Aalto University
School of Chemical
Technology

School of Chemical Technology
Degree Programme of Chemical Technology

Moses Ogunsola

DATA-BASED MODELLING OF A MULTIPLE HEARTH FURNACE

Master's thesis for the degree of Master of Science in Technology submitted for inspection, Espoo, 26 October, 2015.

Supervisor **Professor Sirkka-Liisa Jämsä-Jounela**

Instructor **Ph.D. Alexey Zakharov**

Aalto University
School of Chemical
Technology

Aalto University, P.O. BOX 11000, 00076 AALTO
www.aalto.fi
Abstract of master's thesis

Author Moses Ogunsola

Title of thesis Data-based modelling of a multiple hearth furnace

Department Department of Biotechnology and Chemical Technology

Professorship Process control and automation **Code of professorship** Kem-90

Thesis supervisor Professor Sirkka-Liisa Jämsä-Jounela

Thesis advisor(s) / Thesis examiner(s) **Ph.D. Alexey Zakharov**

Date 26.10.2015 **Number of pages** 75 + 47 **Language** English

Abstract

Monitoring and control of process operations is highly essential in process industries for the successful operation of a chemical process. Control over process variables and other process variations ensure a reliable end product quality and provide stability and efficiency for the process. The process considered in this thesis is the calcination of Kaolin in a Multiple Hearth furnace which consists of 8 hearths with four burners each on hearths 4 and 6 that supply the energy required for calcination.

The aim of this thesis is to develop data based models for the gas temperature profile in the multiple hearth furnace which is a key process variable determining the gas-solid heat exchange, and thus, affecting the final product quality. The models can be utilized to forecast furnace dynamics, to develop a model-based control which reduces variations in the gas flow rates into the hearths as well as for model based optimization which determines the optimal gas flow rates to hearths 4 and 6. These benefits of the gas temperature profile prediction may help to minimize the energy consumed by the burners and also to improve the control of the final product quality while maintaining the quality constraints.

In this thesis, the relevant literature on statistical data processing methods are reviewed and case studies are presented to demonstrate the application of data based modeling in mineral processing. Thereafter, required data-based static and dynamic models are constructed using statistical techniques such as the Principal Component Analysis (PCA), and the Partial Least Squares (PLS). The model accuracy is improved by combining the process data with the chemical engineering knowledge of the process.

The models are constructed for the most common feed rates and finally validated using process data not used for training. Results are presented and the models were able to predict the gas temperature profiles in the furnace in each of the hearths; the dynamic models improved the model quality when compared to the static models. In addition, a future prediction of the temperature profile was carried out to confirm the ability of the dynamic models to predict the furnace behavior. Also, the possibility of utilizing the dynamic models for process control and optimization is discussed.

Keywords Multiple hearth furnace, data-based modelling, PCA, PLS.

Preface

This master's thesis has been written in the Research Group of Process Control and Automation, at Aalto University School of Chemical Technology during the period 2. March 2015 – 31. October 2015. This work is a part of the STOICISM project. STOICISM (The Sustainable Technologies for Calcined Industrial Minerals) is a major innovative research project launched in the beginning of the year 2013 under the Framework Programme 7 for the "New environmentally friendly approaches to mineral processing".

Firstly, I would like to express my gratitude to my professor Sirkka-Liisa Jämsä-Jounela for the opportunity to write my masters thesis in the research group, and particularly in this project. Her guidance, advice and invaluable feedback are highly appreciated. Also, I would like to thank my instructor, Ph.D. Alexey Zakharov, for his support and expertise during the course of the work.

In addition, I appreciate my colleagues in the lab for encouragement, motivation and for creating a friendly environment. Thank you Palash, Rinat, Miao, Sasha, Jukka and Jose.

Sincerely, I appreciate my family for their support all through the years, not forgetting my friends for their understanding and encouragement when required.

Espoo, 26.10.2015

Moses Ogunsola

Contents

LITERATURE PART

EXPERIMENTAL PART

Appendices

1. Prediction of PCA scores for feed rates 100, 105, 110, 115 kg/min using gas flows to hearths 4 and 6 (Static Models).

2. Prediction of PCA Scores for Feed Rates 100, 105, 110, 115 Kg/Min Using Gas Flows and Walls Temperature (Static Models).

3. Prediction of GPCA Scores for feed rates 100, 105, 110, 115 kg/min using Gas Flows and Walls Temperature (Static Models).

4. PLS results for the prediction of Gas Temperature profiles using methane gas flows (Static Models).

5. PLS results for the prediction of Gas temperature profiles using Methane gas flows and Furnace Walls temperature for feed rates 100, 105, 110, 115 kg/min (Static Models).

6. PLS results for the prediction of Gas temperature profiles using Methane gas flows, Furnace Walls temperature and delayed gas temperatures for feed rates 100, 105, 110, 115 kg/min (Dynamic Models).

7. PLS results for the Prediction of Gas temperature profiles using the ratios of Methane gas flows to each burner, Furnace Walls temperature and the delayed gas temperatures (Dynamic Models).

ABBREVIATIONS

DSC	Differential Scanning Calorimetric
MHF	Multiple Hearth Furnace
PCA	Principal Component Analysis
PLS	Partial Least Squares
SOM	Self Organizing Map
STOICISM	Sustainable Technologies for Calcined Industrial Minerals
TG	Thermogravimetric analysis

1 Introduction

Kaolin, also known as china clay, primarily consists of the mineral kaolinite, a hydrous aluminium silicate formed by the decomposition of minerals such as feldspar. The kaolinite content in processed grades of kaolin varies between 75 to 94%.

The properties and quality of kaolin are enhanced by the calcination process which is a heating process that drives off water from the mineral kaolinite ($Al_2Si_2O_5(OH)_4$), collapsing the material structure, which results in the kaolin becoming whiter and chemically inert. Calcination process usually undergoes several reactions starting with dehydration which drives off the free moisture. Next, a dehydroxylation reaction occurs whereby the chemically bound water is removed and amorphous metakaolin is formed at a temperature of 450-500^{o}C. The third reaction is the transformation of metakaolin to the 'spinel phase' by exothermic recrystallization which occurs at a temperature of 980^{o}C. Above 1000^{o}C, a hard and abrasive substance called mullite begins to form, and this can cause damage to process equipment.

Calcined kaolin has a broad range of applications including serving as a binding agent, a filler, fixing agent, heat transfer agent and catalyst support. This makes it an important raw material for a variety of industries such as paper, rubber, paint and pharmaceuticals. In the paper industry, it is used both as filler and a coating medium, thereby enhancing the surface characteristics of paper, reducing cost and improving its printing characteristics. In addition, the ceramics industry utilizes kaolin to improve the brightness, strength and flow properties of the ceramic material. Other applications of kaolin are in the manufacture of paints, adhesives, rubber and plastics, where it is used as fillers [1].

Specifically, in the process studied in this thesis, kaolin is calcined in a multiple hearth furnace called the Herreschoff Calciner which consists of eight hearths. Heat required for calcination is supplied by burners in hearths 4 and 6, each hearth has four burners which are aligned tangentially. Raw material is fed in at the top and gets hotter as it moves down through the furnace. Inside the furnace, material is moved by metal blades which are attached to the rotating rabble arms. The product starts to cool at

hearth 7 and finally leaves at hearth 8. The burners have the potential to use 8000KW of power in total, hence, it is necessary to minimize the energy consumption in the furnace while ensuring a good product quality that has low mullite and soluble aluminium content.

This thesis is part of the STOICISM (Sustainable Technologies for Calcined Industrial Minerals) project. The project is a major innovative research project which began in 2013 under the Framework Program 7 for the 'New environmentally friendly approaches to mineral processing'. The project consists of 18 partners from 8 different European countries, with the consortium being led by IMERYS group. The responsibility of Aalto University is to develop and design the concept for the online monitoring and control of the calcined mineral processes.

The data-based modeling approach taken in the thesis is frequently used in the process monitoring because of its scalability and feasibility for complicated industrial processes. In particular, Principal Component Analysis and Partial Least Squares methods employed in the thesis are frequently utilized for process data analysis and building process models.

The aim of this thesis is to develop static and dynamic data based models to predict the gas temperature profile in the multiple heath furnace, which is beneficial to forecast furnace dynamics. In particular, predicting the uncontrolled process variables, such as some of the gas temperature measurements in Hearth 4, and also predicting the temperature dynamics while plant control saturation could serve for monitoring the plant operations. Secondly, the models obtained in this thesis could be used to develop a model based control as well as for model based optimization. Hence the temperature profile prediction may help to minimize the energy consumed by the methane burners and also to improve the control of the final product quality while maintaining the quality constraints.

The thesis is divided into two separate parts: the literature part which consists of chapters two, three, four and five and the experimental part which consists of chapters six, seven and eight. Chapter 2 explains the structure, composition, chemistry and formation of kaolin while Chapter 3 describes the kaolin preprocessing chain from the pit to the calciner, the calcination reaction and the factors affecting the reaction.

In Chapter 4, the process description in the Herreschoff calciner is presented including the solid and gas process routes and the flow of material through the hearths. In Chapter 5, process monitoring methods are classified and the theories behind them explained. Also, some case studies are included to show the applications of process monitoring in mineral processing. The aim of the experimental part is to develop static and dynamic PCA and PLS models for the MHF and this is explained in details in Chapter 6. Chapter 7 presents the data preprocessing methods, testing environment, PCA and PLS models and their validation. The results are presented, analyzed and discussed. Finally, conclusions and topics for further research are presented in Chapter 8.

LITERATURE PART

2 Formation and Properties of Kaolin

Kaolinite's structure is composed of Silicate sheets (Si_2O_5) bonded to aluminium oxide-hydroxide layers ($Al_2(OH)_4$). This layer is referred to as gibbsite. It is an aluminium oxide mineral with a structure similar to kaolinite. The silica layer consists of silicon atoms interconnected with oxygen atoms in a tetrahedral co-ordination. In the gibbsite layer, aluminium atoms are octahedrally coordinated with hydroxyl group. Silicate and gibbsite are weakly bonded together which causes the cleavage and softness of the mineral [5].

The resulting structure of kaolinite is the combination of both layers resulting into a hexagonal structure comprising of both the octahedral and tetrahedral groups as shown in Figure 2.1.

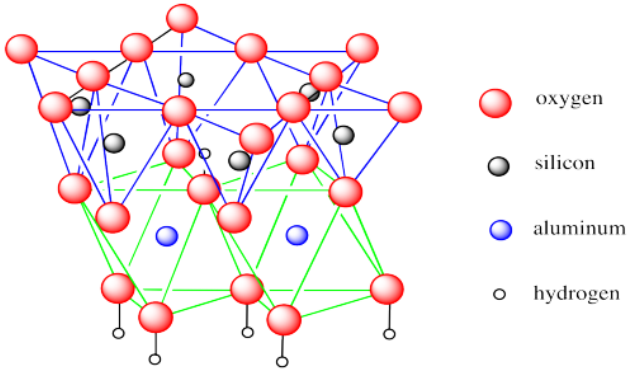

Figure 2.1: Structure of kaolinite [22]

2.1 Kaolin Formation

Usually, kaolin is formed in a process known as kaolinisation by the alteration of feldspar-rich rocks, majorly granites. The process can occur in two ways: Chemical weathering of Feldspar bearing rocks and by hydrothermal alteration.

In chemical weathering, clay formation is initiated by the acid hydrolysis of feldspar according to Equation 1. In this reaction, plagioclase feldspar is broken down during weathering to form kaolinite releasing sodium or calcium ions.

$$(Ca, Na)Al_2Si_2O_8 + 2H^+ + H_2O \leftrightarrow Al_2Si_2O_5(OH)_4 + Na^+ + Ca^{2+} \quad (1)$$

The mechanism of weathering is complex and may involve several stages during kaolin formation. The process is more favorable at acidic pH but less effective under alkaline conditions.

Hydrothermal alteration can also form kaolin. However, this method is far less important as an inherent process compared to weathering. [3] In the hydrothermal theory, it is believed that kaolinite formation was an end product of a long period of paragenetic sequence which occurred after granite emplacement. The formation process was then terminated with the circulation of low temperature meteoric fluids.

It is generally believed that the process of kaolinite formation was a combination of both weathering and hydrothermal processes. This is necessary because it is difficult to dissociate the two processes, hence it can be concluded that both a late hydrothermal process and a tertiary weathering event contributed to kaolinite formation. [2, 3]

2.2 Properties of Kaolin

The physical and chemical properties of kaolinite vary, however, irrespective of the variations, the properties of the mineral are affected by minor amounts of other clay minerals, non-clay minerals and other impurities. [4]

The mineral usually appears as white, colourless, greenish or yellow. The mineral has a melting point of between 740-1785^{o}C and a density of 2.675g/cm^{3}. It is insoluble in water but when wet, it develops an earthy odour. Kaolin is generally stable and chemically unreactive under ordinary conditions. [6]

Mostly, kaolin deposits are affected by various impurities which greatly reduce their value. Some common impurities include:

- Iron oxides and hydroxides, which affects the colour of calcined products
- Smectites, which affects the behavior of kaolin slurries used in paper coating.
- Silica and fine-grained feldspar, which produce an abrasive slurry that causes wear to machinery.

The type and amount of impurities are dependent on several factors among which are the method of formation (secondary deposits are purer), formation conditions (conditions determine the products formed), materials present in the parent rock (any untransformed impurities present in the parent rock will be present in Kaolin).

3 Kaolin Processing and Calcination

The kaolin utilized in the calcination process is usually processed by a method known as wet processing. This process is described in details in next sub section. Processing of kaolin yields a product of considerably higher quality and in addition it helps to substantially remove the impurity minerals that discolour the crude. Also, the removal of coarse particles can be achieved by settling using vibrating screens, chemical bleaching to remove some coloration, filtration and finally, drying. The overall objective is to produce highly refined kaolins ready to be calcined. [7]

3.1 Preprocessing of Kaolin for Calcination

The processing of kaolin can be divided into three main steps: pit operations, refining processes and drying. An example of the process flow diagram describing the entire process is presented in Figure 3.1.

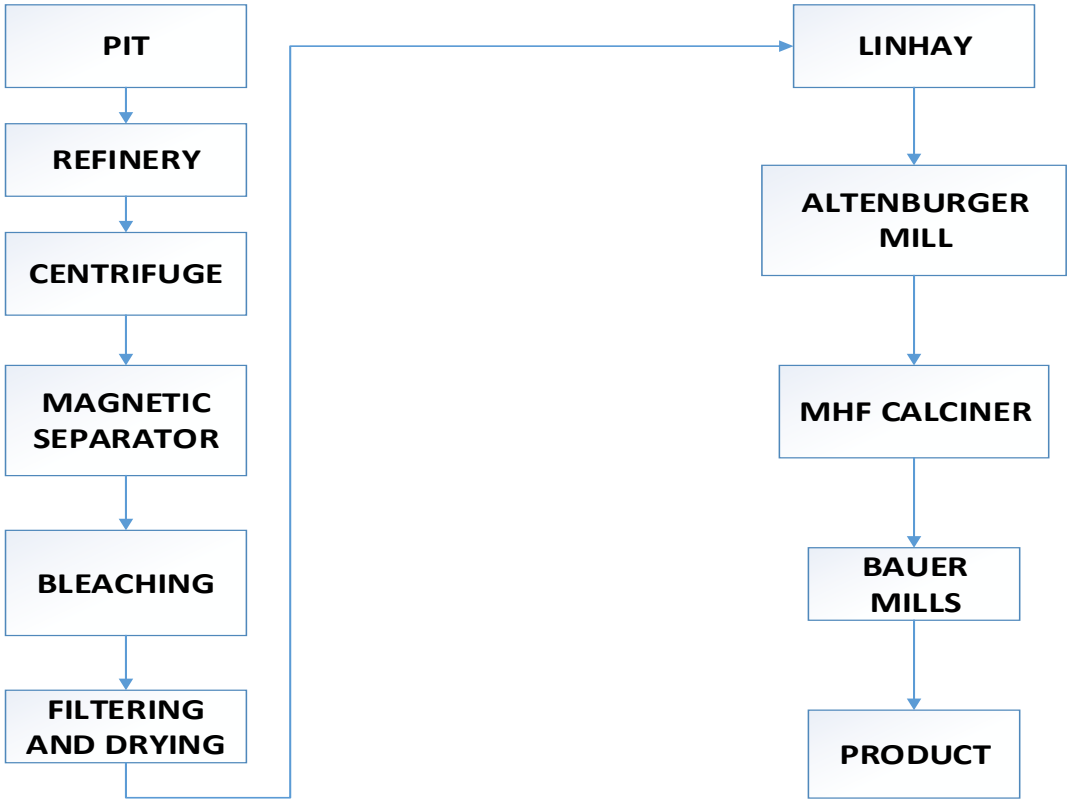

Figure 3.1: Simplified Flow diagram for kaolin production

3.1.1 Pit Operations

Pit operations generally involve the breaking down of kaolinized granite forming a suspension of clay and sand, which are thereafter separated.

The process starts by removing the overburden which consists of two layers: a brown stained granite layer and a layer of top soil. This overburden covers the decomposed granite of interest. This is usually removed by using large shovel loaders and dumpers. The material removed can be subsequently utilized for landscaping work sites where clay extraction has taken place.

Secondly, the pit is blasted to break up the hard ground by drilling holes of 150mm wide and 15m deep. The holes are charged with explosive emulsions which are produced on site. The quality of clay can be analyzed by the piles of sand and dust produced during

drilling. Next, the kaolinized granite goes through a process known as dry mining. In this process, the granite is excavated after blasting and is transported to a 'make down' plant where the material is washed to remove sand and stones. This plant utilize the traditional washing method whereby small water jets are used to break down the granite transforming it into a mixture of clay, sand and stones. The stones are separated by vibrating screens or rotating trommels leaving a mixture of sand and clay.

The next stage involves the removal of sand from clay. Older methods involved the separation of sand from clay by settling method in specialized pits which is a time consuming process. More recently, new and improved methods employed the use of bucket wheel classifiers or large settling pits. In the bucket wheel classifier method, the coarsest particle (quartz, sand and undecomposed feldspar) settle more quickly than the finer particles of clay and mica. The sand removed is placed on vibrating screens to remove more water from the sand before transporting it away by conveyors for use in other applications. Alternatively, in the settling pit method, the sand is allowed to settle in a pit ultimately leading to the formation of a thick bed of sand. This is thereafter loaded by shovel loaders and dumpers and can be sold to sand plants for further refining and use in building industry.

Lastly, fine sand and coarse mica are separated from clay. This is done by pumping the mixture into large hydrocyclones. Centrifugal forces in the cyclone aid the separation of coarse particles (larger than 50microns) from finer particles (lesser than 50 microns). The finer particles are the desired clay which are transported to the refineries for further processing, while the coarser particles are dumped into mica lagoons.

3.1.2 Refining Processes

Kaolin pumped to refineries still contains some amounts of fine sand and mica. At the refinery, these components are completely separated from clay. Furthermore, the clays are sorted into grades of different qualities depending on the requirements of the industry that needs the material.

The first stage in the refining process is thickening. The clay suspension is pumped into circular tanks which have floors that slope towards a central discharge point. The radial

arms inside the tanks push settled material towards the bottom central outlet. To aid thickening, flocculants can be added to encourage clustering of smaller particles into larger ones. The thickened clay settles down and is collected by the underflow pipe which channels it to the next refining stage. The overflow water is collected near the top of the tank and is usually used for clay washing during pit operations.

After the thickening operation, fine mica is separated from clay by adding deflocculants in a series of raked tanks. This allows the particles in suspension to repel each other and subsequently, clay particles are collected as an overflow from the tanks while fine mica is coarser and settles to the bottom of the tanks where it is removed by pumps. Alternatively, this process can be carried out using hydrocyclones.

After separating fine mica from clay, the underflow from the previous stage is grinded. This is because it contains large particles of china clay whose sizes are similar to the size of the unwanted mica and sand. Hence, the grinding process is used to recover the clay by using the principle that the china clay particles are easily broken down within a relatively short period of time. The ground material is then classified in hydrocyclones producing an overflow of china clay.

Furthermore, impurities such as mica, iron oxides and tourmaline are separated from clay. These materials all contain some iron which can cause specks in ceramics and also reduces the brightness of clay used for paper making. The removal of these materials is performed using a powerful electromagnet. Mostly, two kinds of machines are used, depending on the size of clays involved. In both cases, super-conducting electromagnets are employed to create a high magnetic field.

For coarser clays, a large electromagnet with a circular chamber is used which is filled with stainless steel wool. This wool attracts magnetic particles when clay passes through the machine. For finer clays, a machine with a pair of reciprocating canisters is used. The canisters are packed with wire wool they undergo a back and forth movement from a magnetic field. Magnetic particles are held on to the wire wool and the movement mechanism ensures that clay is treated almost continuously.

Lastly, iron oxides which frequently stain the clay are removed by bleaching using sodium hydrosulphite. In the bleaching process, the clay passes through a tower to remove

air trapped which helps to increase bleaching efficiency. The clay then passes through a system of pipes where the bleaching chemical is added. This chemical helps to convert the insoluble iron oxide into iron sulphate which is less coloured and soluble; hence it is removed from the process when the clay is dewatered.

3.1.3 Drying of refined clay

Refined clay is transported to drying plants where it is initially thickened in settling tanks and thereafter passed through a filter press to produce a solid cake of china clay. The cakes are cut and fed to a mechanical dryer before sending to storage.

Firstly, the clay is thickened by removing clear water from the top of the storage tanks located in the refiners and drying units. Addition of an acid flocculant aids this process. Next, the clay is pumped under pressure into a series of chambers lined with tightly woven nylon cloth. This allows only water, but not clay particles to pass through. The chambers may be circular or square in shape. This process is known as filter pressing.

Before clay is eventually dried, it passes through a pug mill. The mill helps to round clay particles and improve their flow properties, which is very useful in some applications.

Before drying, china clay is converted into a pelletized form. Firstly, the clay is mixed in a trough with paddles to break down any lumps that might be present. Next, it is conveyed to a drum enclosing a rotating vertical shaft carrying pegs known as a pelletizer. This process forms pelletized clay which is a preferable form for drying.

Pelletized clay is finally dried either by using the Buell Tray Dryer or the fluidized bed dryer. The Buell dryer consists of thirty layers of trays stack together in a circular tower and rotated in a current of hot air, drawn into the dryer by fans. Clay is fed into the top of the dryer and when the trays completes one revolution, the clay on them is pushed off by fixed arms onto the next tray layer , hence moving down gradually to the bottom of the dryer. In total, the clay spends about 45minutes before emerging from the bottom and it contains about 10% moisture.

A more recent drying method is the fluidized bed drying. In this method, hot air is introduced under slight pressure through a perforated floor into a horizontal cylindrical

chamber. The hot air dries the clay pellets quickly and uniformly. This process can be operated either by the separate cooling method or the combined cooling method. In the separate cooling systems, the hot dried clay is transported to another chamber where cooling takes place using atmospheric air. This method is usually employed to dry tonnages of about 6000 tons per week. On the other hand, the combined cooling method uses a single fluidized bed for both drying and cooling and it is suitable for drying of about 3000 tons per week.

The final product can be used in a variety of industries for different applications. However, depending on the specific requirement, some kaolin is further processed. For instance, in many industries, high quality kaolin is required to produce a wide range of products. Once of such treatment method is Calcination. This is described in details in the next section. [8]

3.2 Calcination of kaolin

Calcination is the process used to produce anhydrous aluminate silicate by heating china clay to high temperatures in a furnace. This process gives an increase in hardness and alters the shape of the kaolin. This heat treatment process gives kaolin an excellent insulation performance and low dielectric loss due to the lack of crystallinity. In addition, calcined kaolin has numerous industrial applications in the plastic industry, pharmaceutical industry, paint industry and many others. This process successfully improves brightness, opacity and other characteristics of kaolin. [9, 10].

Generally, there are two different industrial calcination methods; conventional calcination and flash calcination. Conventional calciners are typically large multi-hearth furnaces or kilns which are operated at temperatures between 1400^{o}F (760^{o}C) and 2000^{o}F (1000^{o}C). In the process, about 14 % of the crystalline bound water of hydration is driven off. Impurities retained in the beneficiation stage are oxidized. To ensure consistency, it is essential to monitor the process through advanced technology and process controls. After calcination, the calcined kaolin is cooled and milled to ensure a reduction in aggregates formed during calcination. In contrast to the conventional calcination method, flash

calcination involves the introduction of water washed kaolin to a hot gas stream for a few seconds. In this way, the crystalline-bound water is rapidly removed. [11]

Calcined kaolin can be divided into two products. The first product known as metakaolin. It is formed after the dehydroxylation of kaolinite at a temperature range of 450°C to 700°C. During this period, the crystal structure of kaolinite is altered resulting in an amorphous mixture of alumina and silica ($Al_2O_3.2SiO_2$). Thermal transformation of kaolin is affected by several factors: temperature, heating rate and time and cooling parameters can significantly affect the dehydroxylation process. Metakaolin has increased brightness and improved opacity. The major characteristic of metakaolin is its pozzolanic nature, which is its ability to react with Calcium hydroxide in the presence of water. This property is very useful in cement production. [12] In addition, metakaolin can be used to enhance resilience and opacity in paper production when used as an additive. Also, metakaolin contains alumina which can react with carbon-hydrogen compounds to form several alumina-containing compounds.

When heating is prolonged to around 980°C, recrystallization occurs leading to the formation of spinel phase. Further heating to about 1050°C leads to the formation of mullite ($3Al_2O_3.2SiO_2$). Mullite is the main crystalline phase detected in a kaolinite sintered above 1000°C. The kinetics and the growth of mullite are largely dependent on the structural characteristics of the kaolin raw material and the thermal cycle. [13] The spinel phase and the mullite make up the second product. This product has a brightness that ranges between 92 and 94 %. It is also whiter and more abrasive compared to the original kaolin. Mullite possess many desirable properties such as its high thermal stability, low thermal expansion and conductivity, good strength and fracture toughness, high corrosion stability and creep resistance. [19] However, the product is coarse and abrasive which can cause machinery damage. The abrasive property can be reduced by carefully selecting the feed and controlling the entire calcination process including the final processing. The product can be utilized as an extender for titanium dioxide in paper coating and also in the paint industry. Table 3.1 shows a comparison of the two calcination products and their properties. [14]

Table 3.1: kaolin grades and property changes [14]

Property	Product 1	Product 2
Shape	Changed	Changed
Particle size	Changed	Changed
Brightness	Increased	Increased
Opacity	Improved	-
Colour	-	Whiter
Abrasion	-	Increased
Specific surface area	-	Increased
Temperature range	500 – 700^{o}C	950-1100^{o}C

The entire kaolin process can be described by the following reaction stages: [15]

1. Removal of adsorbed water (Dehydration)

$$H_2O(l) \xrightarrow{70-110^oC} H_2O(g) \quad (2)$$

2. Dehydroxylation reaction to produce metakaolin

$$Al_2O_3.2SiO_2.2H_2O \xrightarrow{400-700^oC} Al_2O_3.2SiO_2 + 2H_2O \quad (3)$$

3. Spinel Phase formation

$$(Al_2O_3.2SiO_2) \xrightarrow{925-1050^oC} 2Al_2O_3.3SiO_2 + SiO_2\ (amorphous) \quad (4)$$

4. Nucleation of the spinel phase and transformation to mullite

$$3(2Al_2O_3.3SiO_2) \xrightarrow{\geq 1050^oC} 2(3Al_2O_3.2SiO_2) + 5SiO_2(amorphous) \quad (5)$$

5. Cristobalite formation

$$SiO_2(amorphous) \xrightarrow{\geq 1200^oC} SiO_2(cristobalite) \quad (6)$$

Figure 3.2 is a list of all occurring that and it also shows the temperature range for each reaction.

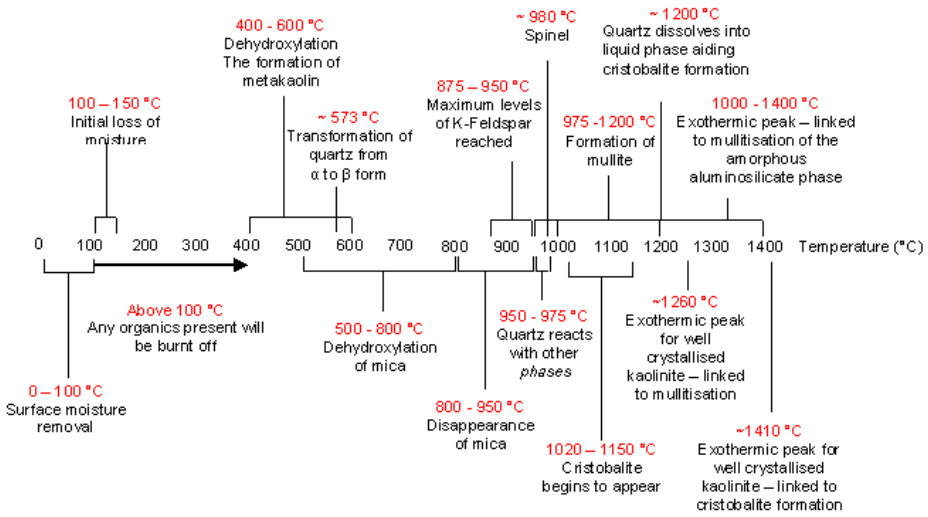

Figure 3.2: Reactions occurring in the Calcination reaction and their temperature range [16]

In addition, a Thermogravimetric analysis and Differential Scanning Calorimetry Curve (TG-DSC curve) is presented in Figure 3.3. TG curve measures the change in mass of a sample over a range of temperatures. This change can be used to determine the composition and thermal stability of a material. Weight losses can be due to decomposition, reduction or evaporation and specifically much of the weight loss in calcination is due to the loss of water. DSC curve on the other hand monitors heat effects associated with the chemical reactions as a function of temperature. In a DSC experiment, a reference material (usually an inert) is used and the difference in heat flow to the sample and the reference at the same temperature is recorded.

The major reactions that occur in the furnace are clearly visible on the curve. The initial dehydration reaction shown in equation (1) takes place between 0-150^{o}C and is

characterized by the first endothermic peak observed on the curve. In this reaction, free moisture is driven from the sample and the temperature of kaolin does not increase despite the addition of energy. In general, 0.5 % weight loss occurs in this reaction.

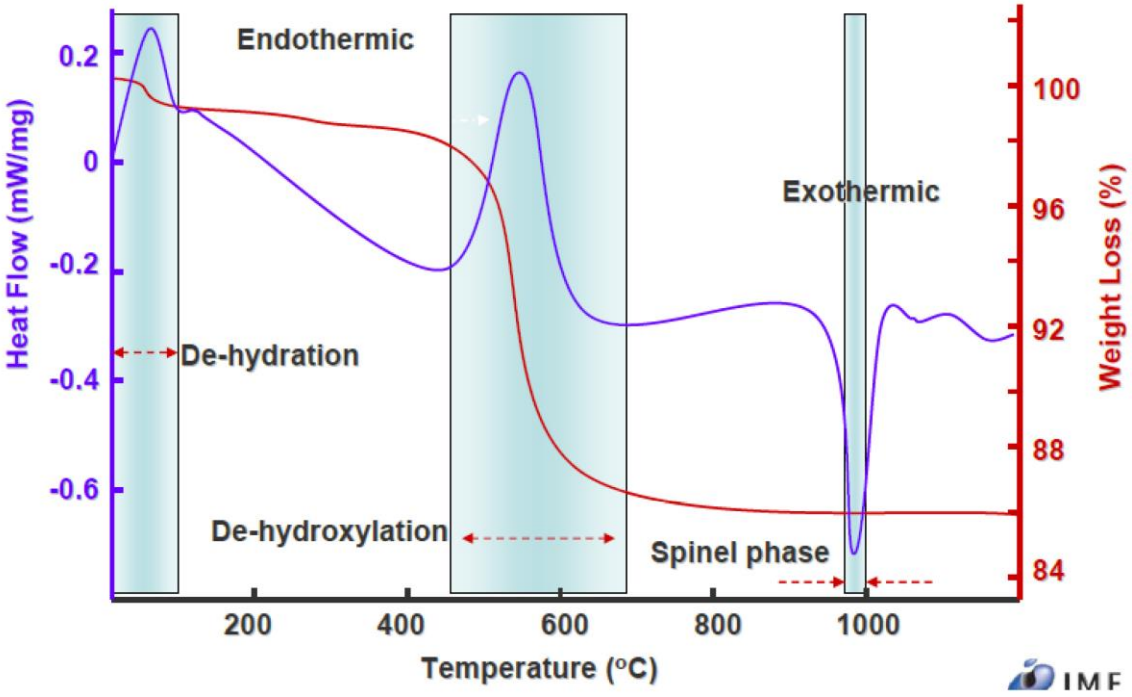

Figure 3.3: TG and DSC curves of kaolin Calcination

Above 100°C, any organic material present in the kaolin will be burnt off. Organic materials can include wood, leaf matter and spores. At low temperature, the organic materials have a charring effect on the product and also lead to a reduction in brightness.

The next visible reaction is also endothermic and here kaolin undergoes a dehydroxylation reaction as shown in equation (2). This reaction can be identified as the large endothermic curve between 450 and 700°C. Chemically bonded water is removed and metakaolin is formed which is an amorphous form of kaolin. The dehydroxylation of kaolin to metakaolin is an endothermic process because of the large amount of energy required to remove the chemically bonded hydroxyl ions. The main constituents of metakaolin are silicon oxide (SiO_2) and aluminium oxide (Al_2O_3) and other minor components are ferric oxide, calcium oxide, Magnesium oxide etc. Table 3.2 shows a typical metakaolin composition for three different grades of metakaolin. [17]

Table 3.2: Typical Metakaolin chemical composition [17]

Components (%)	Grade 1	Grade 2	Grade 3
SiO_2	51.52	52.1	58.10
Al_2O_3	40.18	41.0	35.14
Fe_2O_3	1.23	4.32	1.21
CaO	2.00	0.07	1.15
MgO	0.12	0.19	0.20
K_2O	0.53	0.63	1.05
SO_3	-	-	0.03
TiO_2	2.27	0.81	-
$L.O.I$	2.01	0.60	1.85

The third reaction is the transformation of metakaolin to the spinel phase (equation 3). The transformation occurs by exothermic recrystallization which is visible in figure 2.3 as the sharp exothermic peak around 980^{o}C. In many studies dealing with the spinel phase reaction, the main contention has been identifying the reaction product that results in the exothermic reaction. Experiments carried out by Sonuparlak et.al (1987) was able to confirm the existence of a spinel phase and that it is solely responsible for the exothermic reaction. In addition it was shown that the spinel phase contains less than 10 wt % silica and very close to pure alumina. [18].

When heated further, the kaolinite continues to react. At a temperature range of 975^{o}C to 1200^{o}C, mullite ($2Al_2O_3.3SiO_2$.) begins to form, thereby getting rid of more silica from the structure. Usually some mullite starts to form at the spinel phase. This is known as primary mullite. It has an elliptical shape with random orientation. However, as temperature starts to increase to around 1300^{o}C, the crystallinity of the mullite increases forming needle-like crystals. In addition, the orientation becomes more ordered and hexagonally shaped. In some applications such as in the paint, polymer and paper industries, the coarse product is not needed, therefore it is essential to prevent mullite formation. This achieved by 'soft calcining' for a shorter duration at temperatures below 1100^{o}C. The resulting product is white and has low reactivity, but the abrasive property

is absent [16]. An undesired product can be formed at about 1410^{o}C known as cristobalite as shown in equation (6).

Besides the main reactions described above, other reactions occur simultaneously in the furnace. For example, between 500 and 800^{o}C, any mica present in kaolin will undergo dehydroxylation. By the time temperature reaches 950^{o}C, almost all the mica present in kaolin would have disappeared. Also, the amount of potassium feldspar increases to a maximum before declining or disappearing and the highest amount usually occurs in the temperature range of 875 to 950^{o}C. This is just above the temperature where mica disappeared. Hence, it appears the breakdown of mica provides the necessary raw material for the formation of new potassium feldspar.

In addition, reactions involving quartz are visible. At about 573^{o}C, quartz undergoes a phase change, from the standard and denser alpha form to the less dense and more stable beta form. As a result, between 950 and 975^{o}C, the beta-quartz begins to react with the potassium-rich phases, which causes them to melt.

3.2.1 Effects of heating rate on Calcination

Heating rates in the furnace have significant effects on kaolin calcination and more importantly on the thermal changes that occur in the process. The main reactions such as dehydroxylation to form metakaolin, exothermic recrystallization to form spinel phase and especially mullite formation are all sensitive. Mullite formation below 1100^{o}C is the most affected and the process can be enhanced by increasing the heating rate from 3 to 20^{o}C $/min$ [20]. Mullite forms at a higher temperature with a rapid heating rate. For example, for the kaolin grade considered in the thesis, mullite amount reaches a value of 55% when heated to 1100^{o}C in 25 hours or about 1300^{o}C in 30 minutes. This clearly shows the effect of rapid heating [16].

Also, the processes leading to the formation of metakaolin usually involve three distinct steps. The usual sequence of delamination, dehydroxylation and formation of metakaolinte will only take place in that order if the heating rate is higher than 1^{o}Cmin^{-1}. When heating rate is between 0.03 to 1 ^{o}C/min, the dehydroxylation step occurs first followed by delamination and metakaolinite formation. This implies that at high heating

rate, the rate of delamination prevails over the dehydroxylation. If the heating rate used is below 0.03 ^{o}C min^{-1}, the delamination process reaches its maximum rate after dehydroxylation and formation of pre-hydroxylated metakaolin [21].

3.2.2 Effects of particle size on Calcination

Kaolin with a fine particle size possesses a large surface area which increases its reactivity and consequently its rate of mullite formation. If particle size increases, dehydroxylation and other reactions become much slower. This situation occurs mostly with particle sizes larger than 20µm. A decrease in particle size results in a decrease in the spinel phase reaction, thereby reducing the intensity of the exothermic peak. The particle size of the kaolin feed also affect the size of its calcined products. In addition, a finer product has an increased porosity which affects its oil absorption capability. Also, as particle size decreases, the opacity increases, thereby providing a good raw material additive for paint industries. [14]

3.2.3 Effects of Impurities on Calcination

Iron and organic components are the two categories of impurities present in kaolin. The effect of iron is greater than the effect of organic compounds in calcination. When kaolin is heated to a high temperature in the furnace, the iron oxides are oxidized from Fe^{2+} (green/blue colour) to Fe^{3+} (red colour) giving the product a shade of pink. Also, correlations have been found between the iron content and product properties such as brightness, yellowness and light absorption coefficients. In addition, kaolin whose iron content was reduced through beneficiation produced a brighter product than kaolin with a naturally low iron content. The iron removal process is usually carried out by magnetic separation or reductive chemical bleaching [14].

Organic materials on the other hand, can contaminate kaolin by natural or artificial means. Natural contaminants include wood particles, leaf matter and spores. Artificial contaminants are contacted during processing. An example is polyacrylate which a refinery dispersant added to prevent settling. At high temperatures (above 1000^{o}C), all

organic materials are removed from kaolin. However at temperatures below 700°C, organic compounds give a charring effect on kaolin and changes the colour to grey [14].

Also, the presence of some elements can influence the spinel phase formation reaction and affect the presence of the free amorphous silica. For example, it has been discovered that $Cu^{2+}, Li^{+}, Mg^{2+}\ and\ Zn^{2+}$ promote the recrystallization of metakaolin, while elements with significant alkali content like $Na^{+}\ and\ Ca^{2+}$ have some negative effects, while $K^{+}\ and\ Ba^{2+}$slow down the reaction [16].

4 Process Description of the Herreschoff Calciner

The Multiple Hearth furnace considered in this Master's thesis is the Herreschoff calciner. The process route from raw material to product can be divided into Solid material process route and the Exhaust gas process route. The overall process usually starts from the mills before it enters the furnace. The exhaust gases are also cooled in a heat exchanger where heat is recovered. The bag filter also helps to remove entrained product. The entire process flow is outlined in this section.

4.1 Description of the multiple hearth furnace

The multiple hearth calciner has eight different hearths. The furnace has four burners each on hearths 4 and 6 which supplies the heat required for calcination and these burners are aligned tangentially and have the potential to use 8000 kW of power in total. Raw material is fed in at the top and gets hotter as it moves down through the furnace. The product starts to cool at hearth 7 and finally leaves at hearth 8.

Inside the furnace, material is moved by metal plates or blades which are attached to the rotating rabble arms. The blades are arranged such that they move material inwards on odd-numbered hearths and outwards on even-numbered hearths. Material moving on the odd-numbered hearths drops down to the next hearth at the centre through a single annulus around the shaft supporting the rabble arms while materials on the even

numbered hearths moves outward to drop through individual holes at the outside of the hearth.

The major heat transfer to the material is through radiation from the roofs of the hearth, heat from the burner flame through conduction and convection and some heat is also transferred as the material contacts exhaust gases in the drop holes.

Kaolinte is transformed to metakaolin in hearths 3, 4 and 5. This happens between 500-900^{o}C. The material leaves hearth 5 at around 900^{o}C and its temperature continues to rise in hearth 6. Figure 4.1 is a diagram of the Herreschoff furnace showing the 8 hearths, the location of the burners and the material flow line.

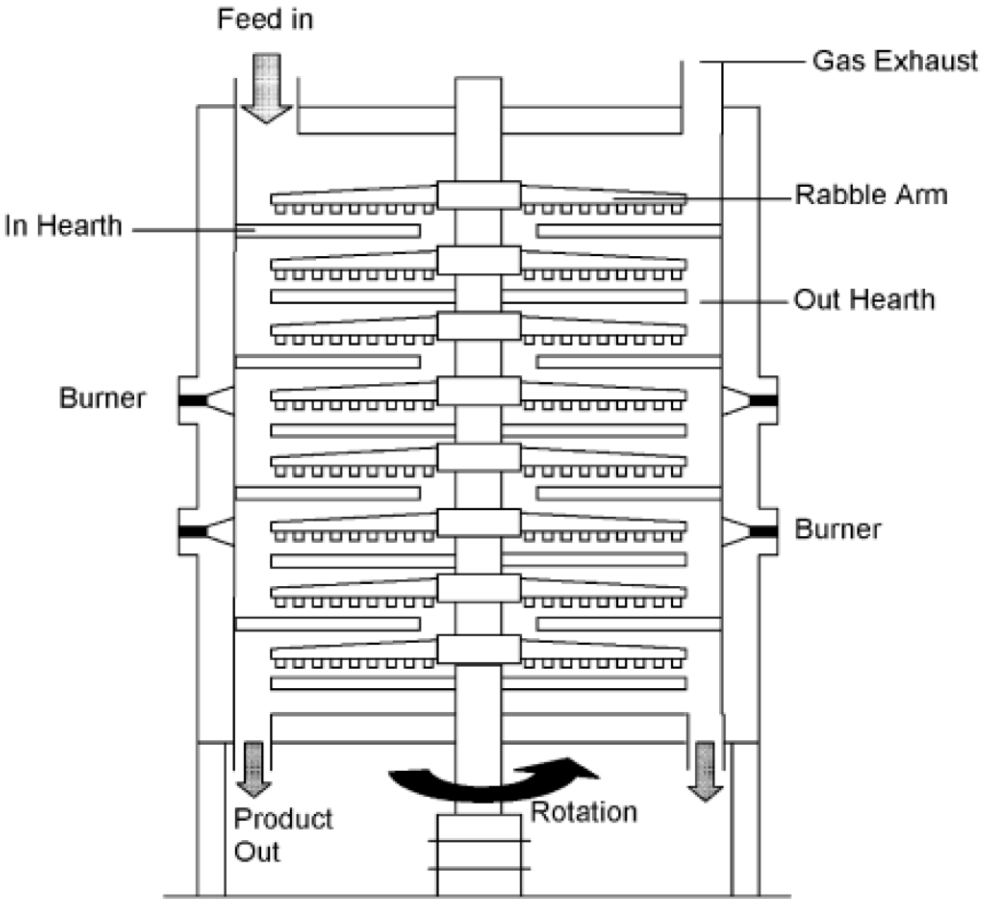

Figure 4.1: Diagram of a Herreschoff furnace [14]

To provide energy, the calciner uses natural gas or fuel oil which is combusted in the 8 burners. The temperature in the fired hearths is controlled by adjusting the gas flows. The combustion air is controlled as a ratio of this gas flow. Measurements of gas and air flow are carried out using orifice plate flow meters. The maximum gas flow in hearth 4 varies as a function of feed rate. This helps to prevent the excessive use of gas. The main purpose of hearth 6 is to increase the temperature which facilitates the absorption of aluminium into the silica phase. Temperature control in hearth 6 is very critical to prevent overheating which can result into the formation of a more crystalline structure which gives rise to abrasion problems. The product starts to cool in hearths 7 and 8 and finally leaves from hearth 8 at around 750^{o}C.

Pressure in the furnace is measured by two sensors which are positions in the calciner exhaust duct and operate within 0 to -5.0 mbar. The sensors are fitted with an air purge cleaning system. The calciner pressure is maintained by the main exhaust fan located at the end of the exhaust gas process discharge through the main stack. The pressure depends on the fan speed and operates with a control procedure that keeps the pressure set point constant.

4.2 Solid and Gas routes through the furnace

This section describes the flow of the solid raw material from the feed inception stage to the finished product. Lumped feed containing about 10% moisture is delivered to the plant by trucks, which tip into the in-feed hopper. It is then conveyed to a 350 tonne redlar bin using a bucket elevator, and thereafter conveyed to the Attenburger Mill/Dryer by another bucket elevator.

The Attenburger mill/dryer removes moisture from the feed and thereafter reduces the feed to powder form as the calciner feed. The product from the mill is collected in a bag filter and afterwards transferred to the powder feed silo by a lean phase air conveyor (LPC) and a rotary blow seal. The powder is then transferred from the silo by another conveyor to the upper weigh feeder bin at the top of the calciner. The powder in the upper bin is transferred to the weighed hopper via a rotary valve. The rotary valve is controlled to deliver weights from 0-154 kg/min. After achieving the desired weight of feed, it is

transferred to the lower bin through two side valves. This happens once every minute; therefore the feed rate is expressed in kg/min of dry feed.

The calcined material leaves the calciner via two discharge holes on the 8th hearth and then via water cooled screws into a high flowing stream of ambient air. The temperature of the calcined clay at this point is 700^{o}C. It is the cooled down by the air to about 100^{o}C before reaching the air blast cooler bag filters. The material then collects in the bottom of the bag filter hopper and then conveyed by LPC to the bauer mill feed bin via a blowing seal. The Bauer mill is necessary to reduce the particle size of the calcined product and also remove material greater than 50 microns as rejects.

Exhaust gases leave the furnace via two ducts in the roof of hearth 1, which thereafter combine into a single duct. These gases are then channeled into the AAF (American Air Filter) exhaust gas processing equipment. In emergency situations the exhaust gases can be vented to the atmosphere by the stack vent valve. The valves are operated by air driven actuators which opens the duct to the atmosphere and closes the duct to the AAF process.

The AAF consists of a heat exchanger and a bag filter. The purpose of the heat exchanger is firstly, to cool the exhaust gases which prevents damage to the filters. Secondly the exchanger aims to recover heat which is supplied to the drying process of the calciner feed. The exchanger operates automatically, and alarms are triggered when faults occur and when process extremes are experienced. The maximum temperature of exhaust gas allowed into the exchanger is 650^{o}C. Hence the temperature of the exhaust gases is controlled at the top of the calciner by an exhaust gas dilution damper. Ambient air from outside is combined with exhaust gas whose temperature is higher than 650^{o}C.

Exhaust gases pass inside the exchanger tubes from the top to bottom on one side and from bottom to top on the other side. Cooling is achieved by passing clean ambient air across the outside of the tube bundles. The cooling air enters at the top of the upside passing downward, counter to the flow of the exhaust gases. Some materials are collected in the drop out hopper. They are channeled into a rotary blowing seal and then into an LPC which transports them into the milled feed silo. The hot process air passes into the inlet of the Attenburger mill, and then eventually used to dry the feed clay.

5 Process Monitoring Methods in Process Industries

For the successful operation of a chemical process, it is highly essential to be aware of how the process is running, and how the variations in raw materials and other process conditions after the process operations. This ensures a reliable end product quality in the process industry. Process monitoring provides major benefits which include:

- Increased process understanding
- Early fault detection
- On-line prediction of quality

This helps to provide stability and efficiency for a wide range of processes. Monitoring a process makes it possible to monitor the final product quality, and also all the available variables at different stages of the process, to identify variations in the process. [23, 24].

5.1 Classification and overview of Process Monitoring methods

A common categorization of process monitoring techniques involve division into two groups: model based and data-driven techniques. The model based approach is based on the mathematical model of the system. These methods can be broadly classified as quantitative model-based and qualitative model-based methods (Figure 3.1). However, model based approaches have a number of disadvantages; they are usually not scalable for high dimensional systems, a priori-knowledge of the process is necessary to develop and validate the model, in case of complex systems, construction of the model becomes difficult and in addition, it is difficult to develop a complete model comprehensive of all possible faults. The increasing complexity of industrial systems limits the applicability of model based methods that cannot be scaled to real-world situations. On the other hand, data driven methods can easily adapt to high dimensionality and system complexity. In this methods, raw data is used to process the required knowledge. They are mostly based on the analysis of large historical data bases. Although, a priori knowledge of the system is still necessary to achieve good performances, however, the amount of prior knowledge required does not increase significantly if the target system is very complex. Hence, they can be better scaled with system complexity. Additional priori knowledge is not a major

requirement for this techniques, but a better understanding of the system could be useful to tune the parameters, choose the optimal amount of data to be analyzed and eventually to perform minor modifications on existing methods aimed at improving the effectiveness for the specific problem. [25, 26, 27]

This thesis focuses on Quantitative data based methods namely Principal Component Analysis (PCA) and Partial Least Squares Regression (PLS). These methods are presented in more details in section 5.2.

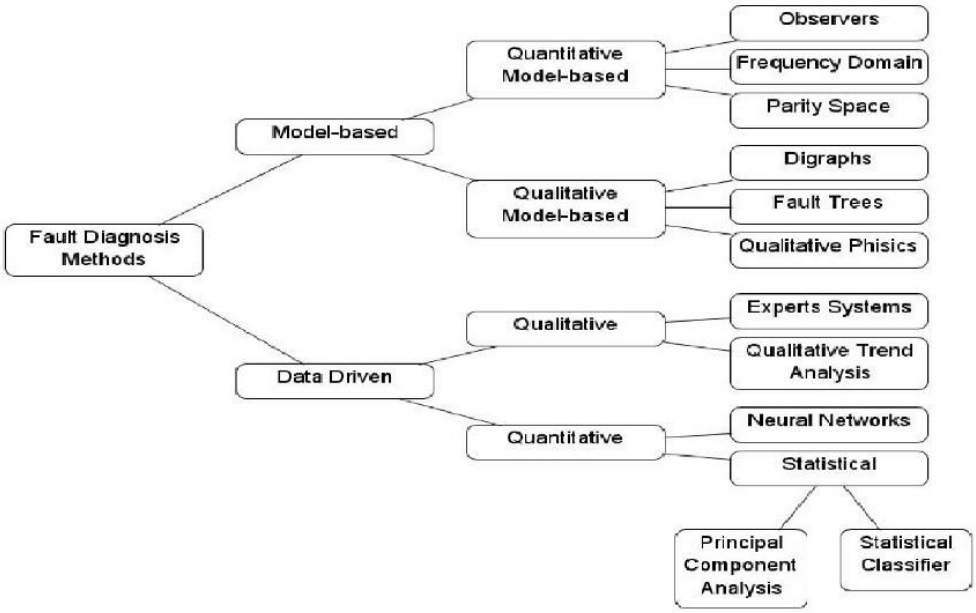

Figure 5.1: Classification of Process Monitoring methods [25]

5.2 Process History based methods

In contrast to model-based methods where a priori knowledge of the process is required, in process history based methods only a large amount of the historical process data is required. These methods can also be qualitative or quantitative. Fig 5.2 shows the classification of qualitative and quantitative process history based methods.

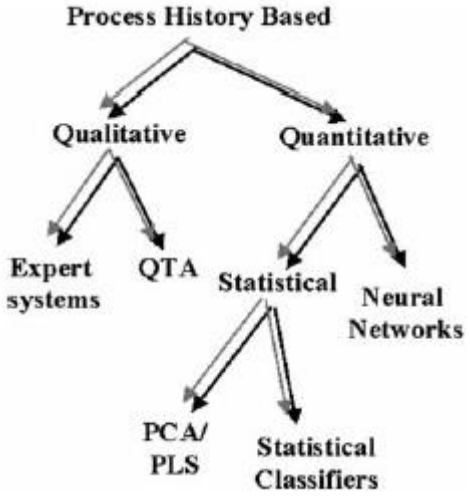

Fig 5.2: Classification of Process history based methods [28]

Expert systems are specialized systems that solves problems in a narrow domain of expertise. Components of Expert systems include knowledge acquisition, choice of knowledge representation, coding of the knowledge in a knowledge base, development of inference procedures and finally development of input-output interfaces. These systems are very suitable for diagnostic problem solving and also provide explanations for solutions provided. Quantitative trend analysis (QTA) aims at extracting trends from the data. The abstracted trends can then be used to explain the important events happening in the process, malfunction diagnosis and also prediction of future states [28]

Quantitative process history methods are divided into statistical methods and Artificial Neural networks. , Neural networks are normally used for classification and function approximation problems. They are used for fault diagnosis and classified based on two dimensions: the architecture of the network and the learning strategy which can be supervised or unsupervised learning. The most popular form of supervised learning strategy is the back-propagation algorithm [28]

The most common statistical methods are Principal Component Analysis (PCA) and Partial least squares (PLS). These methods are explained more specifically in subsequent sections.

5.2.1 Principal Component Analysis

Principal Component Analysis (PCA) is a tool for data compression and information extraction. It finds linear combinations of variables that describe major trends in a data set. It analyzes variability in the data by separating the data into principal components. Each principal component contributes to explaining the total variability, the first principal component described the greatest variability source. The goal is to describe as much information as possible in the system using the least number of principal components. [25]

One of the benefits of PCA is its straightforward implementation because a process model is not needed unlike model-based methods. It is a linear method, based on eigenvalue and eigenvector decomposition of the covariance matrix.

Based on the process measurements, a data matrix, X, is formed. The rows in X correspond to the samples which are n dimensional vectors. The columns on the other hand are m dimensional vectors corresponding to the variables. Prior to performing PCA analysis, it is highly essential to preprocess the data. Specifically, data matrix X should be zero-meaned and scaled by its standard deviation. The result of this normalization is a matrix with zero mean and unit variance.

5.2.1.1 PCA Algorithm

After preprocessing, the next stage is to form the PCA model. This begins by calculating the covariance matrix. The covariance matrix is calculated as shown in equation (8). The Eigen vectors with the largest eigenvalues correspond with the dimensions that has the strongest variance in the data set.

$$C = \frac{1}{N-1} * X^T * X \qquad (8)$$

where C is the covariance matrix and N is the number of observations.

The next step is to calculate the eigenvalues, λ of the covariance matrix. This is shown in equation 9 below.

$$\det(C - I * \lambda_i) = 0 \qquad (9)$$

where I is an identity matrix

The eigenvalues are placed in a diagonal matrix in descending order such that the biggest eigenvalue is in the first row and the second biggest in the second row, and so on.

Also, the eigenvectors are calculated according to equation 10.

$$C * e_i = \lambda_i * e_i \quad (10)$$

The $e_i s$ are the vectors of the corresponding λ_i. These vectors are combined into another vector, V, as shown in equation (11).

$$V = [e_1, e_2, e_3, \dots, e_m] \quad (11)$$

5.2.1.2 Selection of number of principal components

To select the number of principal components, the cumulative variance method is employed. This shows the cumulative sum of the variances captured for each principal component and select the principal component for which 90% of cumulative variance is captured. The variances captured are calculated by the Eigen values as shown in equation (12)

$$Captured\ Variance\ (\%) = \frac{\lambda_i}{\sum_{j=1}^{m} \lambda_k} * 100\% \quad (12)$$

The captured variance method is illustrated in figure 5.3.

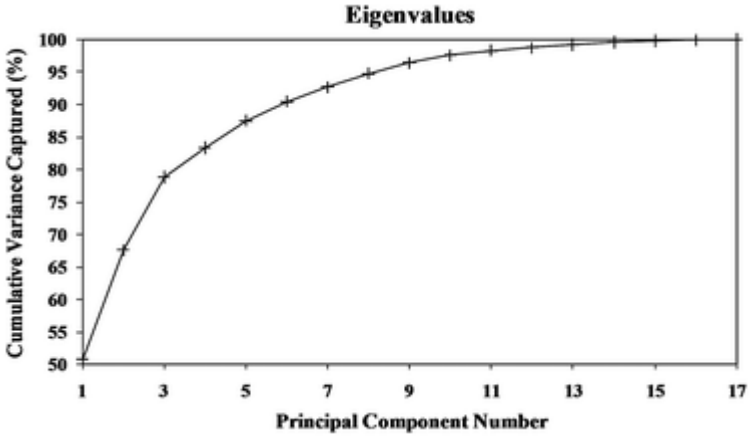

Figure 5.3: Principal Component Selection [32]

After selecting the principal components, k, the PCA model is formed by constructing the transformation matrix V_k and the Eigen value matrix Λ_k as shown in equations 13 and 14.

$$\Lambda_k = \begin{bmatrix} \lambda_1 & \dots. & 0 \\ 0 & \dots. & 0 \\ 0 & \dots. & \lambda_k \end{bmatrix} \quad (13)$$

$$V_k = [e_1, e_2, e_3, \dots, e_k] \quad (14)$$

5.2.1.3 Process Monitoring with PCA

To monitor a process with PCA, control limits are set for two kinds of statistics, Hoteling's T^2 and squared prediction error (SPE), after developing the PCA model. Hoteling's T^2 statistic gives a measure of variation within the PCA model. It is the sum of the normalized square errors. SPE statistic, also known as Q index, on the other hand is the sum of squared errors and a measure of variation not captured by the PCA model [24]. For Hoteling's T^2, the limit for the confidence level, α, is usually taken as 95%. Figure 5.4 shows PCA confidence limits on a model plane.

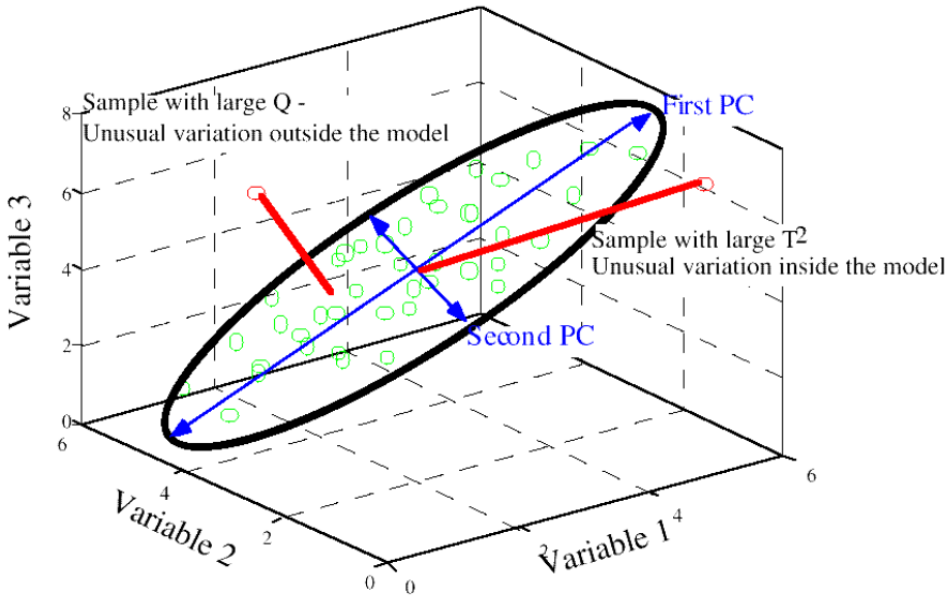

Figure 5.4: Confidence limits of PCA model on a plane [33]

After a fault has been detected, the next phase is to identify the fault. This is achieved using contribution plots. Contribution plots are based on the contribution of each

process variable to the individual score. This include the sum of the scores that are out-of-control. An example of contribution plot is shown in figure 5.7.

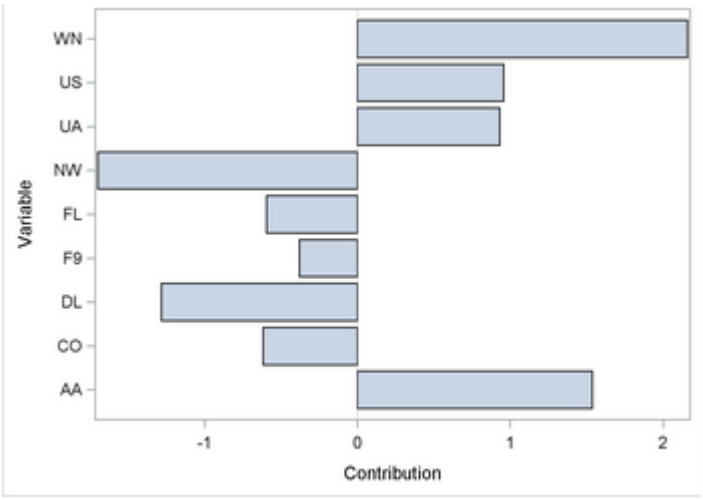

Figure 5.5: PCA Contribution plot [34]

5.2.1.4 PCA modifications

Ordinary PCA is a linear method which makes it limited when applied to some applications. Several PCA extensions have developed. This include dynamic PCA, recursive PCA, nonlinear PCA and multiscale PCA.

Dynamic PCA (DPCA) extracts time-dependent relationship in measurements by forming an augmented matrix of the original data matrix and time-lagged variables. The purpose of introducing time-lagged input variables is to capture the dynamics in the process. This is done by taking into account the correlation of variables. However, the disadvantage is the increased number of variables due to the addition of lagged inputs. DPCA has successfully identified and isolated faults in some processes and it also detects small disturbances better than static PCA.

Due to changes in operating conditions, some processes do not display a stationary behavior. Hence Recursive PCA (RPCA) tries to solve this problem by recursively updating the PCA model. Generally a recursive model recursively updates the mean, number of PC calculation and also the confidence limits for SPE and T^2 in real time. In simple cases, the structure of the covariance matrix is unchanged but the mean and

variance are updated. RPCA helps to build a PCA model to adapt for slow process changes and detects abnormal conditions.

Non-Liner PCA (NLPCA) is used to handle non-linearity in process monitoring. Usually, many process model equations are essentially non-linear and several techniques such as generalized PCA, principal curve algorithm, neural networks and kernel PCA have been proposed. These methods are able to capture more variance in a smaller dimension compared to linear PCA.

In the generalized PCA method, the data is transformed using some given functions by forming new variables before eigen value and eigen vector decomposition. Using process knowledge, the functions can be derived and the resulting PCA model usually represents the modeled system better and for a wider operating region. The main setback of the approach is that a comprehensive knowledge of the process is required and various transformations must be tried [37].

The Kernel PCA method transforms the input data into a high-dimensional feature and thereafter applies the linear PCA technique to the transformed data. In the principal curve technique the data is represented with a smooth curve which is determined by nonlinear relationships among the variables. Each point in the principal curve is equivalent to the average value of the data samples whose projection on the curve aligns with the point, thereby making it possible to construct a principal curve iteratively [37]. To demonstrate the kernel PCA and the principal curve method, a simulated system is used which was driven by a single variable (t) which is inaccessible [32]. The only information available are three measurements which satisfy the equations below:

$$x_1 = t + \epsilon_1 \tag{23}$$

$$x_2 = t^2 - 3t + \epsilon_2 \tag{24}$$

$$x_3 = -t^3 + 3t^2 + \epsilon_3 \tag{25}$$

where t is the sampling time and ϵ_i (i = 1,2 and 3) is a random noise with a mean of zero and variance of 0.02.

A faulty condition is introduced by introducing small changes to x_3 as shown below:

$$x_3 = -1.1t^3 + 3.2t^2 + \epsilon_3 \quad (26)$$

100 samples were collected before the occurrence of faults and an additional 100 samples were collected after introducing the fault. However, PCA analysis is inadequate to detect the faulty condition because the correlations between the variables are nonlinear. Hence, the principal curve method was used to find the nonlinear scores while the multilayer perceptron was used to find the nonlinear function between the scores and the original data. The SPE plot is presented in figure 5.6. The onset of the faulty condition can be easily noticed from the chat.

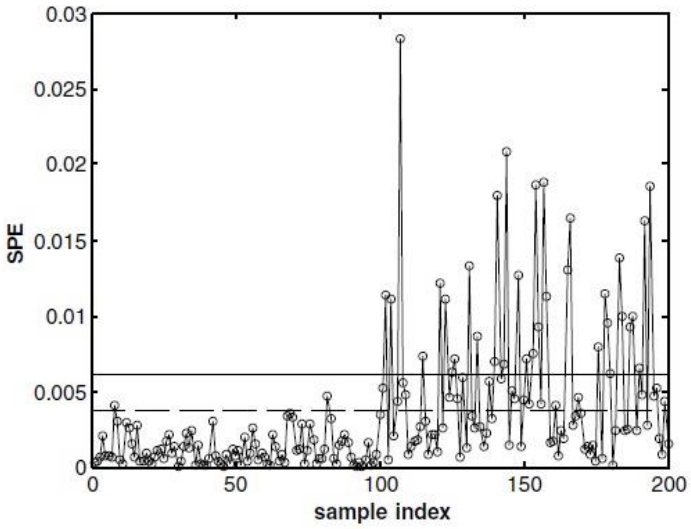

Fig 5.6: SPE statistics plot using principal curves-multilayer perceptron method

Thereafter, the proposed kernel PCA method was also performed on the same data and the results are presented in Fig 5.7. In this approach, kernel PCA was used to extract nonlinear features from the data and then linear PCA was performed on the residuals. Both T^2 and SPE statistic plot indicates a shift in the data sampled in the presence of faults.

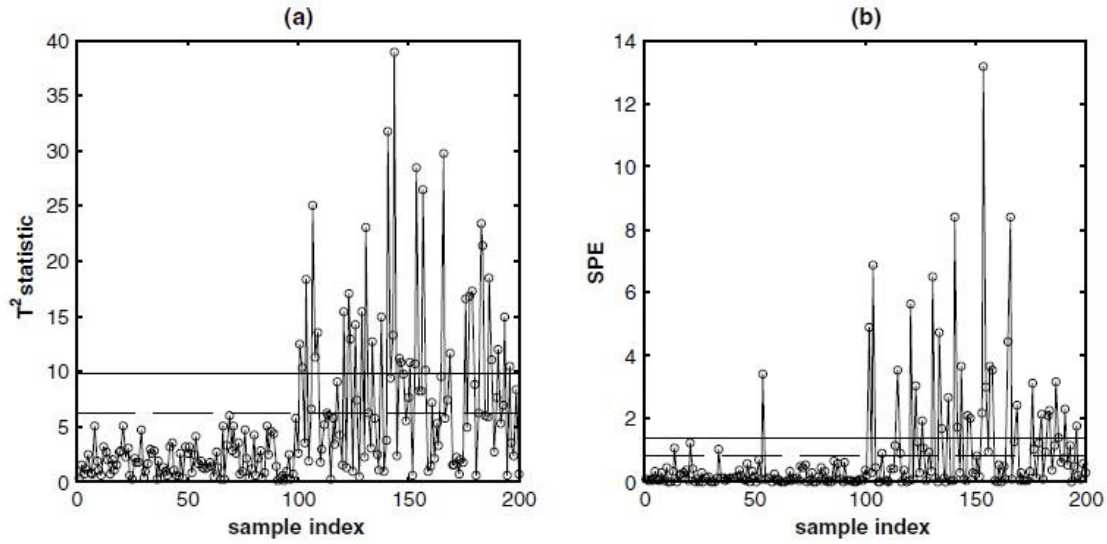

Fig. 5.7: Hoteling T^2 and SPE statistics using Kernel PCA to extract nonlinear features.

Multiscale PCA combines the benefits of PCA and wavelength analysis. While PCA identifies linear relationships between variables, wavelength analysis extracts features and detects auto correlated measurements. Therefore this method adequately eliminates stationary and non-stationary noise better than the individual methods in isolation. Monitoring and calculation of confidence limits are carried out by computing SPE and T^2 at each scale. [35]

5.2.2 Partial Least Squares

Sometimes, an additional group of data usually do exist e.g. product quality variables Y. It is often needed to include all the data available and to use process variables X to predict and identify changes in product quality variables Y. This can be achieved using the Partial Least Squares (PLS) method. This method models the relationship between two blocks of data and also simultaneously compresses them [28]. It reduces the dimensionality and also maximizes the covariance between the predictor matrix X and the predicted matrix Y for each component. The dimensionality of the two data sets are reduced such that the reduced X is the most predictive of Y. The first PLS latent variable is the linear

combination of the process variables that maximizes the covariance between them and the quality variable [35].

5.2.2.1 PLS Algorithm

After applying data pretreatment, matrix X is decomposed into a score matrix T and a loading matrix P, plus a residual matrix E.

$$X = TP^T + E = \sum_{a=1}^{A} t_a p_a^T + E \quad (27)$$

Similarly, data matrix Y is decomposed into a score matrix U, a loading matrix Q and a residual matrix F.

$$Y = TU + F = \sum_{a=1}^{A} u_a q_a^T + F \quad (28)$$

Then PLS regresses the estimated Y score matrix U to the X score matrix T using equation 29.

$$U = TB \quad (29)$$

Where B is a diagonal regression matrix. Using the regression of U, equation 30 can be derived as follows:

$$Y = TBQ^T + F \quad (30)$$

where F is the prediction error matrix. This iterative process can be carried out by several algorithms such as NIPALS and SIMPLS.

5.2.2.2 Selection of number of latent variables

Selection of latent variables is based on several indexes such as cross validation PRESS, RMSECV, RMSEC and RMSEP.

PRESS (Prediction residual sum of squares) is calculated according to equation (31). When the PRESS value is minimized, the optimal number of latent variables is defined. The first step is to divide the data into groups. Groups are left outside the model one after

the other, and the model is constructed using the rest of the groups. The model is tested with the group that was left outside. Using this algorithm, PRESS value is calculated for every latent variable. When the cumulative PRESS reaches its minimum value, the optimal number of latent variables is selected.

$$PRESS_i = \frac{1}{mn} ||Y_i - \hat{Y}||_F^2 \quad (31)$$

$$PRESS_{CUM} = \sum_{i=1}^{s} PRESS_i \quad (32)$$

where m is the number of observation in each group i, n is the number of variables, s is the number of groups and F indicates Frobenium norm. Figure 5.8 shows how the latent variables are selected

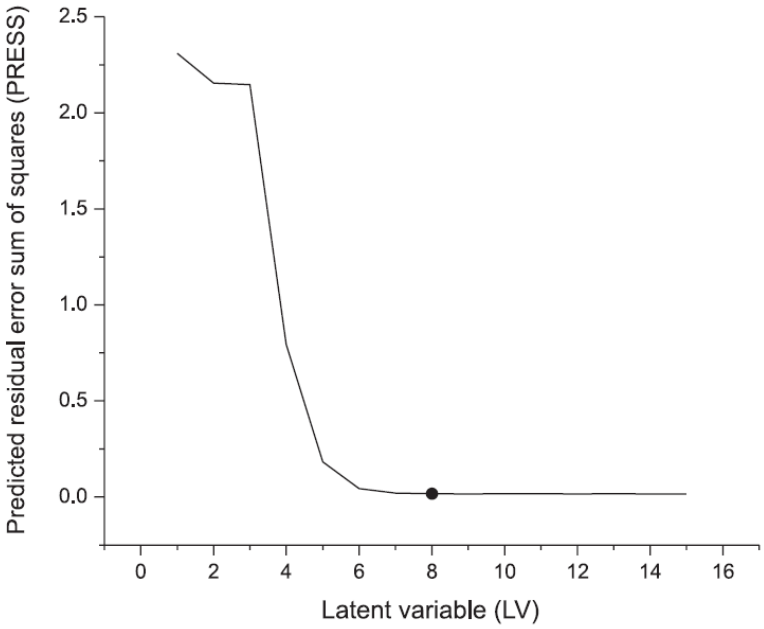

Figure 5.8: Selecting number of latent variables using PRESS [36]

In RMSEC (root mean square error of calibration), the model is compared to the modelling data. The error is calculated using equation 33.

$$RMSEC = \sqrt{\frac{\sum_{i=1}^{n} (\hat{Y}_i - Y_i)^2}{n}} \quad (33)$$

where n is the number of samples in the modelling data and Y_i is the modelling data value.

Alternatively, RMSECV (root mean square error of cross-validation) fits the model quality using equation 34, where s is the number of groups.

$$RMSECV = \sqrt{\frac{PRESS_{CUM}}{s}} \quad (34)$$

RMSEP (root mean square of prediction error), on the other hand, is equal to RMSEC but the model is compared to a separate test data.

5.2.2.3 Evaluation of model quality

Output residuals can be monitored in PLS using equation 35.

$$r = y - \hat{y} \quad (35)$$

For fault detection, identification and diagnosis, the techniques applied for PCA can also be applied in PLS. Therefore SPE, T^2 statistics and contribution plots can be used [35].

5.2.2.4 PLS Modifications

Recursive PLS (RPLS) regression algorithms can be used when the process is time-varying and the model needs to be updated based on the new process data. RPLS does this update without increasing the size of the data matrices. The process starts by formulating data matrices X and Y. The data is scaled to zero mean and unit variance and then the PLS model is updated. Then the new observation pair is scaled and new matrices X and Y are formulated. The previous step is then repeated. This method has been successfully applied to Model predictive control monitoring [35].

5.3 Methodology for Applying Data based methods

The first phase in setting up a monitoring system is to gather the specifications of the target application and the end user requirements. This is usually achieved by interviewing production personnel which include the engineers, operators and the management team. Information obtained from the interviews include a detailed description of the required functionality of the proposed system, the process conditions in the plant, specification of the system environment and the user interface.

The next stage is the selection of the appropriate data based modeling technique to use. Several linear modeling methods are available for selection, however the existence on nonlinear methods are limited, hence processes with nonlinear tendencies are usually modeled with non-linear versions of the linear methods. Also of importance in method selection is the number of operating regions in the process and usually, data representing multiple operating regions are unsuitable for most statistical modeling methods. The intended purpose of the model also needs to be taken into account, for example if the task of building the model is to estimate the values of some process variables, then the values of measures variables are used to estimate the value of another variable, and in this case, the estimates produced by regression models are compared with the equivalent measured values. In addition, the quality of the training data also limits the use of certain modeling methods.

Thirdly the measurement data is analyzed and the modeling data set is prepared. This is usually initiated by applying data preprocessing algorithms to the data set. The outliers in the data are removed by a filtering technique prior to the analysis and compensation of process delays, which can be determined by performing cross correlation analysis between each input and output variable pair. In some methods such as the generalized PCA technique, it is required to augment the original data set with calculated variables, whose values are determined with mathematical functions using a subset of the measured values as inputs. Calculated variables are used to either reduce the number of variables, to form variables describing process phenomena or to linearize the data by converting nonlinear relationships in the process into linear ones, thus making the data suitable to be analyzed by linear modeling methods. To create calculated variables, the role of prior knowledge of the process is very important. Thereafter the consistency of the data and its

suitability for modeling are determined. Data inconsistencies are caused by measurement noise and changes in the process during data collection. For instance, in multivariable cases, data inconsistency is determined by a clustering tool used to find data samples with similar values in the input variables.

Lastly, the data based models are constructed by firstly selecting the input variables and determining the training data set, followed by the model construction. Assessment of the performance of the model is carried out and the input variables can be reevaluated until the required model accuracy is achieved [38].

5.4 Applications of Process Monitoring in Mineral processing

The mineral processing industry currently undergoes several stiff challenges such as high energy costs, tough environmental regulations and stiff competition. Usually, the operations of the processes are controlled by advanced control methods and are highly automated. Hence, it is highly imperative to implement algorithms to detect and classify abnormal trends in the process, therefore, measurements are highly important. Due to this necessity, advanced algorithms and measurement control systems are widely utilized for process performance monitoring. In addition, the efficiency of the process largely relies on the amount of adequate information of the process state available to plant operators. Advanced process monitoring can help to eliminate process upsets and reduce abnormal situations which can yield a greater production capacity [29]. Some industrial applications of process monitoring methods to mining processing are reviewed in this section.

5.4.1 Case 1: Plant wide monitoring of a grinding-separation unit

Process monitoring methods were applied to three Finnish mines; Outokumpu Kemi mine, the Yara Siilinjärvi Mine and the Inmet Pyhäsalmi mine. [30] Plant wide process monitoring was performed at the kemi plant. The objective was to apply advanced monitoring techniques to improve throughput, quality, grade and product recovery of the mineral processing plant or a unit process, ultimately leading to economical improvements of the process operation. The main purpose was to gain prior knowledge

of possible directions of control actions in the grinding circuit. The focus area was the grinding section and gravity separation circuits. Measurement data consisting of 153 samples were collected from the grinding-gravity separation process chain. The output variable is the concentrate grade HR_{Cr2O3} (expressed in $\%Cr_2O_3$). This measurement is carried out by an XRF analyzer after the drum filter. The input variables selected were the feed slurry chromite content and the online analysis of the 50% passing size of the particles (µm) measured from the grinding circuit.

The process was modelled using a recursive partial least squares method. The model structure is illustrated in figure 5.9. The model dynamics was obtained by including a step backward output estimate as an input into the system.

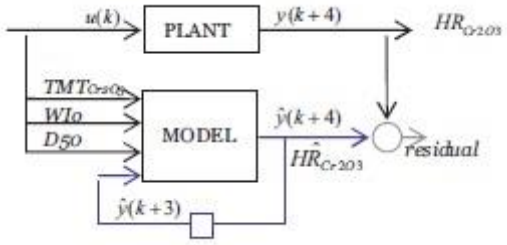

Fig 5.9: Model structure for the grinding gravity separation plant

Next, the model parameters were used for the calculation of the impacts of the changes in the input variables. Table 5.1 is a summary of the effects of the changes in the input variables of the model on the predicted PLS model output, in terms of the originally unscaled Cr_2O_3 (%) concentrate grades. The results indicate the change in model output that resulted from a 10% increase in each input variable.

Table 5.1: Simulation net changes in chromite concentrate grade when 10% increase in each input variable is applied

Input variable	10 % change in the input variable	$\Delta HR_{Cr2O3}(\%)$ when the input changes
Feed slurry chromite content	2.6	0.26
Particle size	1.0	0.08
Bond operating work index	6.7	-0.19

From the results obtained, it can be observed that the feed chromite content and the particle size caused the largest response on the estimated concentrated grade, but in opposite directions. During the process operation, the sign of the impact or its magnitude can change drastically and ultimately change its impact on the system. Hence, a model-based online monitoring system can give useful information in advance regarding the control actions to implement. By detecting early changes in the grinding chain, fluctuations in concentrate grade and recovery losses can be drastically reduced.

5.4.2 Case 2: Monitoring of a Calcium carbide furnace

In this particular case [31], kernel methods are used to remove nonlinear structures from the data and then the residuals from the data are used to monitor the process. The process considers the operation of a calcium carbide furnace and daily average measurements of 10 process variables are collected which are furnace load, electrical power consumption, electrode resistance, lime additive, charcoal, coke, anthracite and three other variables that characterize lime quality. The product of the grade and production rate of the calcium carbide formed a quality index that was used to characterize the performance of the furnace. High grade product can be produced by a high overall furnace load, combined with high loads of coke, lime and charcoal, hence these combination was selected as the normal operating region of the furnace. Also, these four variables were highly correlated when the process data was investigated,

making them suitable for analysis. Kernel PCA was used to remove coherent structures in the data and then Linear PCA analysis was carried out on the residuals to yield a reliable confidence limit on the scores. For discriminant analysis, a discrete version of the quality index was used which are 'low' (for Class 1), 'medium' (for Class 2) and 'high' (for Class 3), where class 3 represents the highest production rates and product grades. Linear and kernel-based discriminant models were constructed from the process data, and the feature maps are presented in figures 5.10 and 5.11. Inspecting the maps visually indicates that there is a better separation between the three classes when the non-linear kernel method was applied.

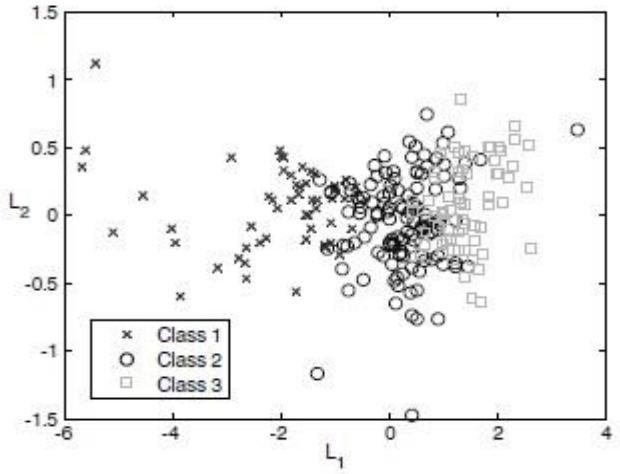

Figure 5.10: Feature extraction of the Furnace data using linear discriminant analysis

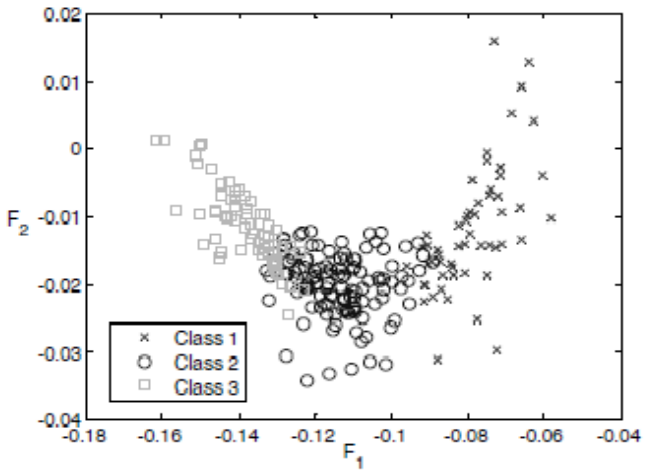

Figure 5.11: Feature extraction of the Furnace data using kernel based non-linear discriminant analysis

EXPERIMENTAL PART

6. Aim of the experimental part

The aim of the experimental part is to develop a data-based model of the gas temperature profile in the multiple hearth furnace, which is a key process variable determining the gas-solid heat exchange, and thus, affecting the final product quality. In more details, both static and dynamic modeling of the temperature profile are considered. In particular, the reason to construct dynamic models is that the recent temperature profile of the gas affects the current state of the solids in the furnace, which in turn affects the future values of the gas phase temperature. Furthermore, the model inputs include the feed rate, the combustion gas and airflow rates as well as the wall temperature. In addition, different process variables and calculated variables selected based on the process knowledge are tried to improve the prediction of the temperature profile.

This thesis proposes static and dynamic data based models to predict the gas temperature profile in the multiple heath furnace, which is beneficial to forecast furnace dynamics. In particular, predicting the uncontrolled process variables, such as some of the gas temperature measurements in Hearth 4, and also predicting the temperature dynamics while plant control saturation could serve for monitoring the plant operations. Furthermore, as the temperature profile in the furnace affects the final product quality, the developed models are suitable to implement a real time optimization system for the furnace to minimize the energy consumption in the process and to improve the control of the final product quality while maintaining the quality constraints. Furthermore, a model-based control of the temperature in Hearths 4 and 6 could be developed to decrease the variations in the temperature profile and especially in the combustion gas flow rate to the furnace, which aims to stabilize the process operations and the product quality. In addition, the developed dynamic models of the gas temperature profile could be employed for more advanced process monitoring.

The model is constructed using the statistical techniques, such as the Principal Component Analysis (PCA), and the Partial Least Squares (PLS). Firstly, plant data is collected and preprocessed. Production breaks and shutdown periods are excluded followed by filtering of noisy signals. The data with a constant feed rate is considered to build furnace models. The delays between the temperature in the earlier hearths and the temperature in Hearths 4 and 6 are removed, and the process variables affecting the gas temperature profile are determined by testing various PCA and PLS model structures, firstly by trying out static models and thereafter dynamic models. Then the models are constructed for the most common feed rates and finally, the model is validated using process data not used for training.

This section is organized as follows. Firstly, in chapter 7, data preprocessing methods, and testing environment are described in details, followed by PCA and PLS models and their validation. Then results are presented, analyzed and discussed, including a comparison between the static and dynamic models. Finally, conclusions and topics for further research are presented in the chapter 8.

7. Determination of the Data-based models of the Temperature profile in the MHF

In this section, the data based models developed in this thesis are presented in details. Firstly, the environment used for process data analysis and models testing is presented followed by a short description of the process data analyzed. Thereafter, the data preprocessing techniques employed to improve the quality of the data are described in details with the outcomes of the data preprocessing stage.

The chapter proceeds with the implementation of the data-based methods aiming to predict the temperature profile in the furnace. In particular, both Static and Dynamic models of the temperature profile are considered. In the simplest case, the flowrates of the combustion gas supplied to the furnace and the kaolin feedrate are utilized to predict the furnace temperature, which results in static models. More accurate modeling of the gas phase temperature profile should also consider the heat transfer between the solid and gaseous phases in the furnace. The solid phase temperature is not measured directly, however, it is determined by the history of the gas phase temperature during the solid stay in the furnace. In other words, the recent temperature profile of the gas affects the current state of the solids in the furnace, which in turn affects the future values of the gas phase temperature. Consequently, the delayed gas temperature profile affects the current gas temperature profile indirectly, through the unmeasured solid phase temperature. As the solid phase residence time is much longer compared the gas residence time, this thesis considers the dynamic models of the gaseous phase, utilizing the past values of the gas temperature profile as their inputs.

The PCA and PLS methods are both utilized to determine gas temperature profile models based on the process historical data. In particular, the PCA models are applied to the gas temperature profile alone to find out the correlations between the temperature in different furnace hearths and to shrink down the dimensionality of the temperature profile data. The outcomes of the PCA method are combined with the simple least-squares regression aiming to obtain a gas temperature profile model. On the other hand, the PLS method is directly applied to obtain the gas temperature profile models.

The different models developed and the motivation behind them is described and the results of the analysis are presented in details. Lastly, the models were validated by using a portion of data not utilized in the model training.

7.1 Description of the test environment and the process data

The testing environment used in this thesis was MATAB. MATLAB (**mat**rix **lab**oratory) is a high-level language and interactive environment used by engineers and scientists to explore and visualize ideas and collaborate across different disciplines. Its capabilities involve performing numerical computations, data analysis and visualization, programming and algorithm implementation and creation of user interfaces. In this thesis, Matlab was utilized for most of the mentioned functionalities including matrix manipulations, plotting of functions and implementation of algorithms.

The data used for analysis was collected between May 2013 to November 2013. The data consists of online furnace measurements during the mentioned period and the variables utilized in the analysis include the following:

- Gas exit temperature from hearth 1
- Gas temperatures in hearths 2, 3, 5, 7 and 8.
- Temperatures of four burners located in each of hearths 4 and 6.
- Kaolin feed rate
- Combustion gas flows to each of the four burners in hearths 4 and 6.
- Combustion air flows to each of the four burners in hearths 4 and 6.
- Walls temperature in hearths 5 and 8

7.2 Data Preprocessing

The data collected from the plant is incomplete (lacking certain attribute values), noisy (i.e. contained errors and outliers) and also inconsistent (i.e. contained discrepancies). Hence, data processing techniques were applied to improve the quality of the data to

enhance the accuracy and efficiency of the data analysis by following the four steps below:

Data Visualization: Data Visualization is the first step carried out to assess the quality of the process data, which is required to select appropriate data pre-processing techniques. In particular, it is important to determine the data relevant for the analysis which is typically achieved by excluding the periods of downtime, containing major disturbances and faulty process operations.

As an example, Figures 7.1 visualizes the kaolin feedrate to the calciner between May and June, 2013. From the plots, it can be seen that the most prominent feed rates during the period observed are 95, 100, 105, 110, 120 kg/min.

Lower feed rates often relate to some abnormal process operations. As an example, in august 2013 the feed rate was down to 85 kg/min as shown in Figure 7.2 due to a problem in the rotary valve. In addition, plant shutdown due to the kiln bottom bearing problem is observed in some months. Both problems are indicated with the red marker on the Figure 7.2 plot. Furthermore, some periods of missing data are clearly recognized in the plots.

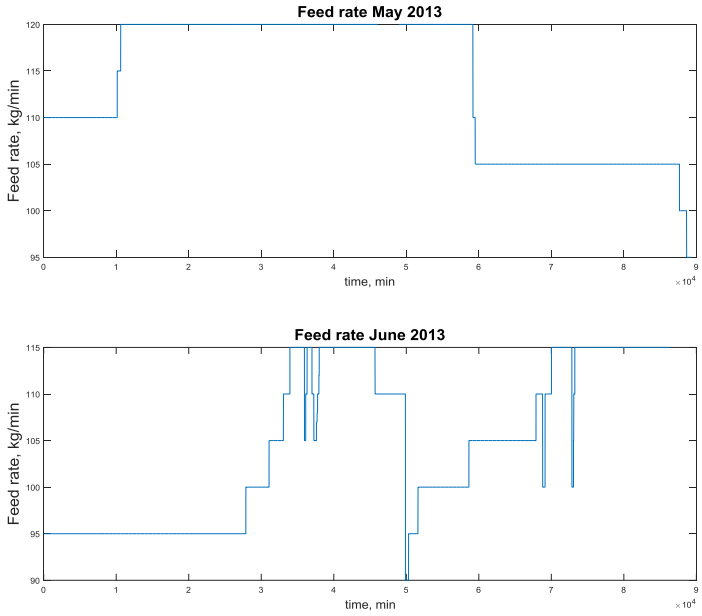

Figure 7.1: Visualizing the Feed to the Calciner (May and June)

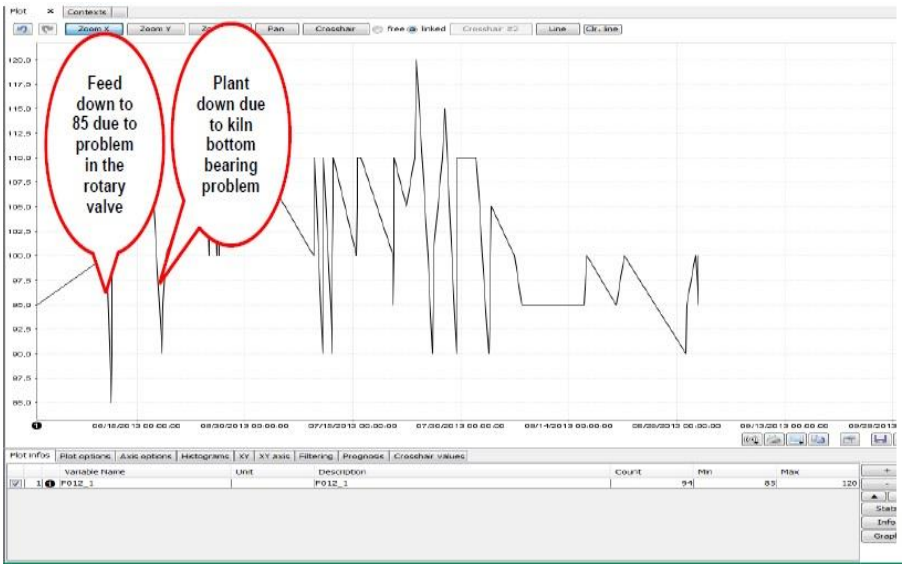

Figure 7.2: Visualizing the effect of rotary valve problem and plant shutdown on the feed rate

In order to determine the periods of furnace downtime, Figure 7.3 examines the temperature of the second burner in hearth 4 during June, 2013. A period of downtime, in which the temperatures in Hearth 4 is much lower compared to the normal operation range, is clearly visible and circled in red. Similarly, other downtime periods can be located and excluded from further analysis.

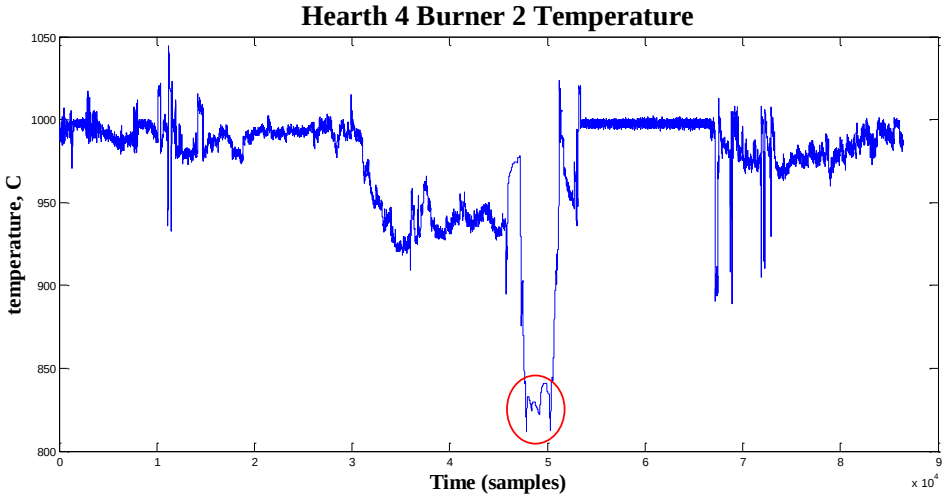

Figure 7.3: Visualizing effect of low fire period on the Hearth temperature

The temperature around four burners located in Hearth 6 is presented in Figure 7.4. It can be concluded that the temperature in Hearth 6 is controlled much more tightly. Some spikes and outliers, not related to the plant downtime, are visible in the figure.

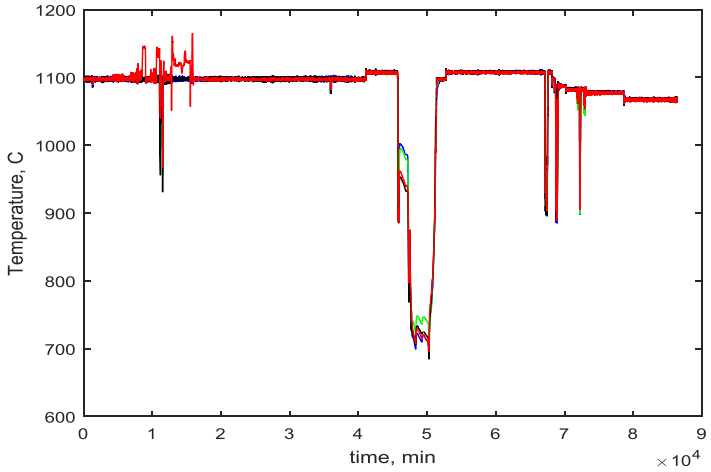

Figure 7.4: Temperature of four burners in hearth 6

Selection of relevant datasets: after excluding periods of shutdown, disturbances and equipment malfunctions, relevant datasets were selected based on the operation regimes.

Scaling: Process data is usually scaled to obtain equal magnitude (or weight) for signals having different scales or units. The purpose is for the data to have zero mean and unit variance as shown in equation 36.

$$\overline{x_i} = \frac{x_i - \mu_x}{\sigma_x} \qquad (36)$$

Data scaling is particularly required for PCA algorithm.

Filtering: Filtering is necessary to suppress undesirable frequency ranges from a signal. To achieve this, the 'filter' function was used in the MATLAB environment as shown in equation (37), where vector X is the signal to be filtered and the filter is

described by numerator coefficient vector b and the denominator coefficient vector a. Y is a vector of the filtered data.

$$Y = filter(b, a, X) \qquad (37)$$

Figures 7.5 and 7.6 contain the outcomes of the filtering procedure for the gas flows and Hearth 4 temperature respectively.

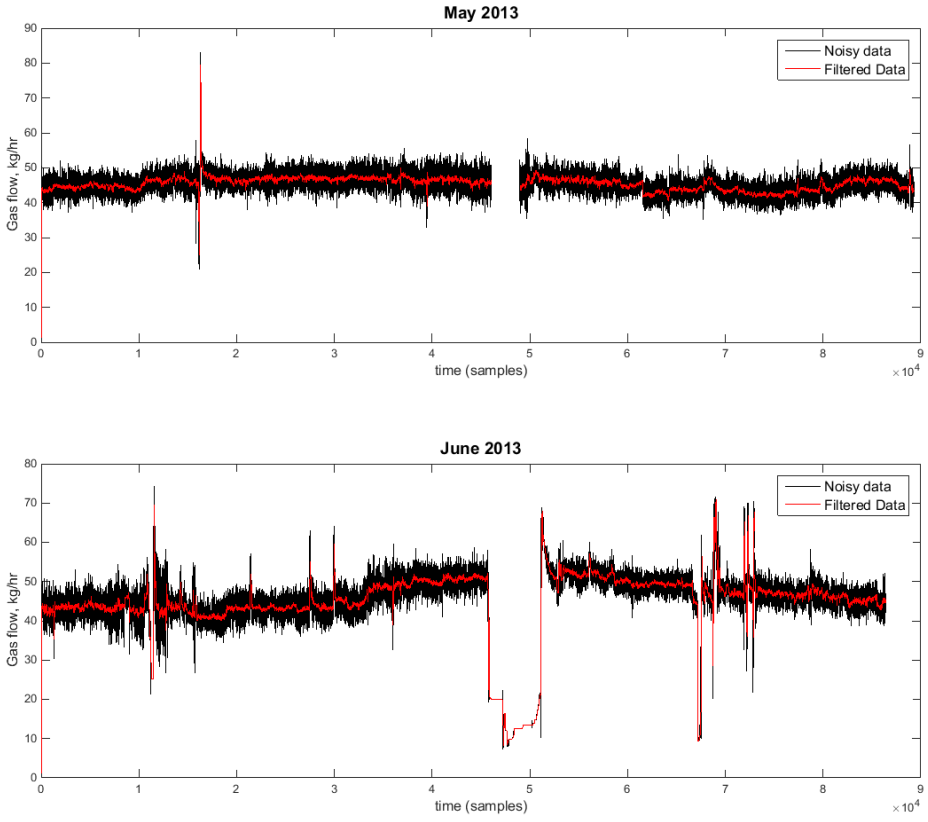

Figure 7.5: Filtered Gas flows in hearth 6

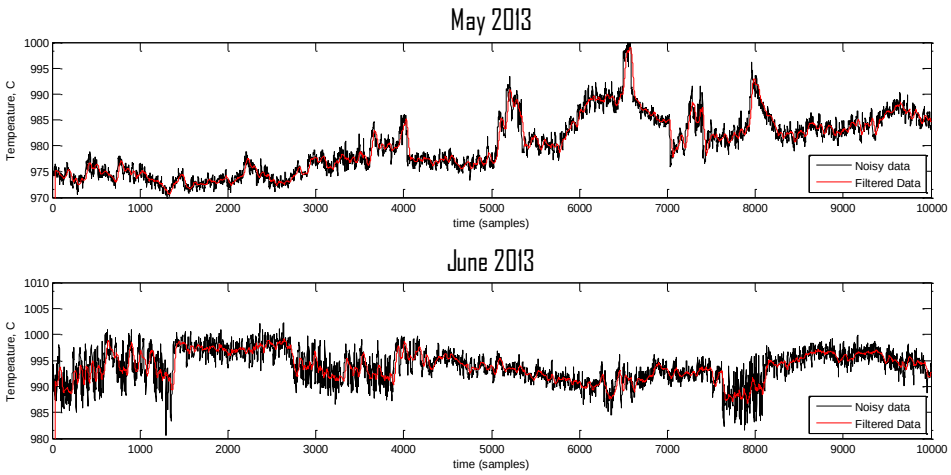

Figure 7.6: Filtered Gas temperature in hearth 4

7.3 Determination of static models using PCA

In this section, static PCA models are developed for the gas temperature profiles in the furnace at different feed rates. This method reduces the dimensionality of the gas temperature measured in the eight hearths by selecting the right number of principal components. Thereafter the PCA scores are predicted using the least squares regression method. In addition, the generalized PCA method is employed to cater for the non-linearity present in the system.

The model inputs are clearly stated and results are presented to compare and show the outcomes of the models. Generally, changing the model inputs based on process knowledge was tried to improve the performance of the obtained models.

7.3.1 Analysis of gas temperature profiles using PCA

Firstly, the data is scaled according to equation (36), then PCA is applied to the gas temperature measurements of hearths 1 to 8 with the aim of forming a number of new variables to describe the variation of the data by using linear combinations of the gas temperatures in the eight hearths. The captured variance from the PCA implementation

on the Temperature profiles in the eight hearths for specific feed rates are presented in Figure 7.7.

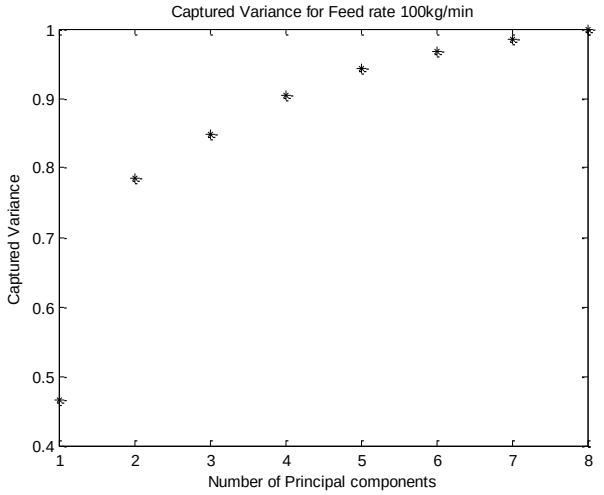

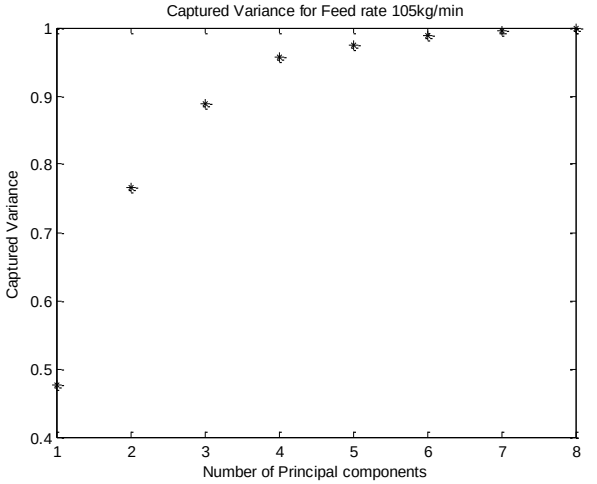

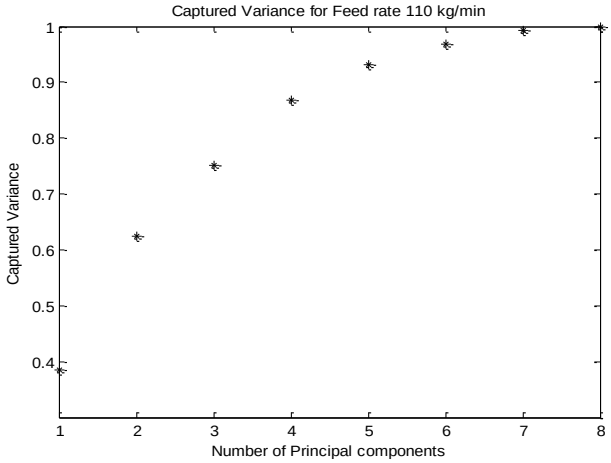

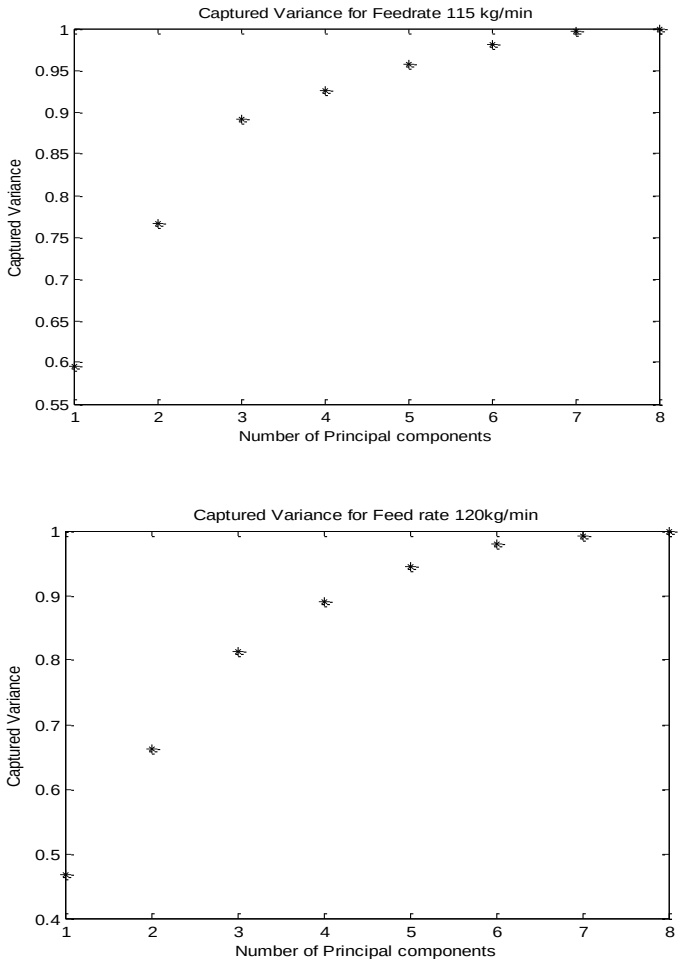

Figure 7.7: Captured variance by the PCA for different models (100, 105, 110, 115, 120 kg/min)

For each of the specified kaolin feedrates, the number of principal components required to capture 90% of the variation in the temperature profile ranges from three to four. Hence, the PCA models with three principal components have been selected for further analysis. Thus, the three scores corresponding to the principal components describing the most variation in the data represent the compressed version of the temperature profile. In other words, the full gas temperature profile in all eight hearths can be approximately calculated from these three scores.

7.3.2 Applying regression to predict PCA scores

Next, the least-squares regression is applied to predict the PCA scores, representing the compressed version of the temperature profile. The scores are predicted independently by using the gas flows into hearths 4 and 6 as the model inputs. The results for the feed rate of 120 kg/min are presented in Figures 7.8, whereas the results for other feedrates can be found in Appendix 1. Based on the observed results, the conclusion is made that the gas temperature profile in the furnace cannot be predicted based on the combustion gas federate alone.

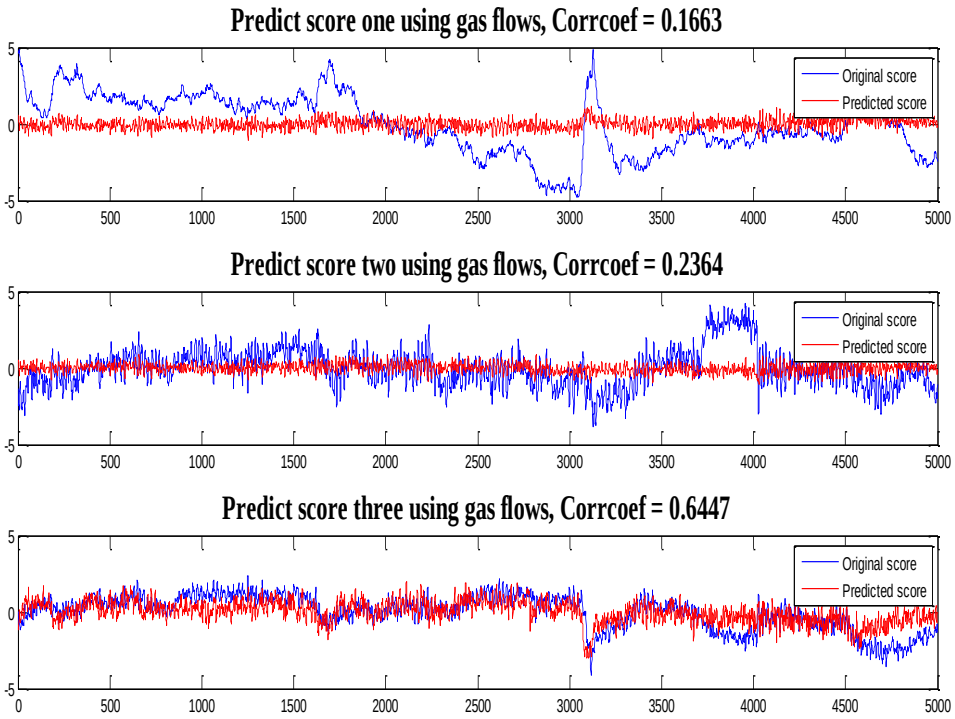

Figure 7.8: Prediction of PCA scores using Gas flows for Feed rate 120 kg/min

As the consumption of the combustion gas is not enough to predict the temperature profile in the furnace, the model inputs were enriched by additional process variables that might represent the process phenomena having effect on the gas phase temperature in the furnace. In particular, it was decided to add the measured furnace walls temperature to the model, as it is known that there is significant heat transfer between the gases in the

furnace and its walls. The walls temperature measurements in hearths 5 and 8 together are added to the model to improve the prediction accuracy. The results are presented in Figure 7.9 for feed rate 120 kg/min, whereas similar results for other feedrates are provided in Appendix 2. It can be concluded, that the temperature profile cannot be satisfactorily predicted using the walls temperature, even though the model accuracy has improved compared to the models utilizing the combustion gas flowrate as the only input.

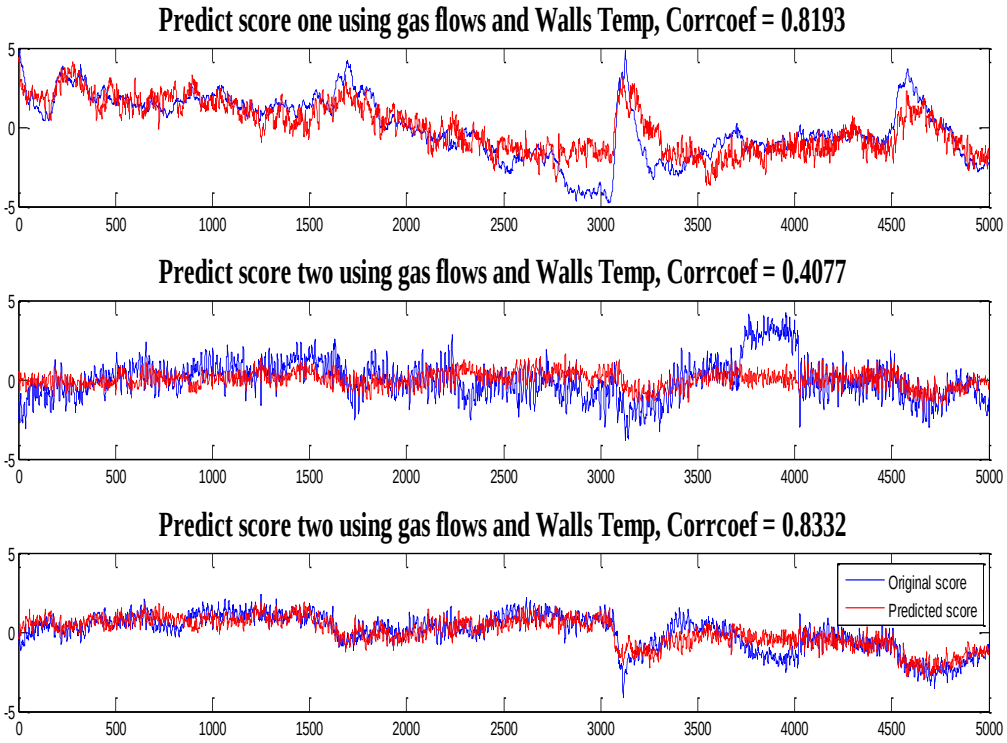

Figure 7.9: Prediction of PCA scores using Gas flows and Walls Temperature for Feed rate 120 kg/min

7.3.3 Analysis of Gas Temperature profiles using Generalized PCA and score prediction

To improve the quality of the results by taking into account the process nonlinearity, the Generalized PCA (GPCA) method was employed. According to this method, new variables, known as calculated variables, are created by applying specified functions to

the process data. The calculated variables are designed based on the process knowledge aiming to represent some valuable information able to describe important process phenomena. Next, the process data is augmented by the calculated variables before applying the PCA technique.

Using process knowledge, the following three variables are formed

- The squared gas flow to Hearth 4
- The squared gas flow to Hearth 6
- The ratio of hearth 4 gas flow to hearth 6 gas flow

In particular, the first two calculated variables are suggested to describe the nonlinear effect of the combustion gas flows on the temperature profile. The last variable aims to represent the effect of the combustion gas distribution between the hearths.

Thereafter, the PCA was applied to the data extended using the calculated variables, and the principal component scores were predicted using the Gas flows to hearths 4 and 6 together with the walls temperature. The result for feed rate 120 kg/min is presented in Figures 7.10, other results can be found in Appendix 3.

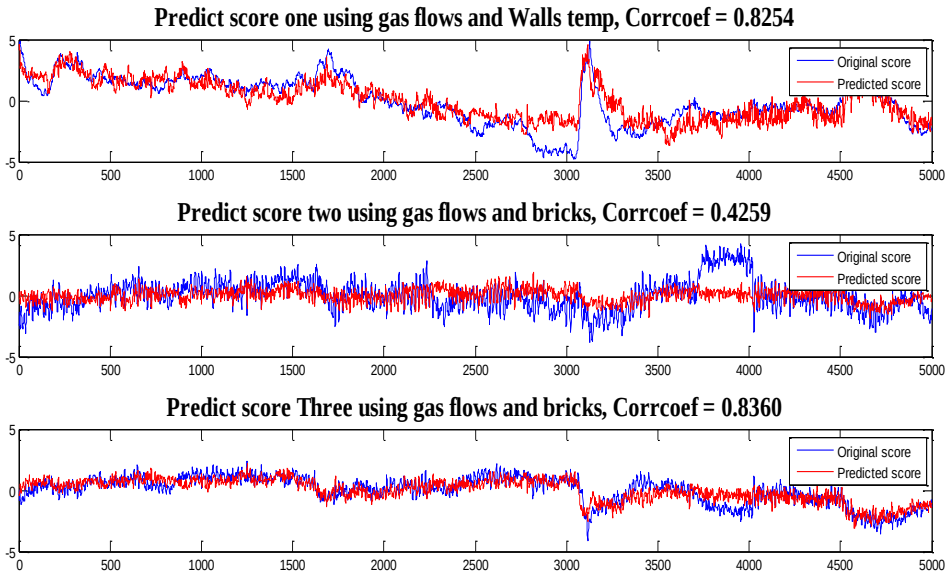

Figure 7.10: Prediction of GPCA scores using Gas flows and Walls Temperature for Feed rate 120 kg/min

7.3.4 Comparison of the obtained models

In order to compare the gas temperature profile models constructed in the previous subsections, the correlation coefficients between the scores obtained from the PCA analysis and the scores predicted by the regression models were computed for the training data and the results are summarized in Table 7.1. The table confirms the conclusions presented previously. Firstly, the combustion gas flowrates alone cannot be used to predict the gas temperature in the furnace. Secondly, even though considering the walls temperature helps to improve the modeling accuracy, satisfactory results are still not obtained. Thirdly, the GPCA method improved the quality of the model greatly as noticed by the increase in the correlation coefficient between the original and predicted scores. The validity of the GPCA model was examined on validation data that was not utilized in training the model, and the result for the feed rate of 120 kg/min are presented in Figure 7.11. For each of the scores, the correlation coefficient between the values obtained by the PCA method and the regression prediction stays above 80%.

Table 7.1: Comparison of the model quality for different Static PCA models

Models	**Ordinary PCA (Score Prediction with Gas flows)**	**Ordinary PCA (Score Prediction with Gas flows and Walls temperature)**	**Generalized PCA (Score Prediction with Gas flows and Walls temperature)**
100 kg/min	0.3125 0.1136 0.0191	0.4815 0.8895 0.6980	0.7918 0.6162 0.5155
105 kg/min	0.3393 0.2422 0.5629	0.9688 0.8221 0.6180	0.9691 0.8311 0.6204

110 kg/min	0.2584	0.7659	0.7665
	0.3421	0.5436	0.6282
	0.4422	0.5523	0.5533
115 kg/min	0.5886	0.9205	0.9240
	0.2261	0.7134	0.7503
	0.4910	0.6895	0.6900
120 kg/min	0.1663	0.8193	0.8252
	0.2364	0.4077	0.4259
	0.6447	0.8332	0.8360

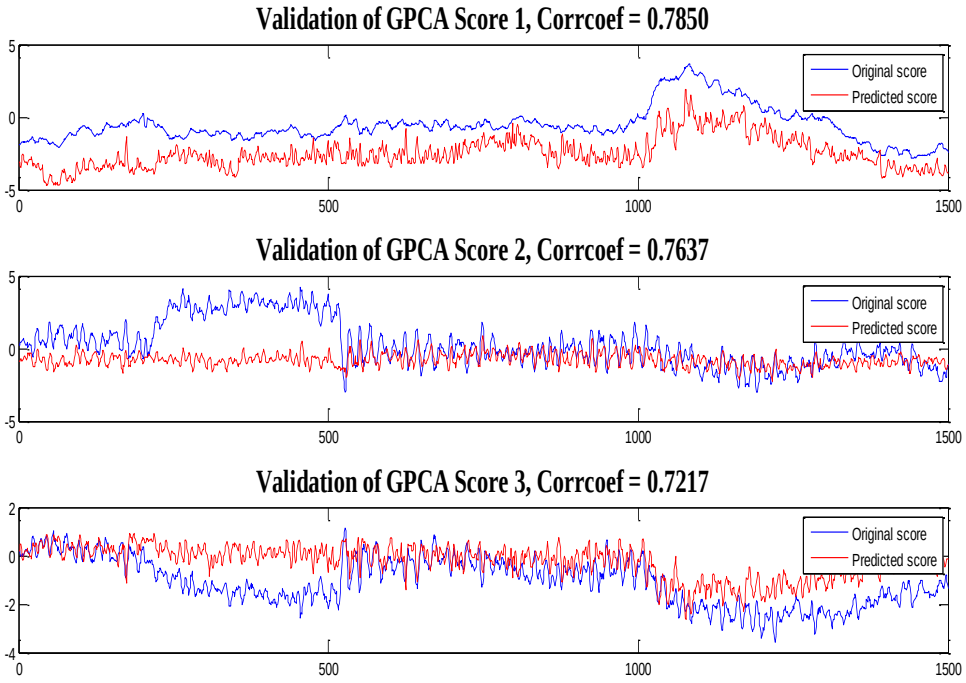

Figure 7.11: Validation of GPCA scores prediction

In conclusion, the PCA analysis shows that it is possible to select principal components according to the highest variation in the original data set, and in this particular case it is shown that there are a few variables describing the whole temperature profile in the furnace. In particular, the Generalized PCA model was able to represent the modeled

system better and for a wider operating region, which confirms the nonlinear character of the dependences between the process variables. In general, it can be concluded that the static modeling of the gas temperature profile fails to achieve accurate prediction. This can be explained by the effect of the past gas temperature on the unmeasured solid phase temperature in the furnace, which in turn effects the future gas temperature profile.

7.4 Predicting the temperature profile in the Furnace using Partial Least Squares method

This sections aims to improve the accuracy of the models presented in the previous section, which is achieved by constructing dynamic models of the temperature profile in addition to the static ones. The models are developed using the Partial Least Squares (PLS) regression method presented in the next section.

Denote T to be the gas temperature profile of hearths 1 to 8. Starting from the simple PLS model considering the combustion gas flows to hearths 4 and 6 alone, the model inputs are extended based on the process knowledge aiming to improve the model accuracy. Thus, the simple model is improved by adding walls temperature to the inputs.

Next, a dynamic model is created by including the past gas temperature profile as the delayed temperature values affect the unmeasured solid temperature in the furnace, which in turn affects the current gas temperatures. Lastly, it was observed that the burners located in the same hearth affect the temperature measurement in this hearth slightly differently, which probably happens because the burners are not arranged in a symmetrical way. Therefore, the gas flows to each burner are considered as separate model inputs, instead of aggregating them to a single input value. Details of the constructed models and the results are presented in the following subsections.

7.4.1 Prediction of gas temperature profiles using methane gas flows

The models include just the combustion gas flows to hearths 4 and 6 as the inputs were constructed for each of the feed rates. Some examples of the temperature prediction for the federate of 120 kg/min are provided in Figure 7.12 for hearths 4 and 6, whereas the

results for other feedrates are given in Appendix 4. It can be observed from the figures and the correlation coefficients that the model doesn't fit well to the data. The conclusions coincide with the ones made in Section 7.3.2 using the PCA method.

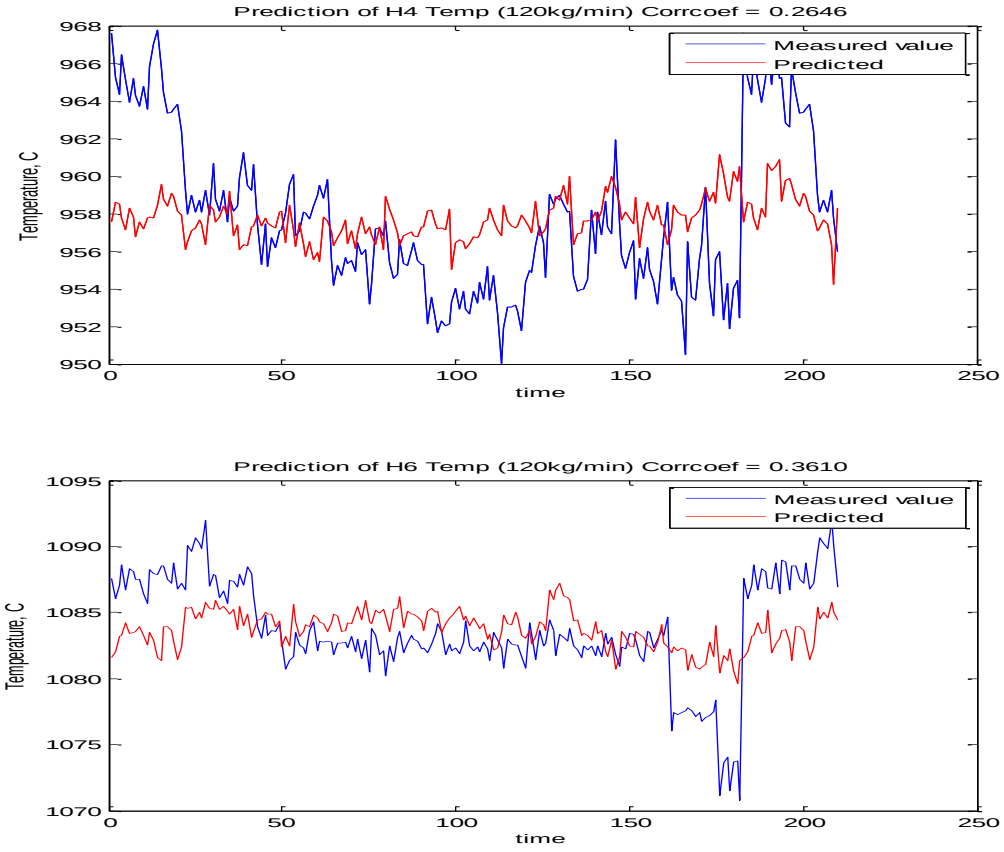

Figure 7.12: Prediction of Gas Temperature profiles in Hearths 4 and 6 for Feed rate 120kg/min using methane gas flows

7.4.2 Prediction of Gas temperature profiles using Methane gas flows and Furnace Walls temperature

Gas temperature profiles is predicted using the combustion gas flows to hearths 4 and 6 together with the walls temperature as the inputs to improve the quality of the static model presented in the previous subsection. Some examples of the temperature prediction for the federate of 120 kg/min are provided in Figure 7.13 for hearths 4 and 6, whereas the

results for other feedrates are given in Appendix 5. It can be noticed that the addition of walls temperature to the model improved the prediction quality.

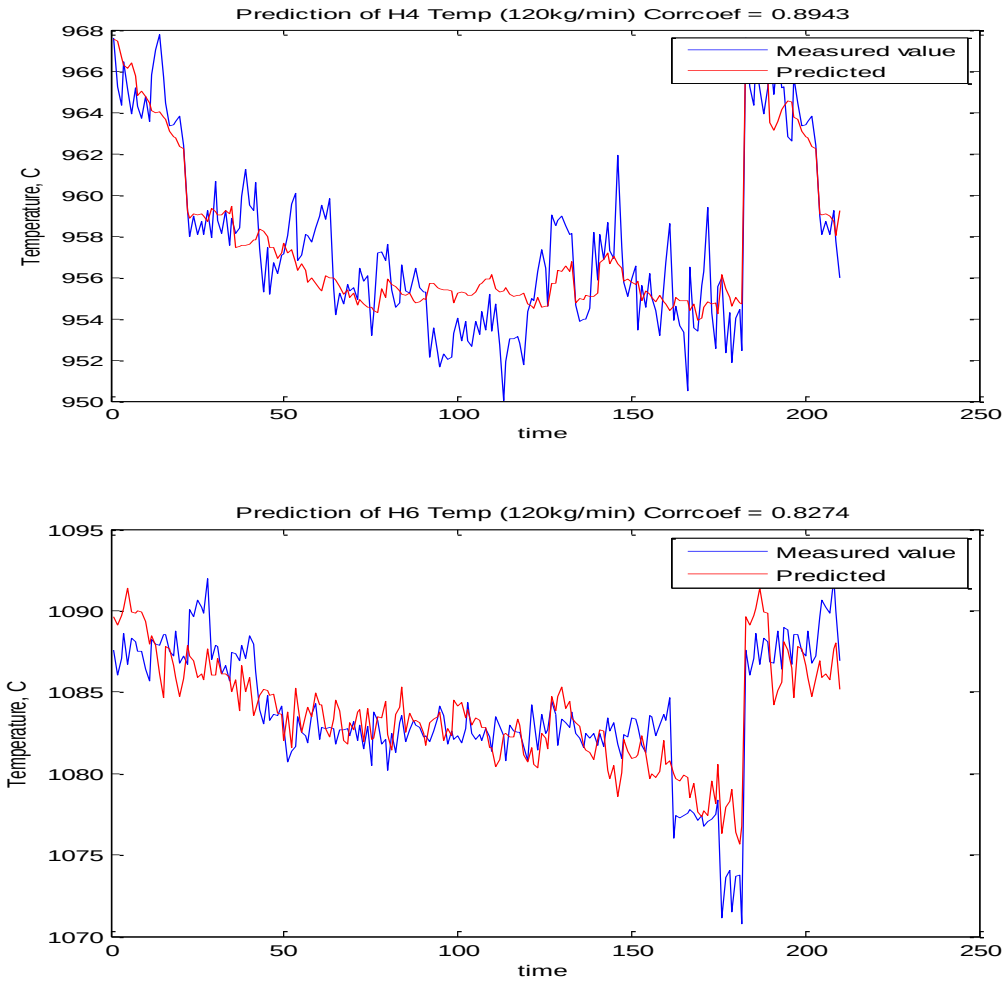

Figure 7.13: Prediction of Gas Temperature profiles in Hearths 4 and 6 for Feed rate 120kg/min using Gas flows and Walls Temperature

7.4.3 Prediction of Gas temperature profiles using Methane gas flows, Furnace Walls temperature and the delayed gas temperatures

In this section, dynamic models are formulated by adding the delayed gas temperatures in the hearths as additional model inputs. Some examples of the temperature prediction for the feedrate of 120 kg/min are provided in Figure 7.14 for hearths 4 and 6, whereas the results for other feedrates are given in Appendix 6. Adding the delayed gas

temperatures improved the model quality considerably as observed with the correlation coefficients obtained. This confirms the assertion that dynamic models can be useful to obtain a better model quality.

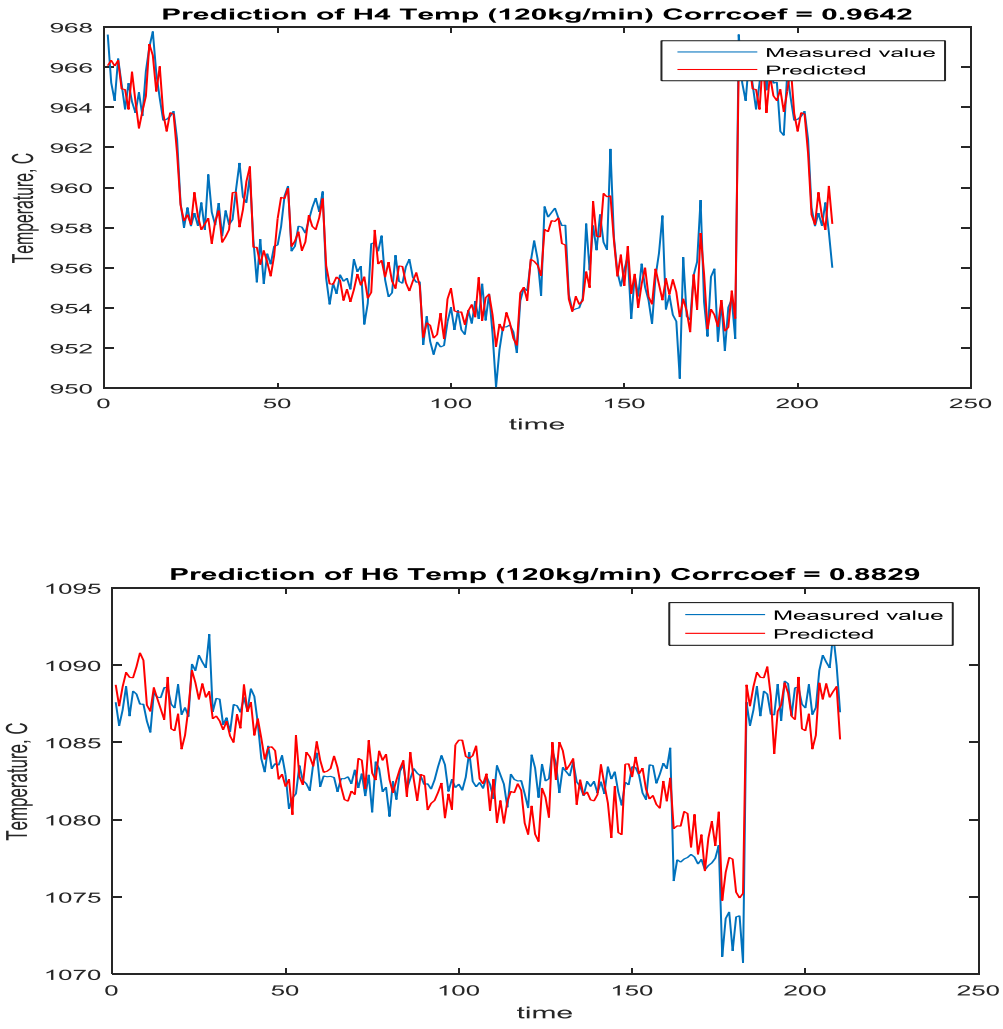

Figure 7.14: Prediction of Gas Temperature profiles in Hearths 4 and 6 for Feed rate 120kg/min using Gas flows, Walls Temperature and delayed gas Temperatures

7.4.4 Prediction of Gas temperature profiles using the ratios of Methane gas flows to each burner, Furnace Walls temperature and the delayed gas temperatures

Lastly, to further improve the quality of the dynamic model, the gas flows to the burners were considered separately in the model and the temperature prediction for hearths 4 and 6 for the feed rate of 120 kg/min is presented in Figure 7.15. Results for other feed rates and hearths are shown in Appendix 7. Compared to the dynamic model presented in Section 7.4.3, the prediction quality is slightly improved by considering gas flows to each burner as separate entities in the model.

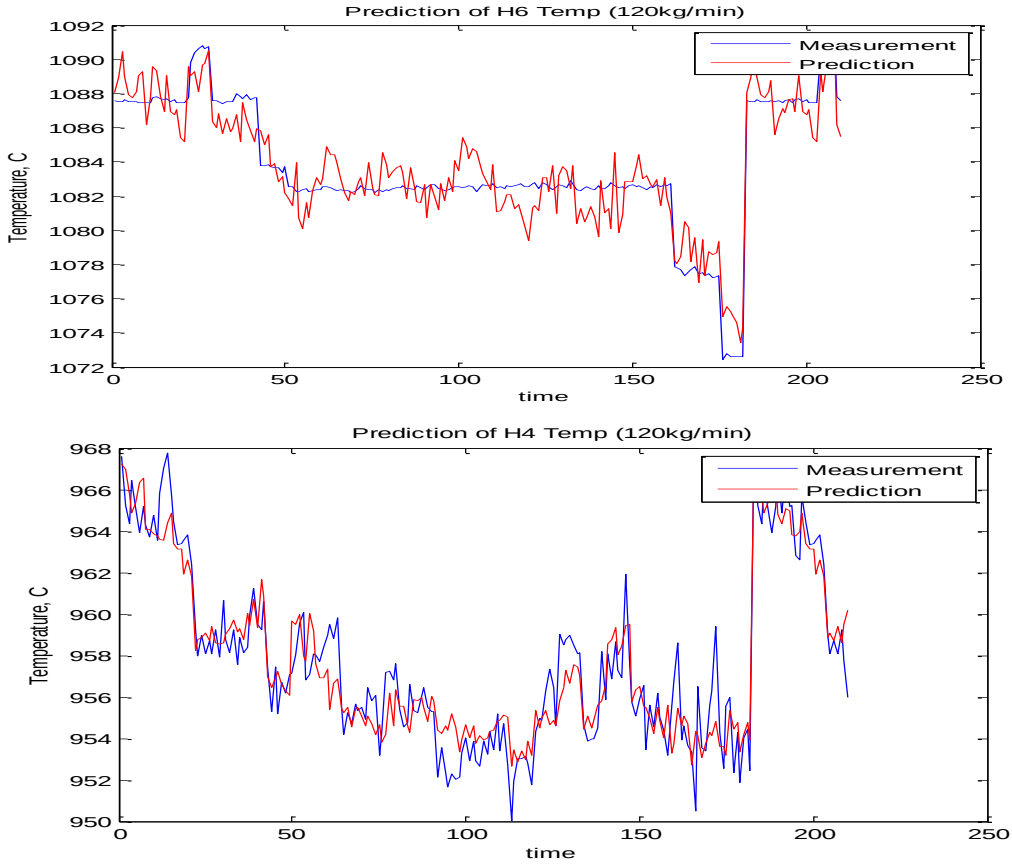

Figure 7.15: Prediction of Gas Temperature profiles in Hearths 4 and 6 for Feed rate 120 kg/min using individual burner gas flows, Walls Temperature and delayed gas Temperature

7.4.5 Comparison of the models

Table 7.2 contains the correlation coefficients for the measured and the predicted gas temperatures for the static and dynamic models constructed in previous sections. The accuracy of the dynamic model is much higher compared to the static ones, which can be observed by an increased correlation values, thus confirming the suitability of dynamic models to represent the effect of past gas temperature on the current furnace state.

Table 7.2: Comparison of the model quality for static and dynamic PLS models

Models	Hearths	Static model (Gas flows)	Static model (Gas + Walls Temp)	Dynamic model (Gas flows + Walls Temp + delayed gas temp)	Dynamic model (Individual burner gas flows + Walls Temp + delayed gas Temp)
100 kg/min	1	0.6990	0.8300	0.9823	0.9903
	2	0.1620	0.6219	0.8431	0.8921
	3	0.5815	0.7305	0.9572	0.9633
	4	0.4360	0.7507	0.8633	0.8808
	5	0.4770	0.7025	0.8687	0.9300
	6	0.5543	0.6285	0.9042	0.8952
	7	0.5636	0.6859	0.9195	0.9264
	8	0.4219	0.7357	0.9239	0.9380
105 kg/min	1	0.7676	0.8955	0.9769	0.9894
	2	0.6569	0.8373	0.9076	0.9473
	3	0.6751	0.9067	0.9895	0.9911
	4	0.7930	0.9539	0.9846	0.9878
	5	0.1999	0.8486	0.9774	0.9801
	6	0.6739	0.9232	0.9696	0.9818

	7	0.2383	0.6723	0.7846	0.8000
	8	0.8829	0.9498	0.9602	0.9643
110	1	0.3028	0.7754	0.9604	0.9687
kg/min	2	0.3254	0.5682	0.6787	0.6820
	3	0.3705	0.7413	0.9309	0.9521
	4	0.4391	0.8877	0.7906	0.8791
	5	0.3609	0.7605	0.8804	0.9130
	6	0.5480	0.7995	0.9472	0.9177
	7	0.1006	0.5768	0.8289	0.8468
	8	0.3248	0.5272	0.8484	0.8663
115	1	0.8863	0.9538	0.9950	0.9945
kg/min	2	0.6847	0.7768	0.9157	0.9289
	3	0.8474	0.9096	0.9821	0.9951
	4	0.8262	0.8606	0.9751	0.9804
	5	0.8893	0.9478	0.9915	0.9930
	6	0.9359	0.9891	0.9950	0.9962
	7	0.1997	0.2578	0.8519	0.8655
	8	0.8151	0.8670	0.9762	0.9825
120	1	0.2014	0.5373	0.7769	0.8027
kg/min	2	0.2228	0.7483	0.7853	0.8157
	3	0.1136	0.5580	0.7552	0.7903
	4	0.2646	0.8943	0.9131	0.9340
	5	0.5683	0.6821	0.7948	0.8521
	6	0.3610	0.8274	0.8880	0.9294
	7	0.2914	0.6143	0.7525	0.7853
	8	0.4156	0.7848	0.8675	0.8960

7.4.6 Model Validation

The models were validated by using three-quarters of data for training and the rest for the validation and the validation results for some of the models are presented in Figures 7.16 to 7.19 for hearths 4 and 8. The model predicted the validation data considerably has shown in the values of correlation coefficient obtained.

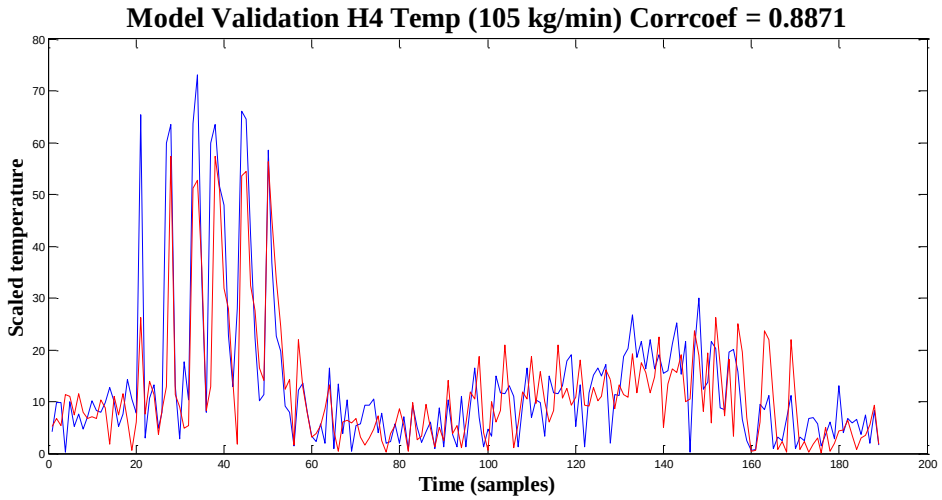

Figure 7.16: Model Validation H4 Temp for Feed rate 105kg/min

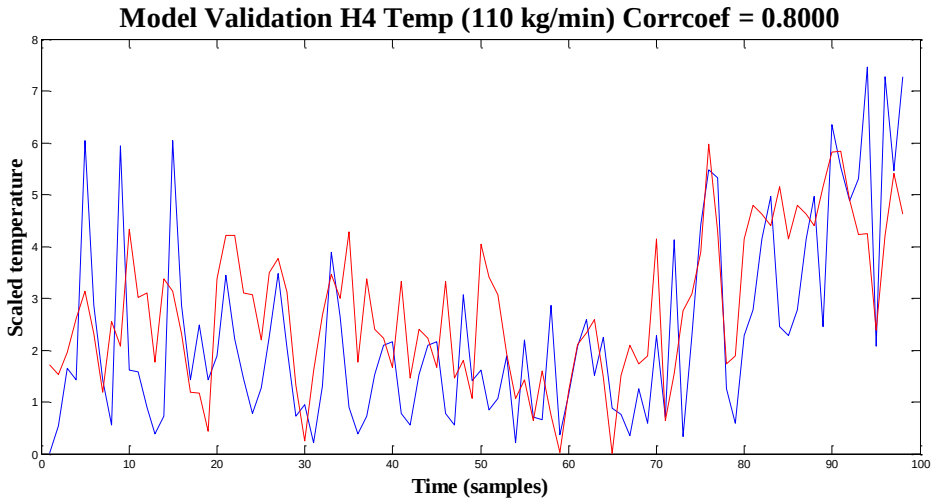

Figure 7.17: Model Validation H4 Temp for Feed rate 110kg/min

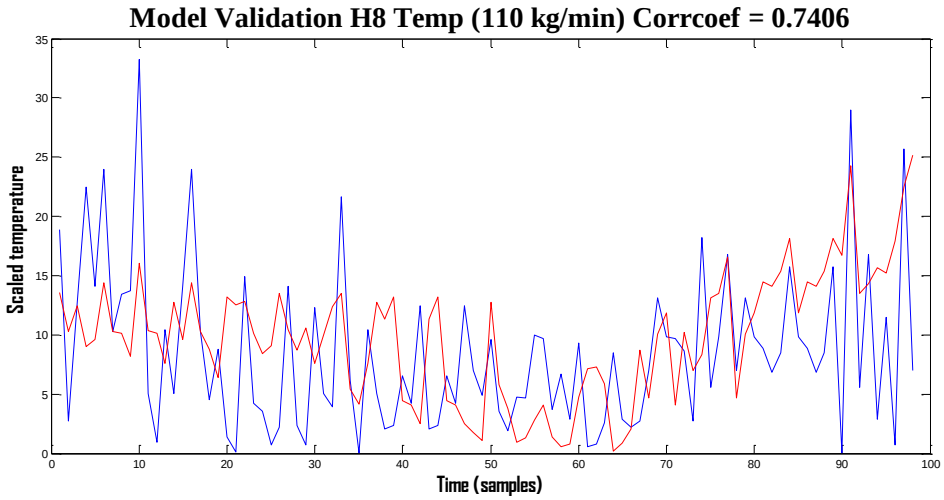

Figure 7.18: Model Validation H8 Temp for Feed rate 110kg/min

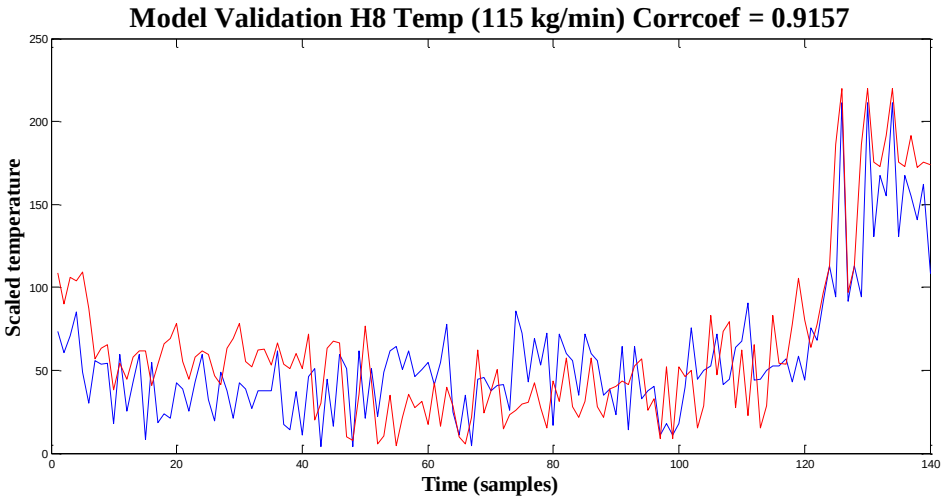

Figure 7.19: Model Validation H8 Temp for Feed rate 115kg/min

In addition, 20 steps ahead (10 min) prediction of the temperature profile has been computed to evaluate the ability of the model to predict the furnace dynamics. The results are presented in the following Figure 7.20-7.23 for the feedrates of 100 kg/min and 110 kg/min, where the solid line represents the dynamics of the gas temperature and the red dotted line denotes the prediction made based on the first 100 samples available. Thus, the figures confirm the ability of the dynamic model to predict the furnace behavior.

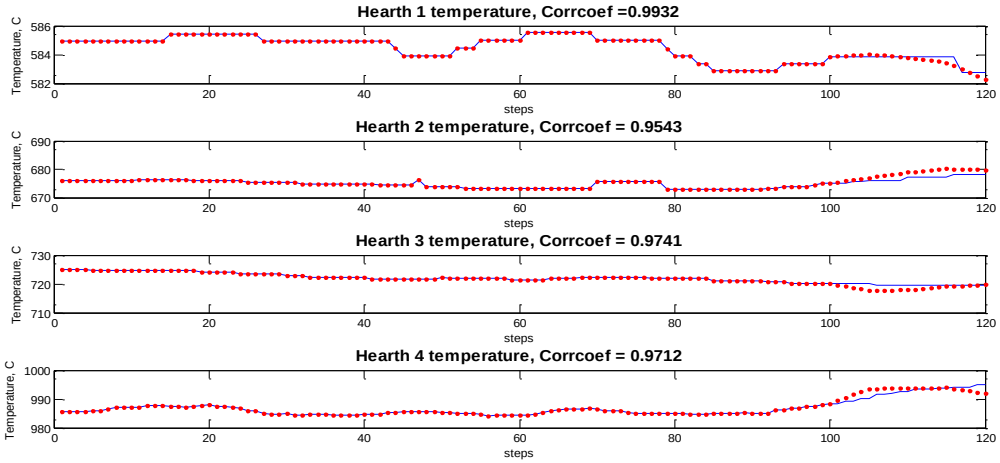

Figure 7.20: 20 steps ahead prediction of Temperatures in H1-H4 for feed rate 100kg/min

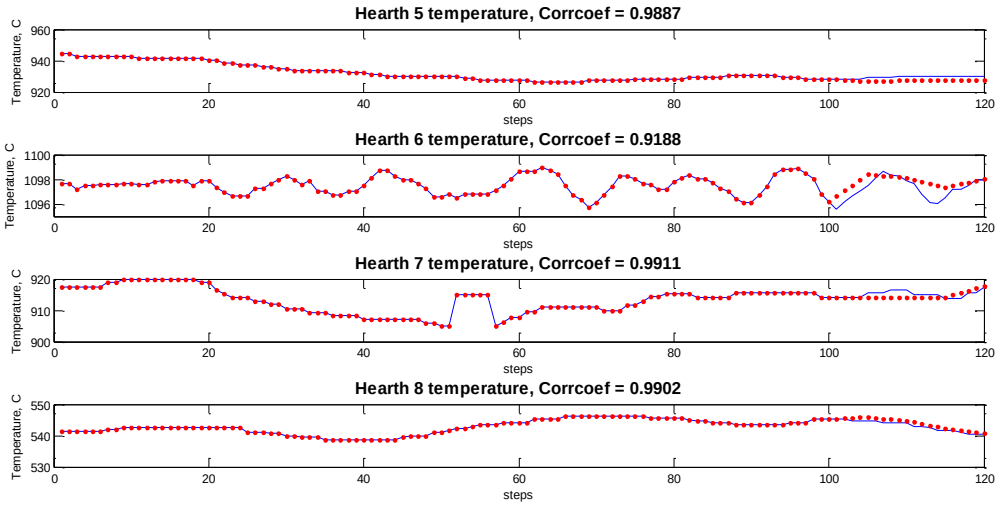

Figure 7.21: 20 steps ahead prediction of Temperatures in H5-H8 for feed rate 100kg/min

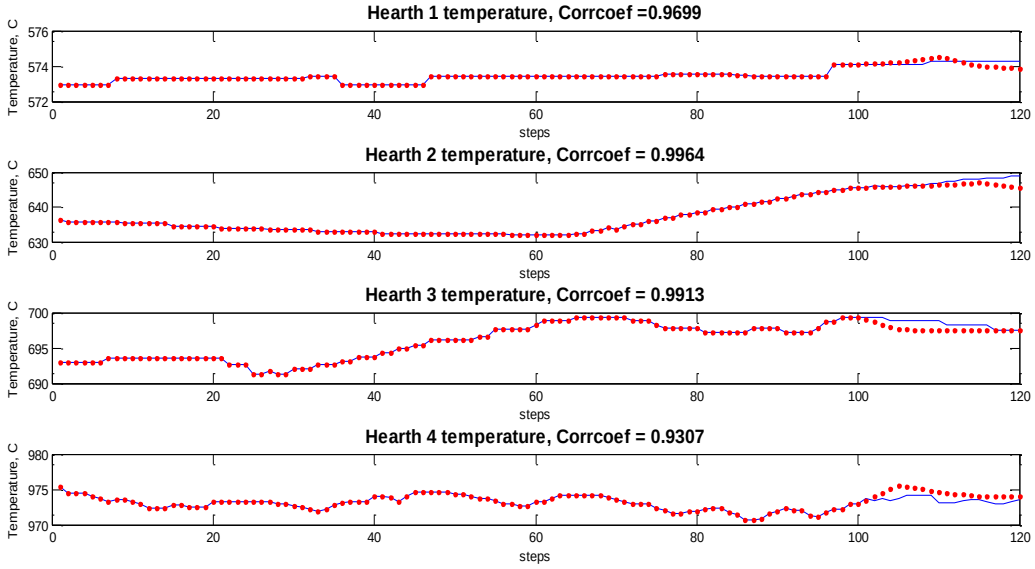

Figure 7.22: 20 steps ahead prediction of Temperatures in H1-H4 for feed rate 110kg/min

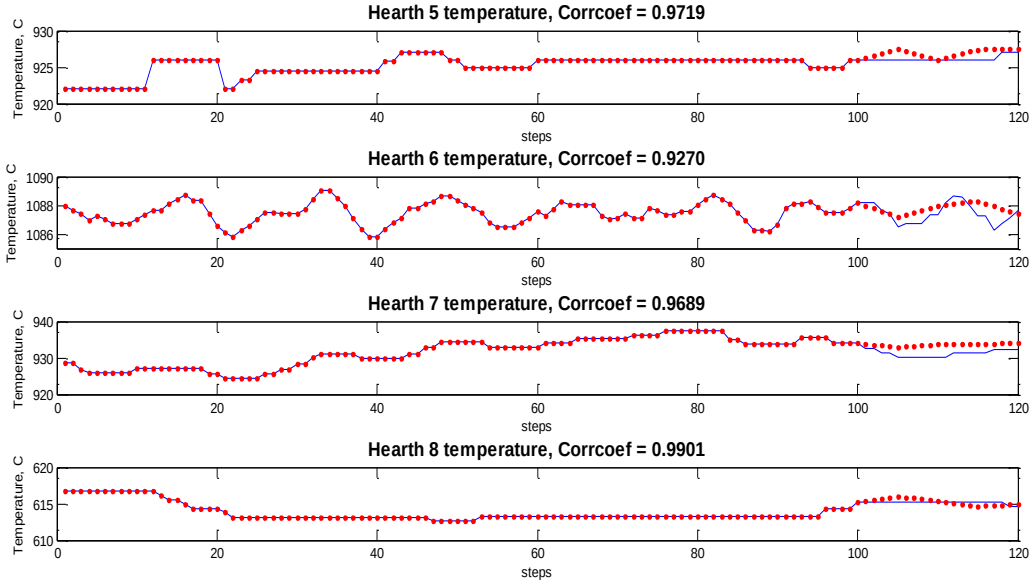

Figure 7.23: 20 steps ahead prediction of Temperatures in H5-H8 for feed rate 110kg/min

7.5 Utilization of the developed dynamic models for process control and optimization

As the calciner is the main energy consumer in the kaolin processing chain, the optimization of its operations should focus on minimizing the fuel gas flowrate in the process. However, the gas temperature profile in the furnace has to be maintained at the level high enough to ensure that the kaolin is completely converted to the spinel phase and the main quality requirements, such as brightness, are met. Therefore, the dependence of the temperature in the furnace on the fuel gas consumption has to be known in order to determine the optimal gas flowrates to Hearths 4 and 6 resulting in the required gas temperature in the furnace. Thus, the developed model can be utilized for the described optimization.

Regarding the gas temperature control in Hearths 4 and 6, it is possible to see a strong coupling between the four temperature measurements in each Hearth, which makes the control a nontrivial task. As an example, four gas temperature measurements and the normalized fuel gas flow to Hearth 6 are presented in Figure 7.24, demonstrating that the precise control of the temperature causes significant variations in the fuel gas flow rate. Thus, a model based control could be developed to reduce the variations in the fuel gas flowrate in the Hearths. The ability of the developed model to predict the gas temperature profile is demonstrated in Section 7.4.6. In addition, the prediction of the model for the mean temperature measured in Hearth 4 is shown in Figure 7.25, for a period when some of the temperature measurements are uncontrolled.

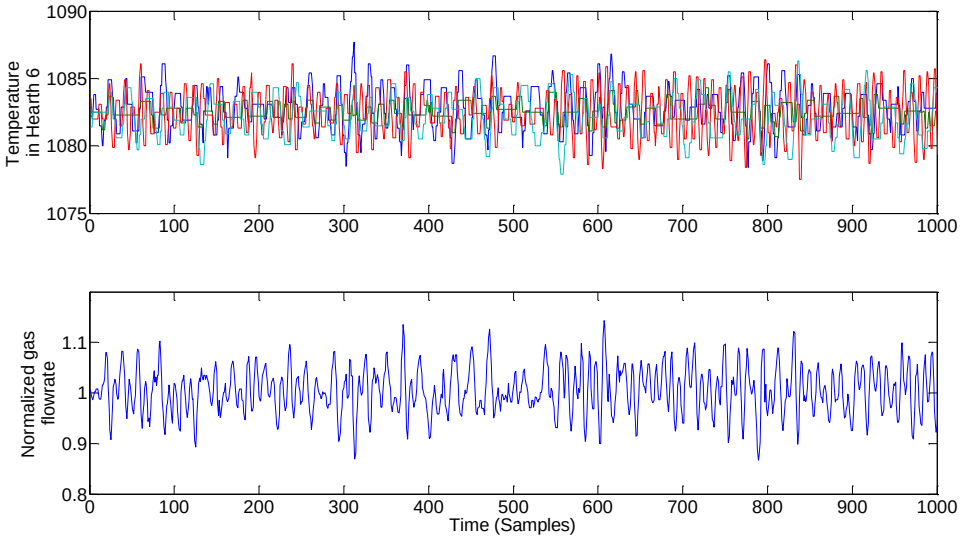

Figure 7.24: An example of the Temperature and the fuel gas flow in Hearth 6

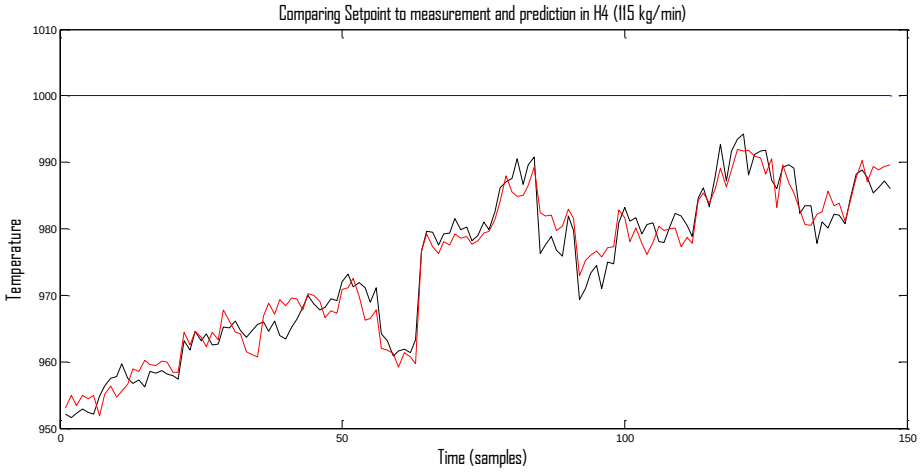

Figure 7.25: The mean temperature in Hearth 4 (black), the estimated temperature (red) and the setpoint for the controlled temperature measurements (blue)

8. Conclusion

The aim of this thesis is to develop data-based models to forecast the gas temperature profile in a multiple hearth furnace used for kaolin calcination. In the Literature section, the structure and formation of kaolin was investigated and presented, including the chemistry of kaolin. Next, the kaolin preprocessing chain was described followed by the study of the Calcination reactions, process description of the calciner and the effects of heating rate, particle size and impurities on the calcination process. This part was concluded with a study of the different process monitoring methods that can be employed to increase process understanding, detect fault early enough and predict quality of products. The methods were classified appropriately, their general operation scheme presented, and lastly, some case studies were presented on the applications of process monitoring in mineral processing.

Afterwards, the data-based models which is the main purpose of the experimental part were developed. Initially, the data was preprocessed to improve the quality and remove inconsistencies. Static PCA models were developed to analyze the gas temperature profiles in the hearths. Three Principal Component scores were selected for each model and regression was applied to predict these scores, firstly by using only methane gas flows and then by using both gas flows and walls temperature as model inputs. The accuracy of both models is considered as unsatisfactory, even though adding the walls temperature improves the model performance. In addition, the Generalized PCA method (a non-linear method) was used by introducing calculated variables to the original data matrix to form an augmented data set. Then PCA was carried out on the new data matrix with three PCA scores capturing a large portion of data. The scores were predicted using regression by the methane gas flows and walls temperature and the models performed better than the initial PCA model. In general, it was concluded that the PCA model is able to describe the whole temperature profile in the furnace with three principal components. In addition, the static modeling approach failed to achieve good model performance. This can be explained by the effect of the past gas temperature on the unmeasured solid phase temperature in the furnace, which in turn effects the future gas temperature profile.

PLS was used to model the temperature profiles in all eight hearths by using different model inputs based on the chemical engineering knowledge of the process. Two static

models and two dynamic models were constructed based on different model inputs, starting from using only the methane gas and progressively adding walls temperature, delayed gas temperature and the ratio of gas flow to each burner. The model quality improved with each progression and the quality of the final dynamic model was good when compared with the measured data.

All models were validated using a portion of data not used for training and a comprehensive result is presented in the appendix. As the gas temperature profile is one of the key process variables to monitor and control in the furnace, the model developed in this thesis can be suitable for various applications. In particular, the model could provide the information regarding the expected furnace operations for uncontrolled process variables, like some of the gas temperature measurement, and also during the periods when some of the gas temperature control loops saturate. Furthermore, the developed models can be incorporated into an optimization procedure to minimize energy consumption in the process by computing optimal values of temperature set points for hearths 4 and 6. In addition, a model-based control of the temperature in Hearths 4 and 6 could be developed to decrease the variations in the temperature profile and especially in the combustion gas flow rate to the furnace. However, this would require extending the dynamic models proposed in this thesis to consider the temperature measurements in hearths 4 and 6 individually. The developed dynamic models of the gas temperature profile could be employed in the future research for the process monitoring aims.

REFERENCES

1. Bloodworth A. and Wrighton C. (2009), Mineral Planning Factsheet: Kaolin, *British Geological Survey*, pp. 1-7
2. Laurence Robb (2005), Introduction to Ore-Forming Processes, Blackwell Publishing Company, Malden, pp. 233-235
3. Evans A.M. (1994), Ore Geology and Industrial Minerals: An Introduction, Blackwell Scientific Publications, London, pp. 274-280.
4. Dogam M., Aburub A., Botha A., and Wurster DE., Quantitative Mineralogical Properties (Morphology-Chemistry-Structure) of Pharmaceutical Grade Kaolinites and Recommendations, *Microscopy and Microanalysis,* Vol 18 (1), pp.143-151.
5. The Mineral Kaolinite, http://www.galleries.com/kaolinite, Retrieved 19/03/2015.
6. Kaolin Chemical Properties, Usage and Production, http://www.chemicalbook.com/ChemicalProductProperty_EN_CB6300504.htm, Retrieved 19/03/2015.
7. Atef Helal (2012), Kaolin Wet-Processing, http://atef.helals.net/mental_responses/misr_resources/kaolin-wet-processing.htm, Retrieved 20/03/2015.
8. Thurlow, C., 2005. *China clay from Cornwall & Devon, An illustrated account of the modern China Clay Industry*. 4th ed. St Austell: Cornish Hillside Publications.
9. DEEngineering , Processes Description Calcination, http://www.dgengineering.de/Rotary-Kiln-Processes-Calcination.html, Retrieved 07/04/2015.
10. Calcines kaolin/ Aluminium Silicad in Plastics & Rubber applications, http://www.mikrons.com.tr/index.asp?action=plastics_rubber_CK_AS , Retrieved 07/04/2015.
11. Burgess Pigment Company, Kaolin, Performance Attributes of Flash vs. Commodity Calcination Methods in Coatings Systems, http://www.burgesspigment.com/burgesswebsite.nsf/Calcine%20methods%20Standard%20and%20Flash.pdf , Retrieved 08/04/2015.

12. Biljana R. Ilic, Aleksandra A. Mitrovic, Ljiljana R. Milicic (2010), Thermal Treatment of kaolin clay to obtain metakaolin, *Institute for Testing of Materials*, Belgrade, DOI: 10.2298/HEMIND100322014I
13. Nimambim Soro, Laurent Aldon, Jean Paul Laval and Philippe Blanchart (2003), Role of Iron in Mullite Formation from Kaolins by Mössbauer Spectroscropy and Rietveld Refinement, *Journal of the American Ceramic Society*, 86(1), pp.129-134.
14. Eskelinen A., Dynamic Modelling of a multiple hearth furnace, Masters Thesis, Aalto University, 2014.
15. Petr Ptacek, Magdalena Kreckova, Frantisek Soukal and Tomas Opravil, Jaromir Havlica and Jiri Brandstetr, The Kinetics and mechanism of kaolin powder sintering I. The dilatometric CRH study of sinter-crystallization of mullite and cristobalite (2012), *Powder Technology*, Volume 232, pp. 24-30.
16. Thomas R.E., High Temperature Processing of kaolinitic Materials, PhD Thesis, University of Birmingham, 2010.
17. Metakaolin, www.download.springer.com, Retrieved 14.04.2015.
18. Sonuparlak B., Sarikaya M., and Aksay I. (1987), Spinel Phase Formation during the 980^{o}C Exothermic reaction in the kaolinite-to-Mullite Reaction Series, *Journal of the American Ceramic Society*, 70 (11), pp. 837-842.
19. Schneider H., Schreuer J. and Hildmann B. (2008), Structure and properties of mullite – A review, *Journal of the European Ceramic Society*, Vol 28, pp.329-344.
20. Castelin O., Soulestin J., Bonnet J.P. and Blanchart P. (2001), The influence of heating rate on the thermal behavior and mullite formation from a kaolin raw material, *Ceramics International*, Vol 27, pp. 517-522.
21. Petr Ptacek, Frantiska Frajkorova, Frantisek Soukal and Tomas Opravil, Kinetics and mechanism of three stages of thermal transformation of kaolinite to metakaolinite (2014), *Powder Technology*, Volume 264, pp. 439-445.
22. Network Solids and Related Materials, http://employees.csbsju.edu/cschaller/Principles%20Chem/network/NWalumina.htm, Retrieved 15/07/2015.
23. Manabu Kano, Koji Nagao, Shinji Hasebe, Iori Hashimoto, Hiromu Ohno, Ramon Strauss and Bhavik Bakshi (2000), Comparison of statistical process monitoring

methids: application to the Eastman challenge problem, *Computers and Chemical Engineering*, Vol 24, pp. 175-181.

24. Frank Westad (2012), Monitoring chemical processes for early fault detection using multivariate data analysis methods, CAMO Software.
25. Paolo Pareti (2010), Mining unexpected behavior from equipment measurements, Department of Information Technology, Uppsala University.
26. Venkat Venkatasubramanian, Raghunathan Rengaswamy, Kewen Yin and Surya kavuri (2003), A review of process fault detection and diagnosis Part I: Quantitative model-based methods, *Computers and Chemical Engineering*, Volume 27, pp. 293-311.
27. Venkat Venkatasubramanian, Raghunathan Rengaswamy and Surya Kavuri (2003), A review of process fault detection and diagnosis Part II: Quanlitative model-based methods, *Computers and Chemical Engineering*, Volume 27, pp. 313-326.
28. Venkat Venkatasubramanian, Raghunathan Rengaswamy, Surya Kavuri and kewen Yin (2003), A review of process fault detection and diagnosis Part III: Process History based methods, *Computers and Chemical Engineering*, Volume 27, pp. 327-346.
29. Success Stories for Control (2011), Performance Monitoring for Mineral Processing, http://ieeecss.org/sites/ieeecss.org/files/documents/IoCT-Part2-04MineralProcessing-LR.pdf, Retrieved 29/05/2015
30. Remes A., Advanced Process Monitoring and Control Methods in Mineral Processing Applications, PhD Thesis, Aalto University, 2012.
31. Jemwa G. and Aldrich C. (2006), Kernel-based fault diagnosis on mineral processing plants, *Minerals Engineering*, Volume 19, pp. 1149-1162.
32. Salinas Y. et al, Monitoring of Chicken meat freshness by means of a calorimetric sensor array, *Royal Society of Chemistry*, Vol 137, pp. 3635-3643.
33. Penha R.M. and Hines W.J., Using Principal Component Analysis Modeling to Monitor Temperature Sensors in a Nuclear Research Reactor, http://citeseerx.ist.psu.edu/viewdoc/download?doi=10.1.1.28.5158&rep=rep1&type=pdf, Retrieved 12/07/2015.

34. Anonymous, http://support.sas.com/rnd/app/qc/qcmvp.html, Retrieved 12/07/2015.

35. Kallioniemi J., Utilizing process Monitoring methods in Biopower plant process, Masters Thesis, Aalto University, 2008.

36. Schwab N.V., Da-Col J.A., Terra, J. and Bueno M.I. (2012), Fast Direct Determination of Titanium Dioxide in Toothpastes by X-Ray Fluorescence and Multivariate Calibration, *Journal of the Brazilian Chemical Society*, Volume 23(3), pp. 546-554.

37. Zakharov A., Tikkala V.-M. and Jämsä-Jounela S.-L. (2013), Fault detection and diagnosis approach based on nonlinear parity equations and its applications to leakages and blockages in the drying section of a board machine, *Journal of Process Control*, Volume 23, pp. 1380-1393.

38. Vermasvuori M., Methodology for utilizing prior knowledge in constructing data-based process monitoring systems with an application to a dearomatization process, PhD Thesis, Aalto University, 2008.

Appendices

1. Prediction of PCA scores for feed rates 100, 105, 110, 115 kg/min using gas flows to hearths 4 and 6.

2. Prediction of PCA Scores for Feed Rates 100, 105, 110, 115 Kg/Min Using Gas Flows and Walls Temperature.

3. Prediction of GPCA Scores for feed rates 100, 105, 110, 115 kg/min using Gas Flows and Walls Temperature.

4. PLS results for the prediction of Gas Temperature profiles using methane gas flows.

5. PLS results for the prediction of Gas temperature profiles using Methane gas flows and Furnace Walls temperature for feed rates 100, 105, 110, 115 kg/min.

6. PLS results for the prediction of Gas temperature profiles using Methane gas flows, Furnace Walls temperature and delayed gas temperatures for feed rates 100, 105, 110, 115 kg/min.

7. PLS results for the Prediction of Gas temperature profiles using the ratios of Methane gas flows to each burner, Furnace Walls temperature and the delayed gas temperatures.

1. **Prediction of PCA scores For Feed rates 100, 105, 110, 115 kg/min using gas flows to hearths 4 and 6 (Static Models).**

   Figures 1 to 4 are the results of PCA model for feed rates 100, 105, 110 and 115 kg/min using gas flows to hearths 4 and 6 as model input.

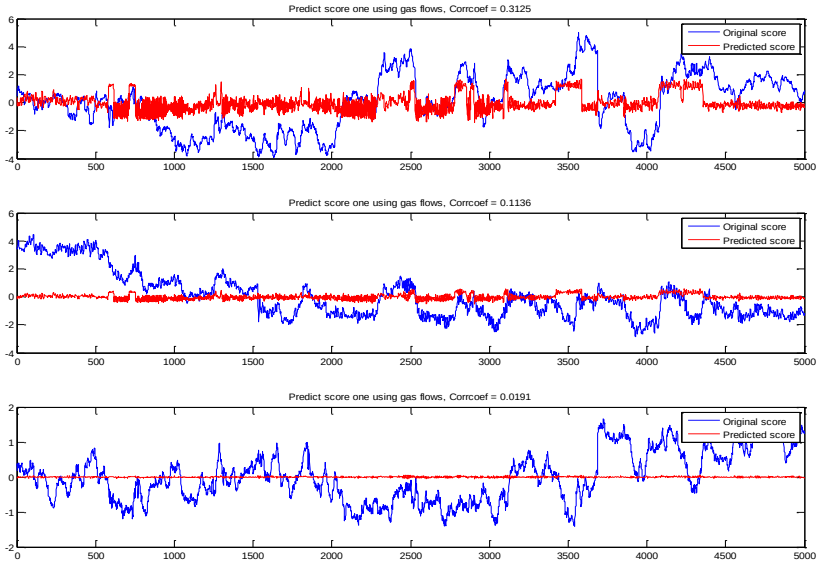

Figure 1: Prediction of PCA scores using Gas flows for Feed rate 100 kg/min

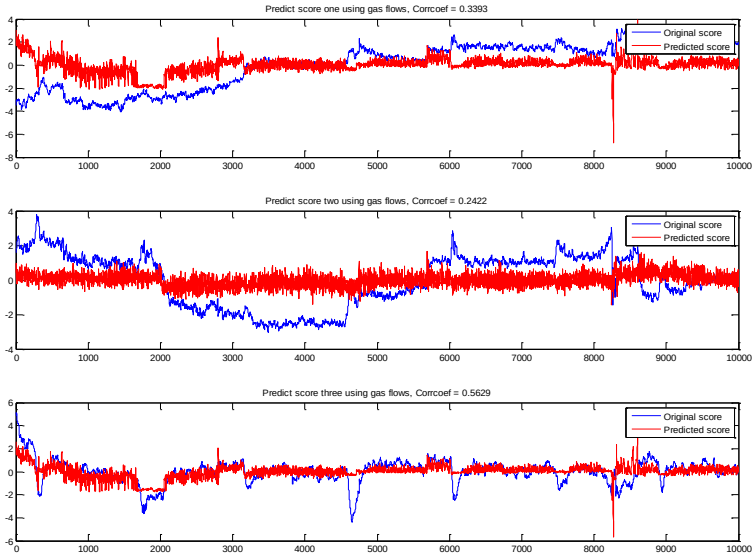

Figure 2: Prediction of PCA scores using Gas flows for Feed rate 105 kg/min

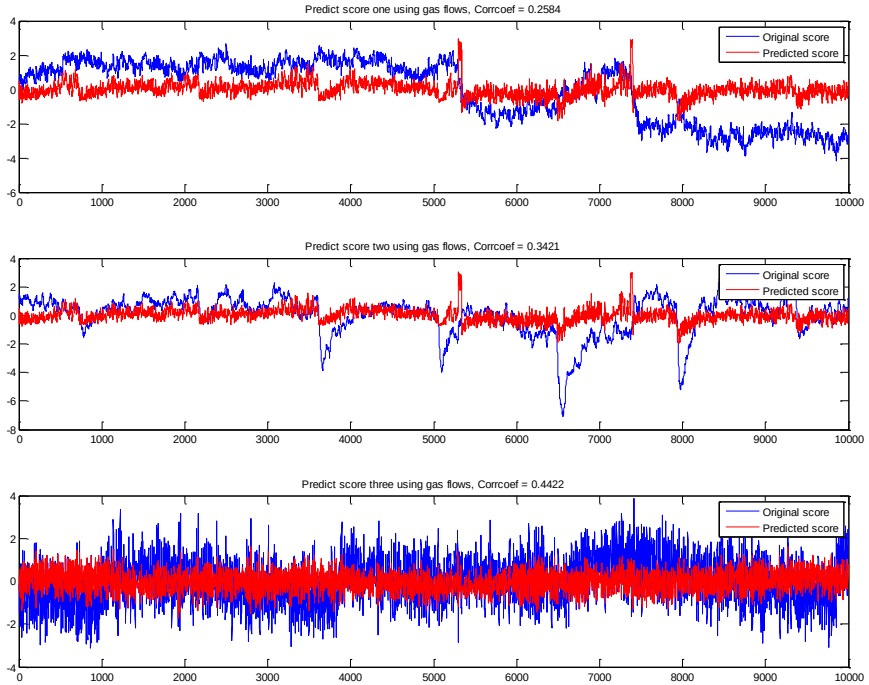

Figure 3: Prediction of PCA scores using Gas flows for Feed rate 110 kg/min

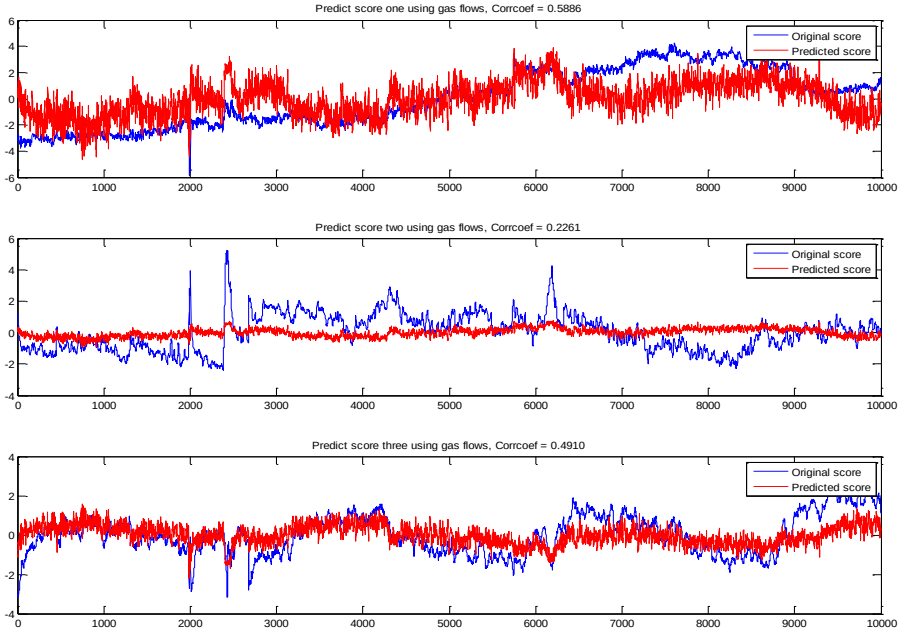

Figure 4: Prediction of PCA scores using Gas flows for Feed rate 115 kg/min

2. Prediction of PCA Scores for feed rates 100, 105, 110, 115 kg/min using Gas Flows and Walls Temperature (Static Models).

Figures 5 to 8 are the results of PCA model for feed rates 100, 105, 110 and 115 kg/min using gas flows to hearths 4 and 6 and Walls temperature of heaths 5 and 8 as model input.

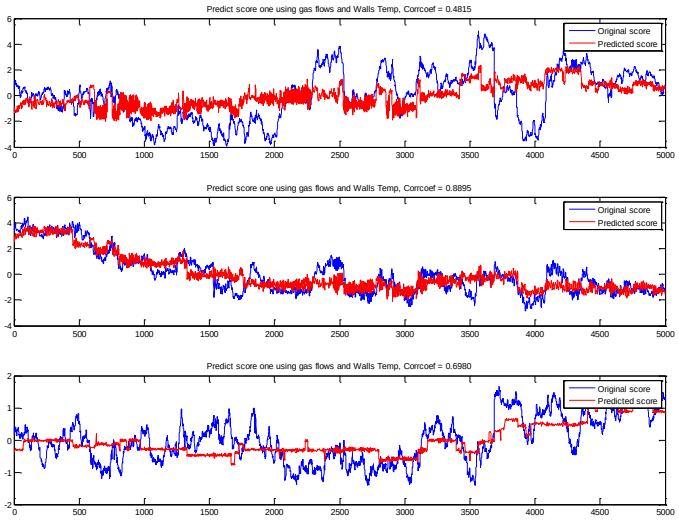

Figure 5: Prediction of PCA scores using Gas flows and Walls Temperature for Feed rate 100 kg/min

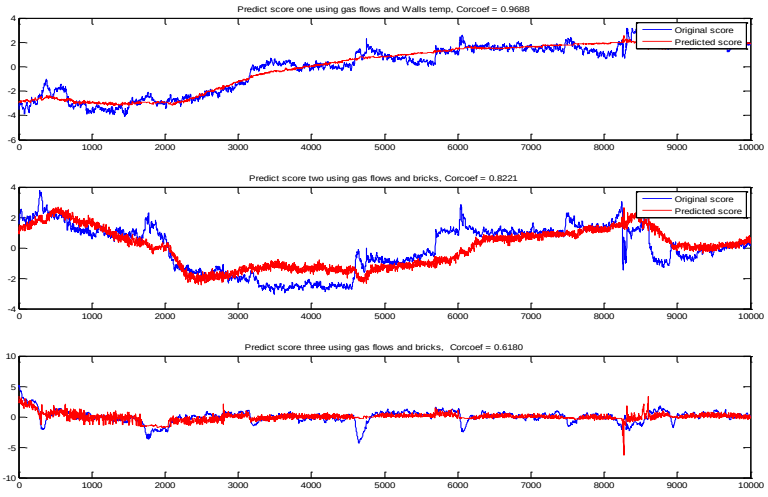

Figure 6: Prediction of PCA scores using Gas flows and Walls Temperature for Feed rate 105 kg/min

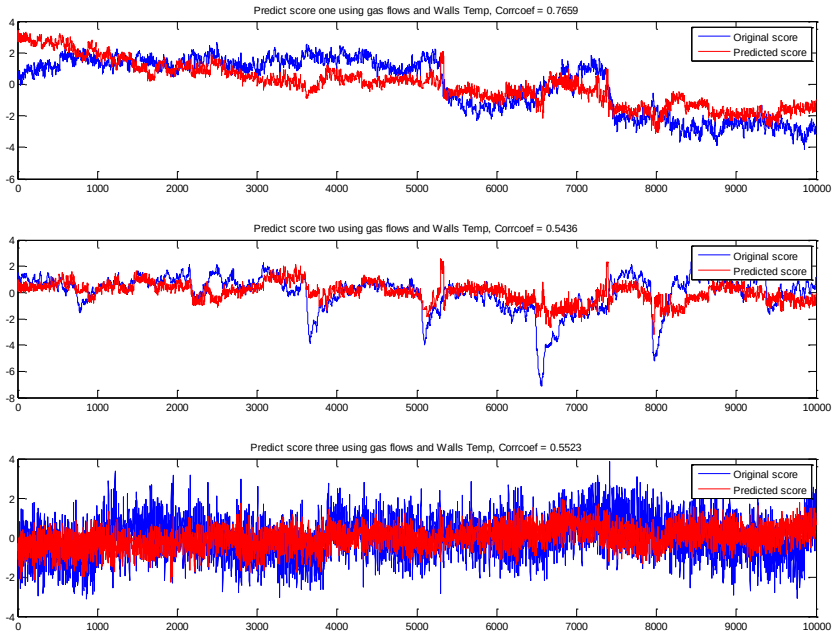

Figure 7: Prediction of PCA scores using Gas flows and Walls Temperature for Feed rate 110 kg/min

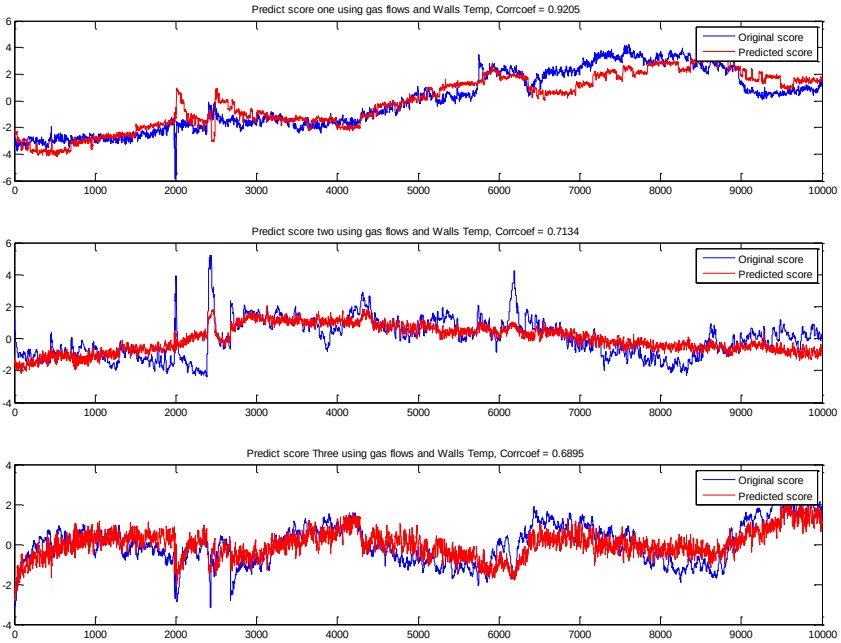

Figure 8: Prediction of PCA scores using Gas flows and Walls Temperature for Feed rate 115 kg/min

3. Prediction of GPCA Scores for feed rates 100, 105, 110, 115 kg/min using Gas Flows and Walls Temperature (Static Models).

Figures 9 to 12 are the results of GPCA model for feed rates 100, 105, 110 and 115 kg/min using gas flows to hearths 4 and 6 and Walls temperature of heaths 5 and 8 as model input.

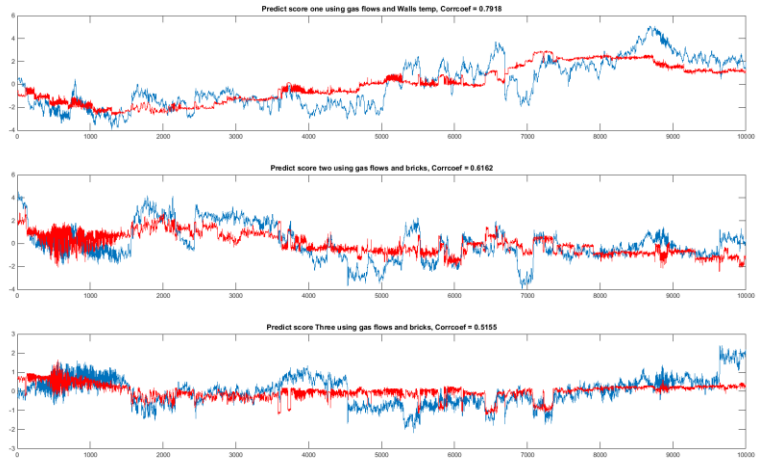

Figure 9: Prediction of GPCA scores using Gas flows and Walls Temperature for Feed rate 100 kg/min

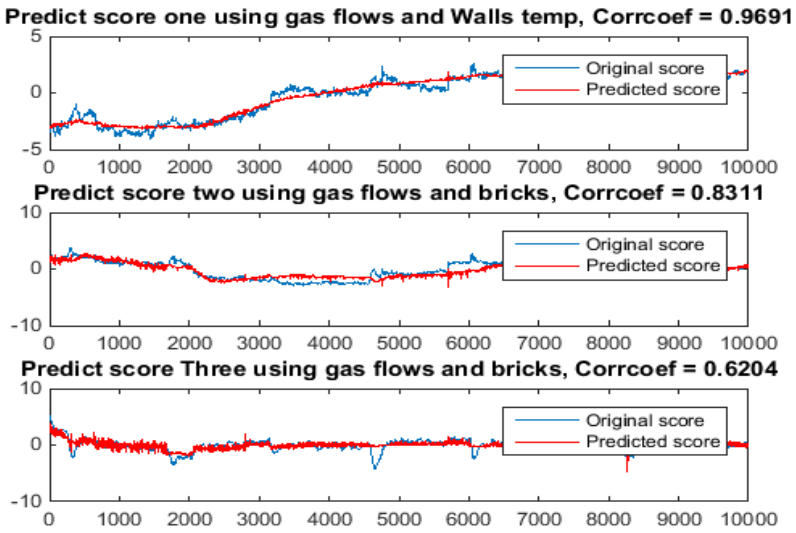

Figure 8.10: Prediction of GPCA scores using Gas flows and Walls Temperature for Feed rate 105 kg/min

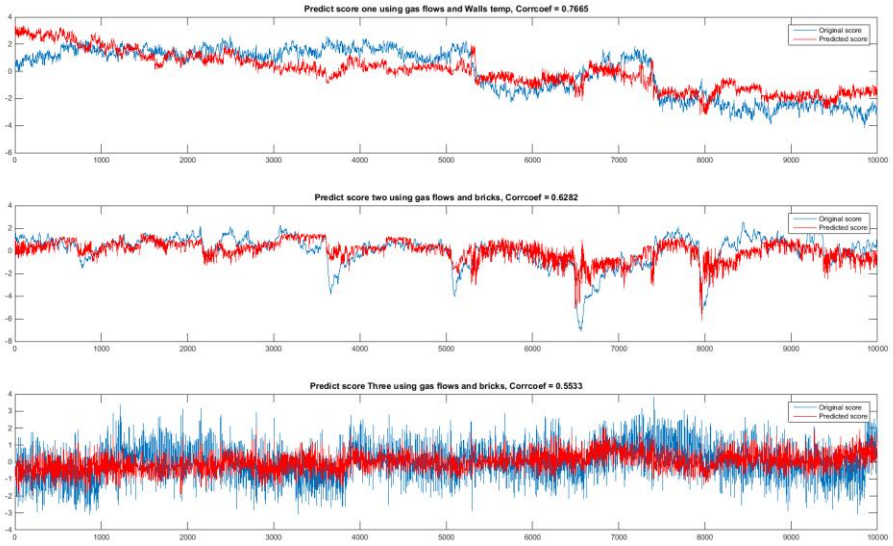

Figure 8.11: Prediction of GPCA scores using Gas flows and Walls Temperature for Feed rate 110 kg/min

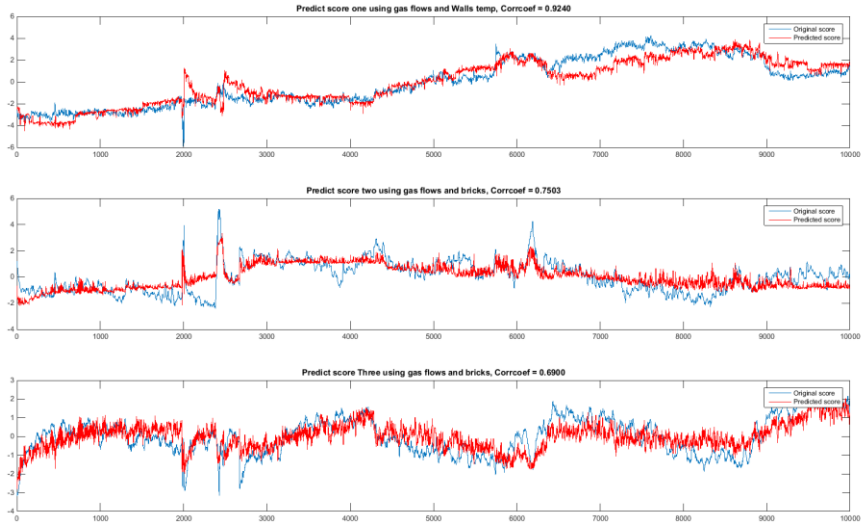

Figure 8.12: Prediction of GPCA scores using Gas flows and Walls Temperature for Feed rate 115 kg/min

4. Prediction of Gas Temperature profiles using methane gas flows (Static Models).

Figures 13 to 52 are the results of PLS for prediction of gas temperature profiles in hearths 1 to 8 for feed rates 100, 105, 110, 115, 120 kg/min using gas flows.

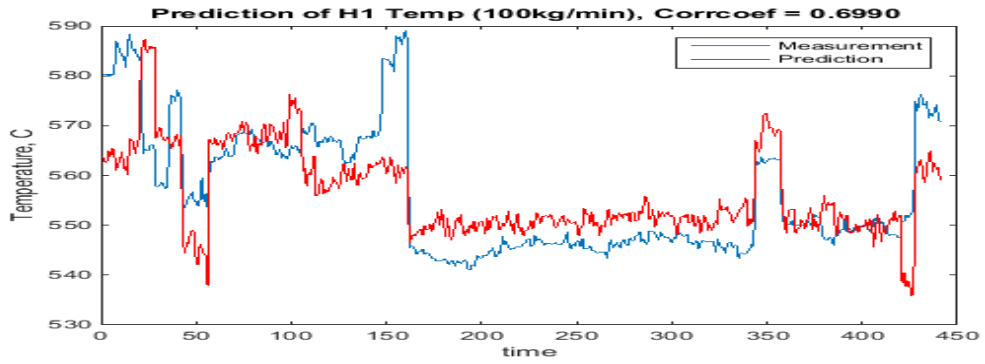

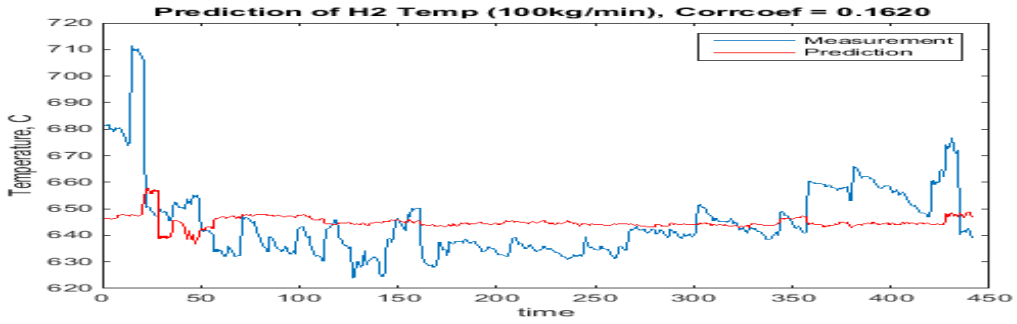

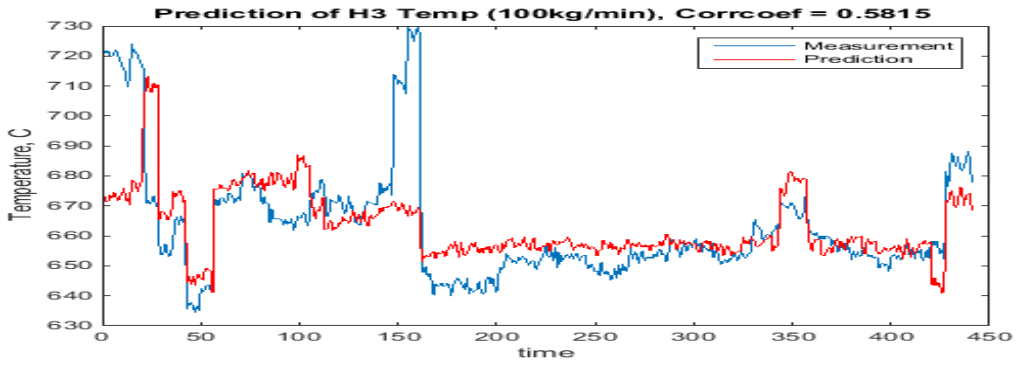

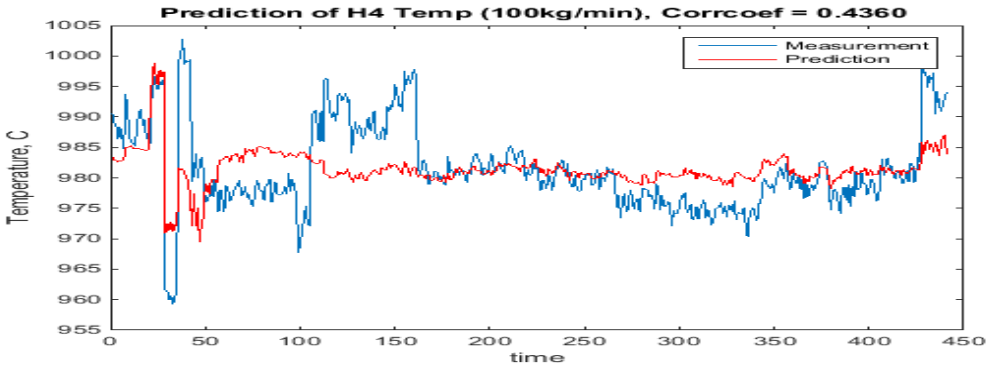

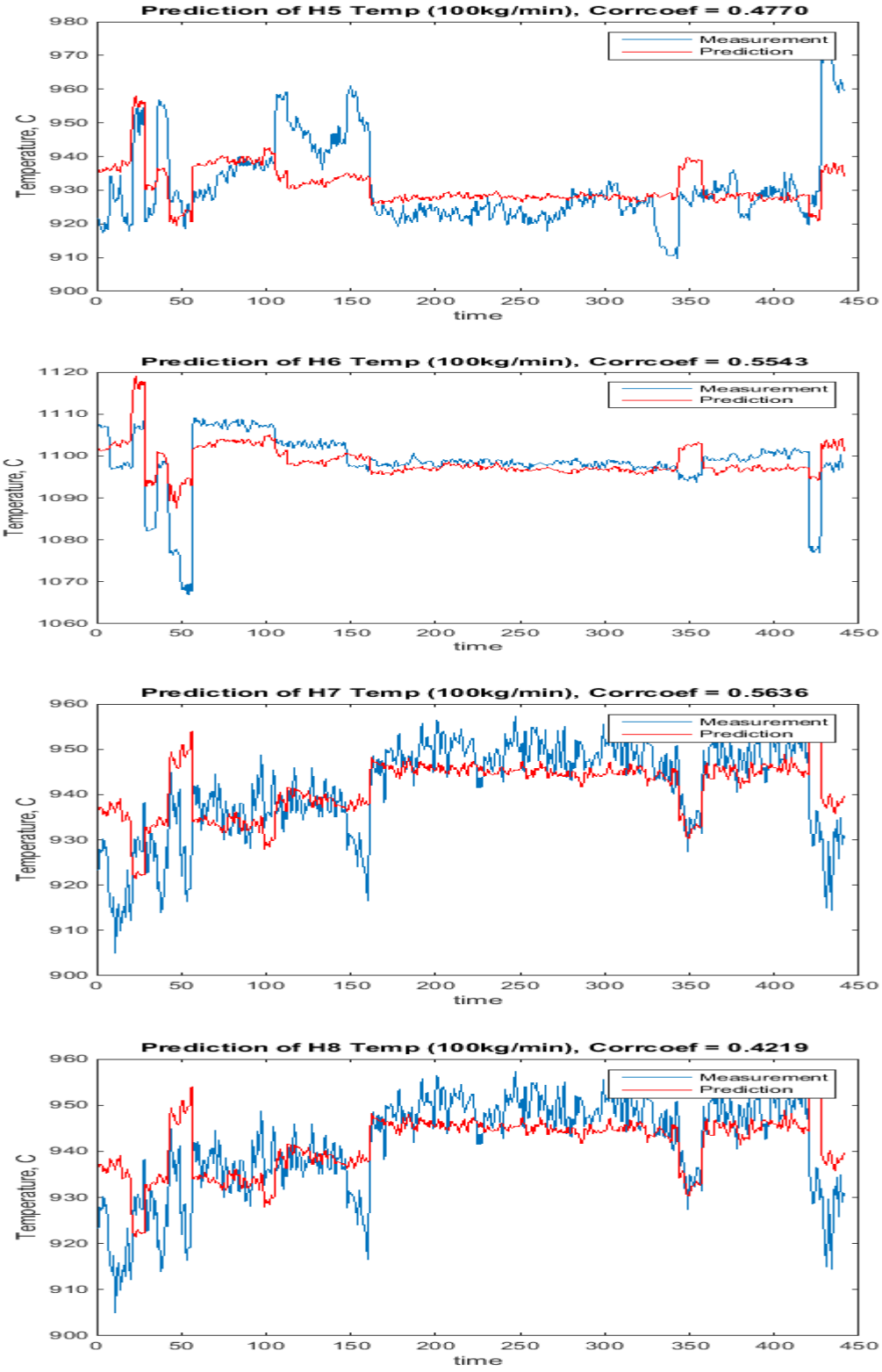

Figures 13-20: Prediction of gas temperature profiles in hearths 1 to 8 using gas flows to hearths 4 and 6 for Feed rate 100 kg/min

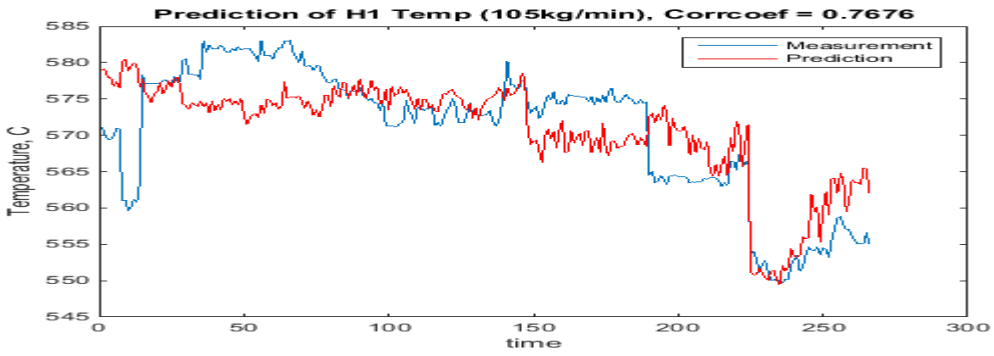
Prediction of H1 Temp (105kg/min), Corrcoef = 0.7676
Measurement
Prediction
Temperature, C
time

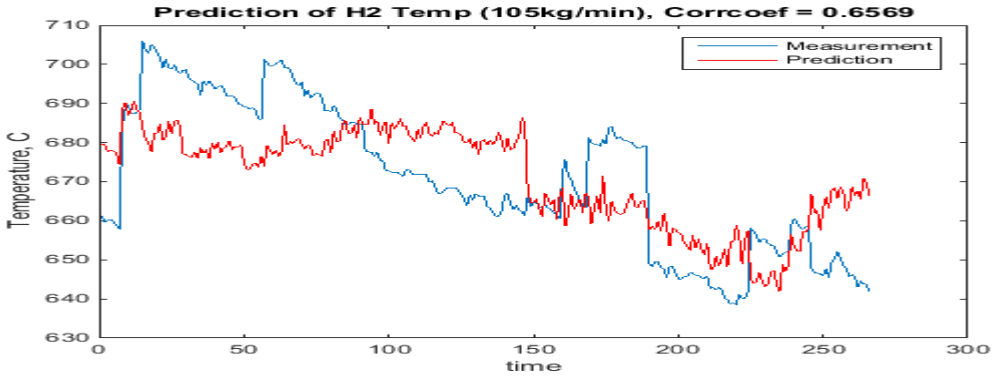
Prediction of H2 Temp (105kg/min), Corrcoef = 0.6569
Measurement
Prediction
Temperature, C
time

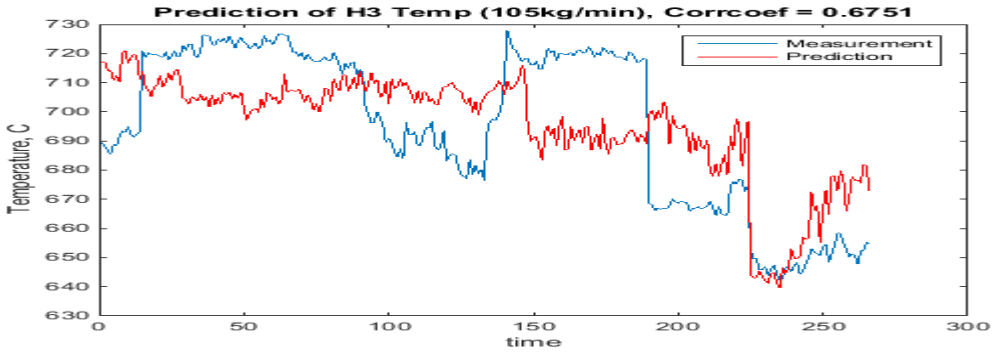
Prediction of H3 Temp (105kg/min), Corrcoef = 0.6751
Measurement
Prediction
Temperature, C
time

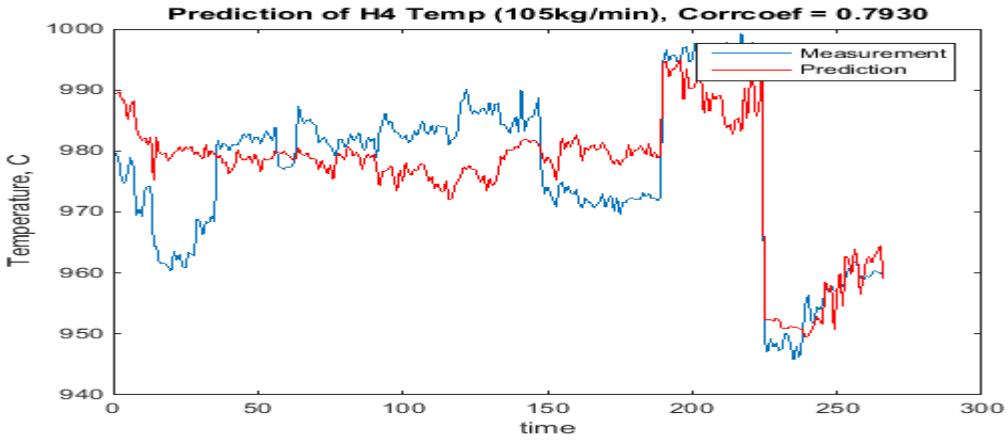
Prediction of H4 Temp (105kg/min), Corrcoef = 0.7930
Measurement
Prediction
Temperature, C
time

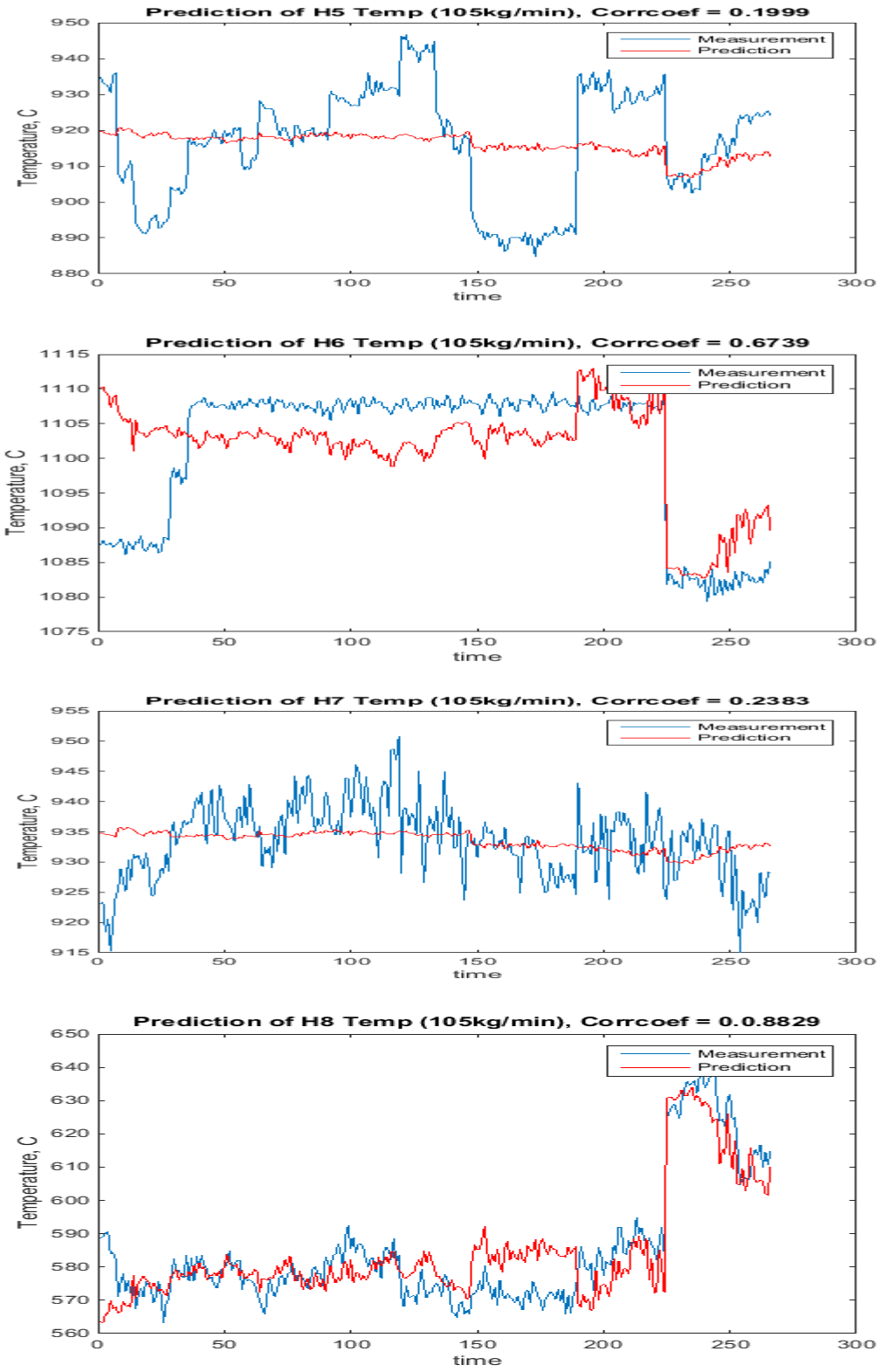

Figures 21-28: Prediction of gas temperature profiles in hearths 1 to 8 using gas flows to hearths 4 and 6 for Feed rate 105 kg/min

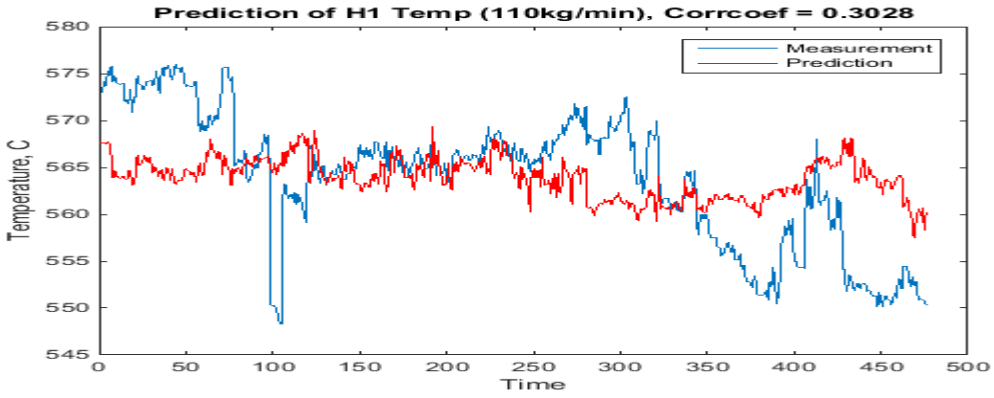
Prediction of H1 Temp (110kg/min), Corrcoef = 0.3028
Measurement
Prediction
Temperature, C
Time

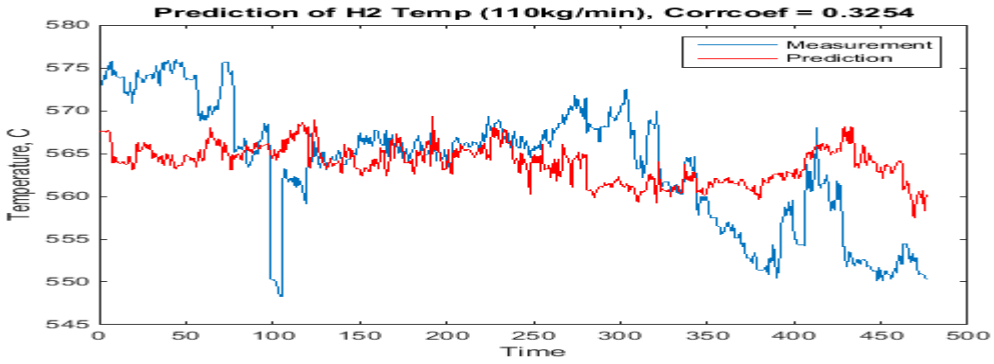
Prediction of H2 Temp (110kg/min), Corrcoef = 0.3254
Measurement
Prediction
Temperature, C
Time

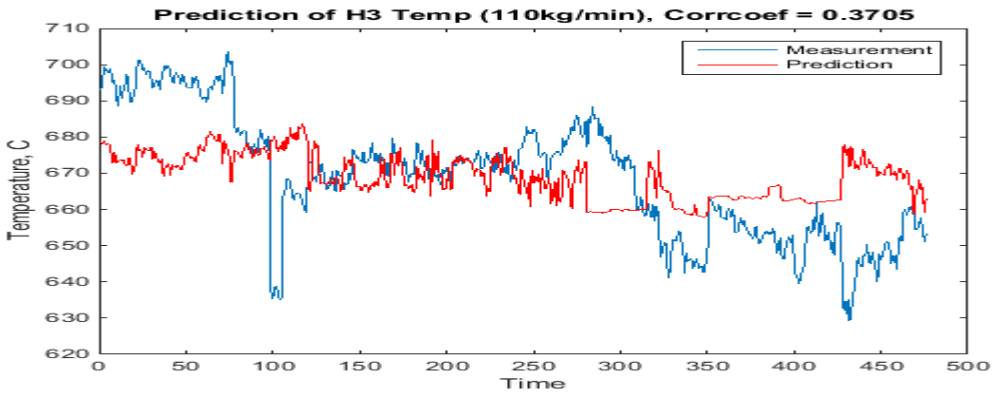
Prediction of H3 Temp (110kg/min), Corrcoef = 0.3705
Measurement
Prediction
Temperature, C
Time

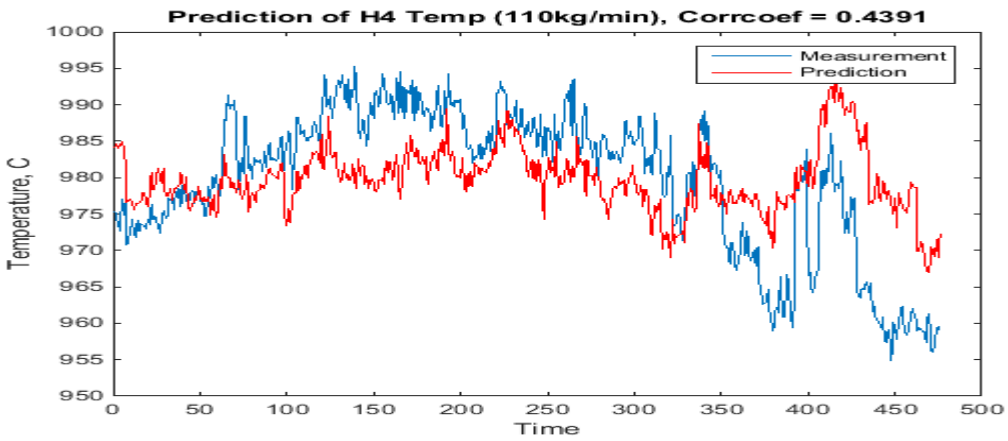
Prediction of H4 Temp (110kg/min), Corrcoef = 0.4391
Measurement
Prediction
Temperature, C
Time

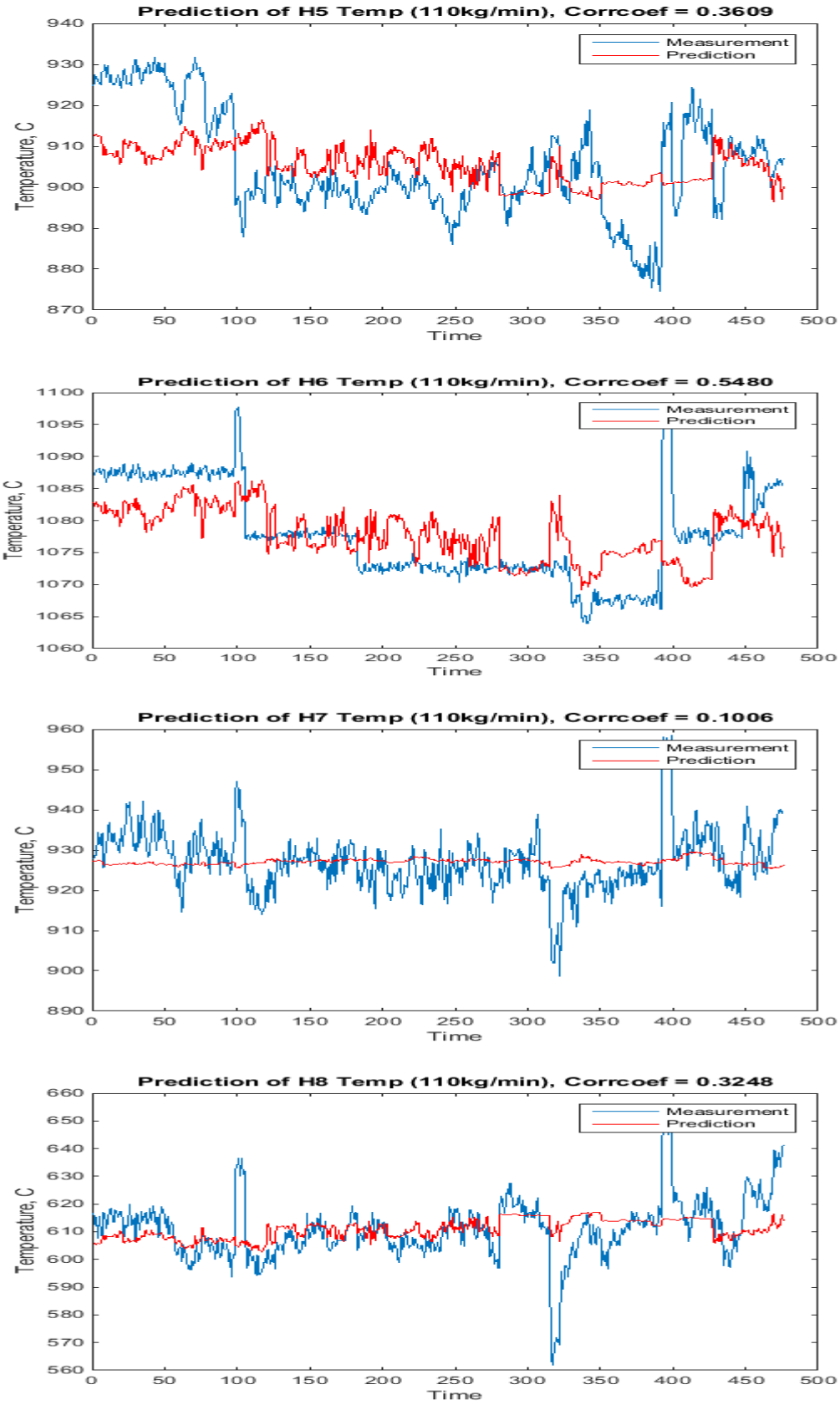

Figures 29-36: Prediction of gas temperature profiles in hearths 1 to 8 using gas flows to hearths 4 and 6 for Feed rate 110 kg/min

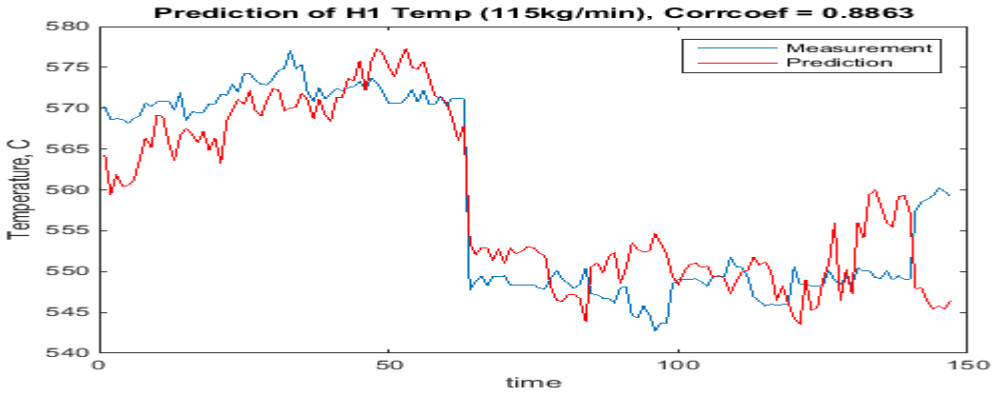
Prediction of H1 Temp (115kg/min), Corrcoef = 0.8863
Measurement
Prediction
Temperature, C
time
580
575
570
565
560
555
550
545
540
0
50
100
150

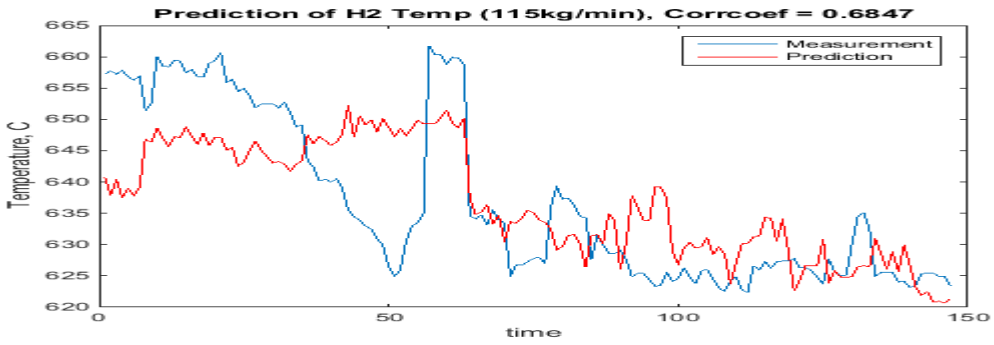
Prediction of H2 Temp (115kg/min), Corrcoef = 0.6847
Measurement
Prediction
Temperature, C
time
665
660
655
650
645
640
635
630
625
620
0
50
100
150

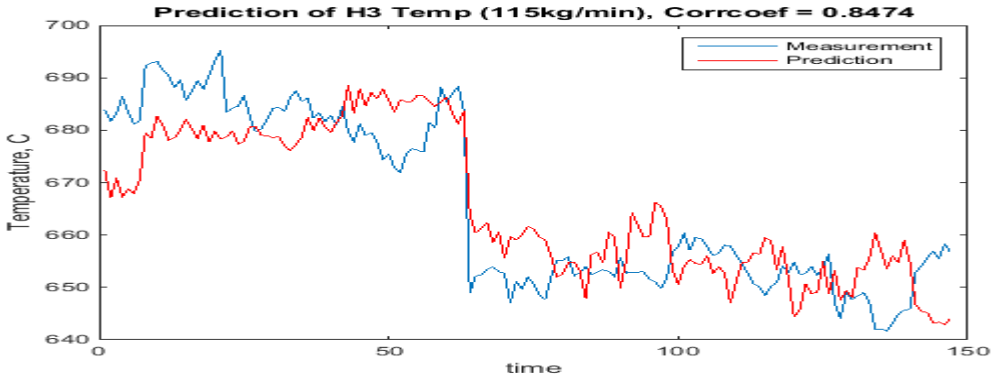
Prediction of H3 Temp (115kg/min), Corrcoef = 0.8474
Measurement
Prediction
Temperature, C
time
700
690
680
670
660
650
640
0
50
100
150

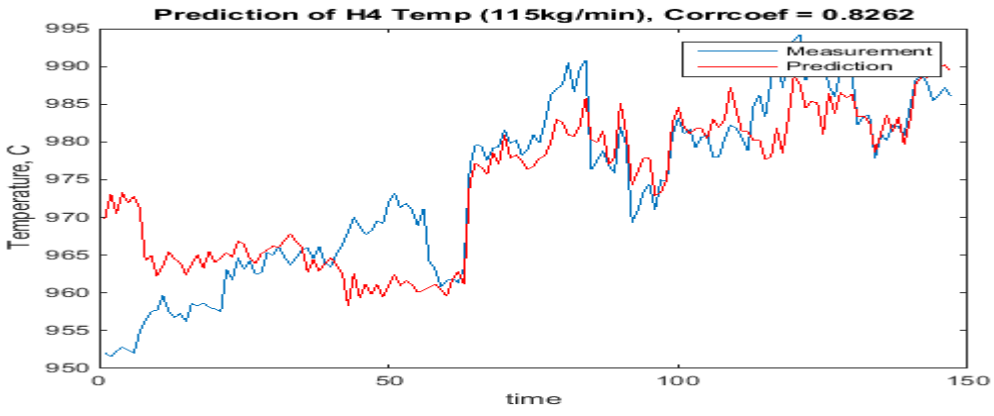
Prediction of H4 Temp (115kg/min), Corrcoef = 0.8262
Measurement
Prediction
Temperature, C
time
995
990
985
980
975
970
965
960
955
950
0
50
100
150

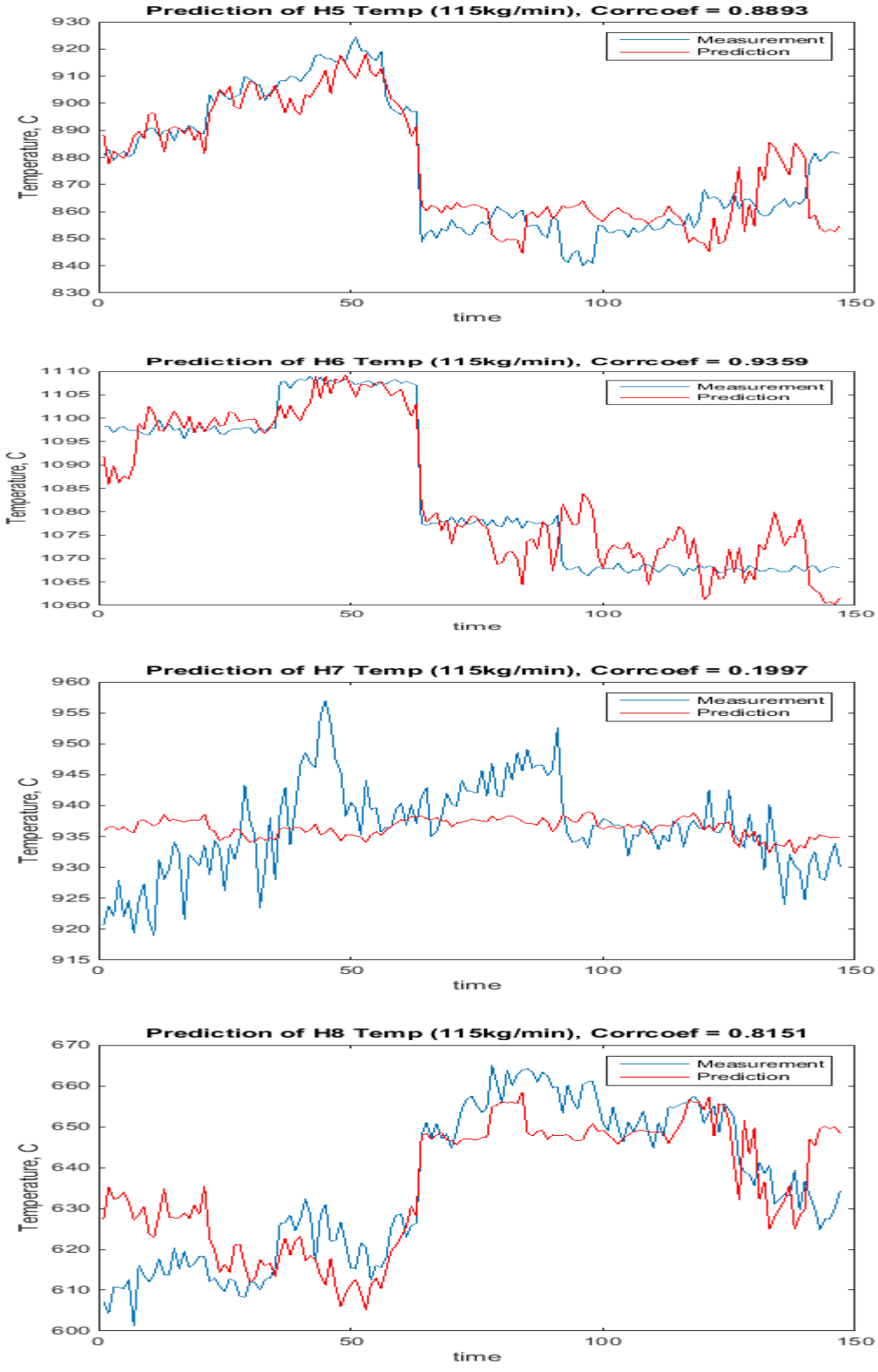

Figures 37-44: Prediction of gas temperature profiles in hearths 1 to 8 using gas flows to hearths 4 and 6 for Feed rate 115 kg/min

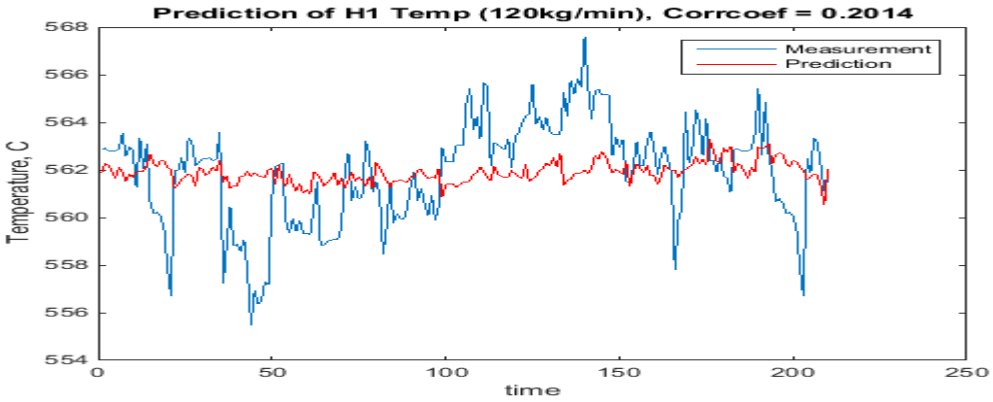
Prediction of H1 Temp (120kg/min), Corrcoef = 0.2014
Measurement
Prediction
Temperature, C
time

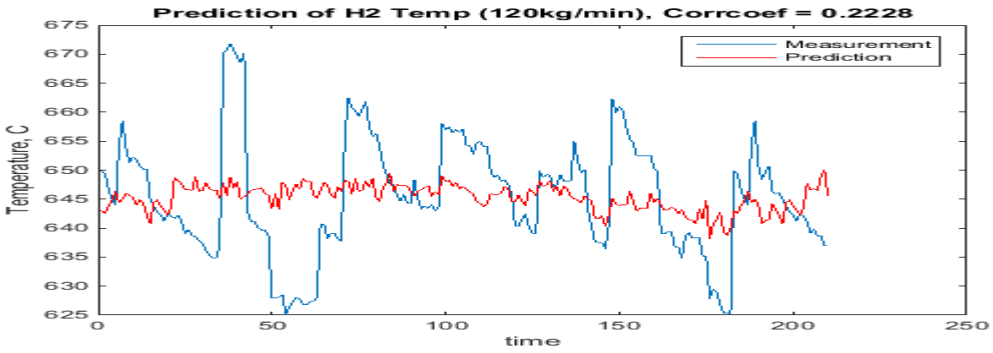
Prediction of H2 Temp (120kg/min), Corrcoef = 0.2228
Measurement
Prediction
Temperature, C
time

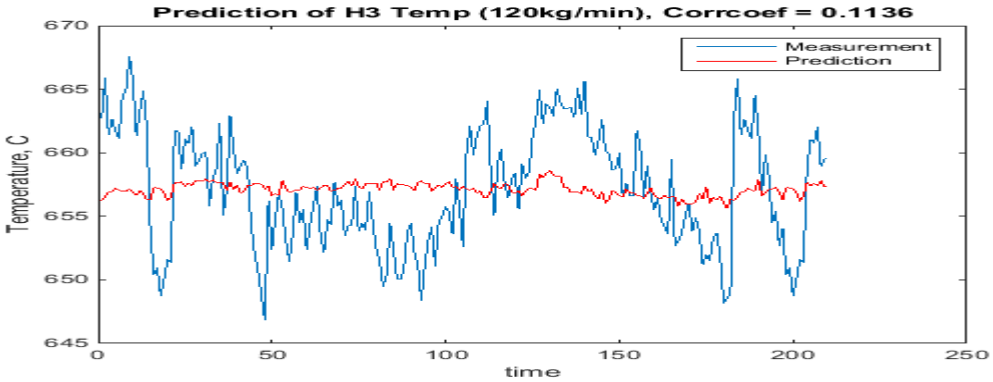
Prediction of H3 Temp (120kg/min), Corrcoef = 0.1136
Measurement
Prediction
Temperature, C
time

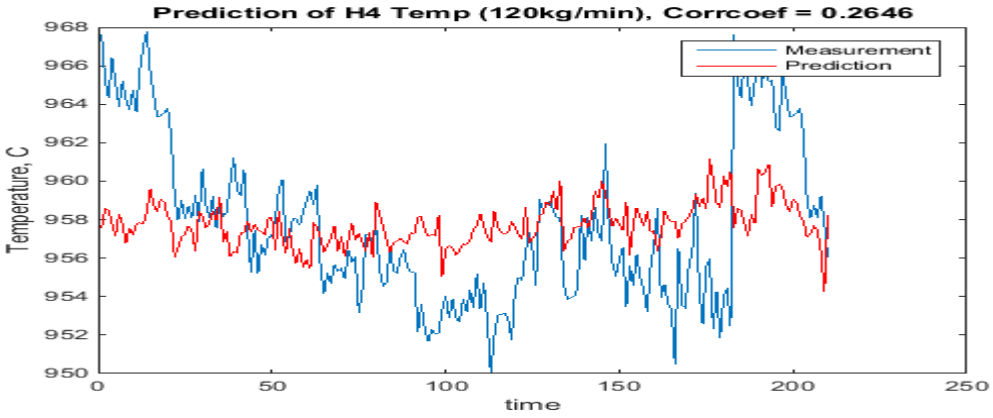
Prediction of H4 Temp (120kg/min), Corrcoef = 0.2646
Measurement
Prediction
Temperature, C
time

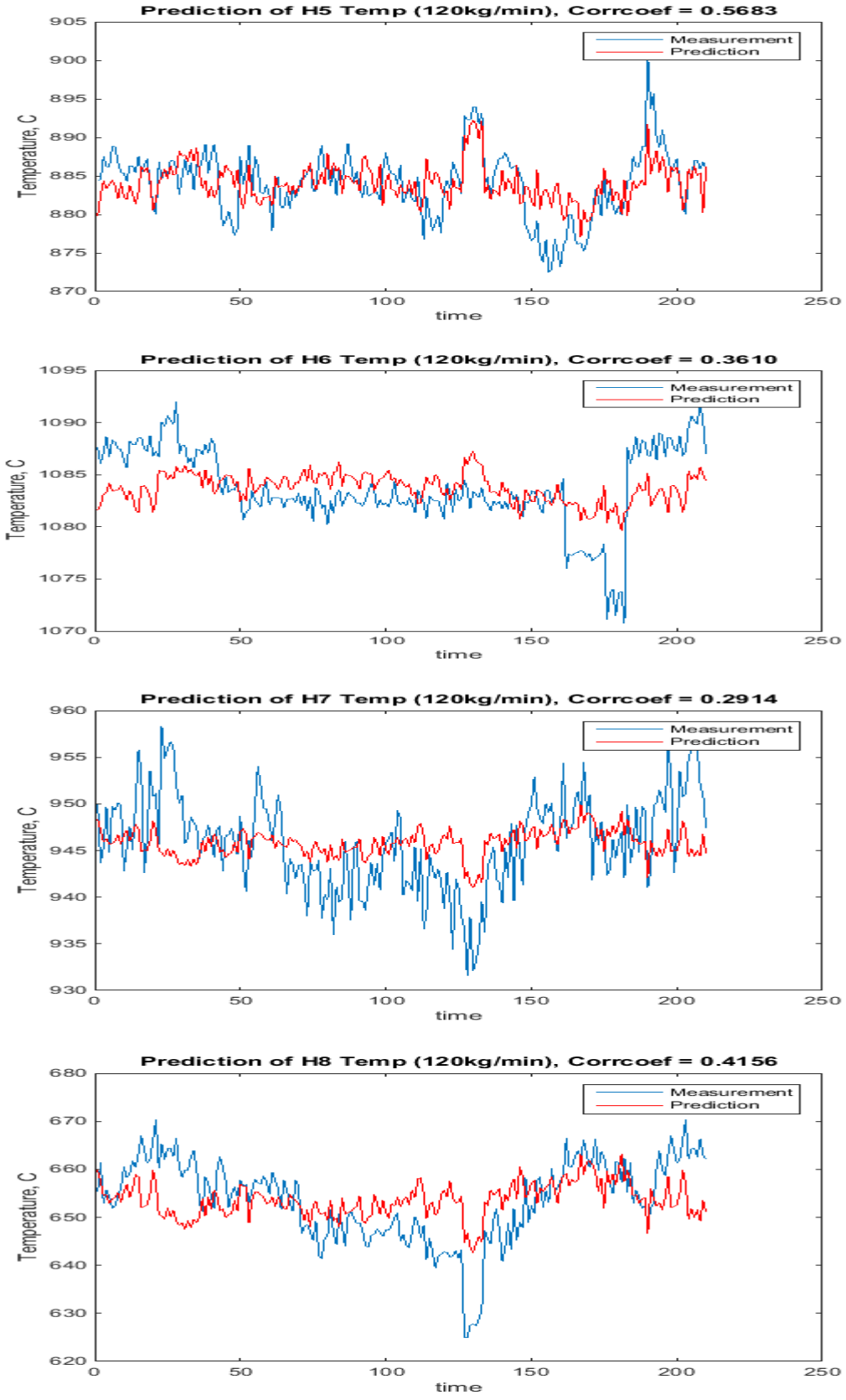

Figures 45-52: Prediction of gas temperature profiles in hearths 1 to 8 using gas flows to hearths 4 and 6 for Feed rate 105 kg/min

5. Prediction of Gas temperature profiles using Methane gas flows and Furnace Walls temperature (Static Models).

Figures 53 to 91 are the results of PLS for prediction of gas temperature profiles in hearths 1 to 8 for feed rates 100, 105, 110, 115, 120 kg/min using gas flows.

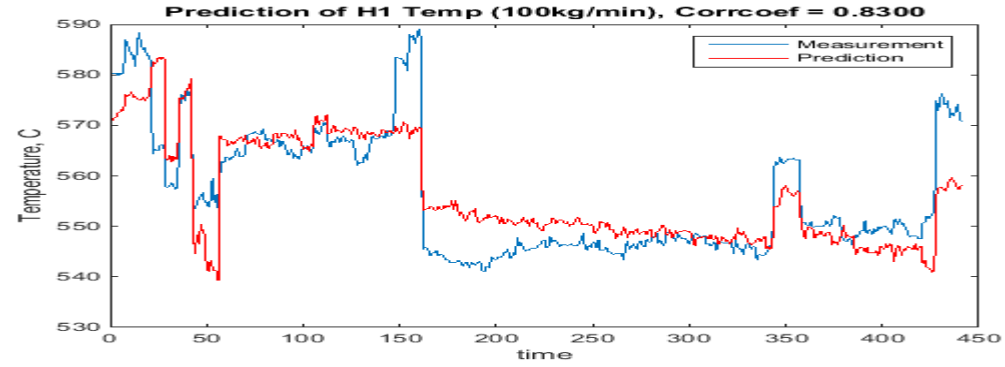

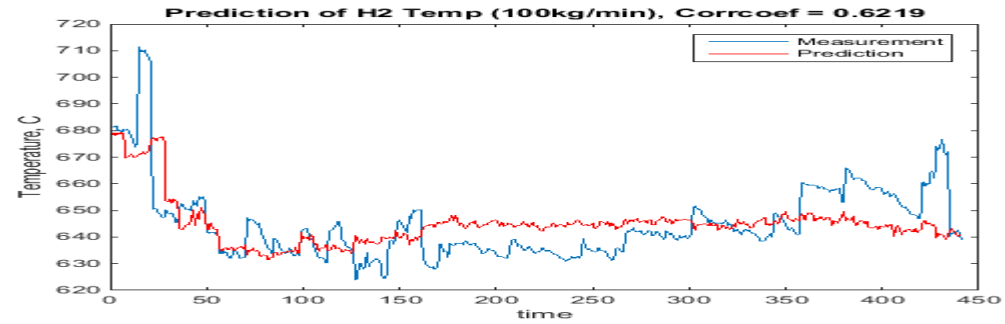

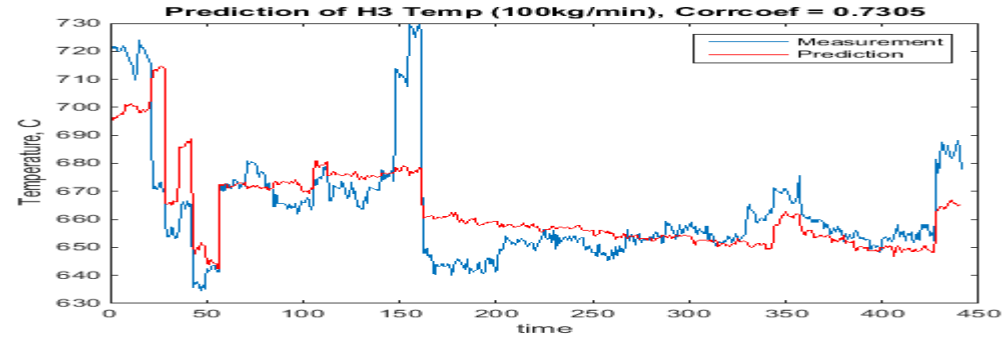

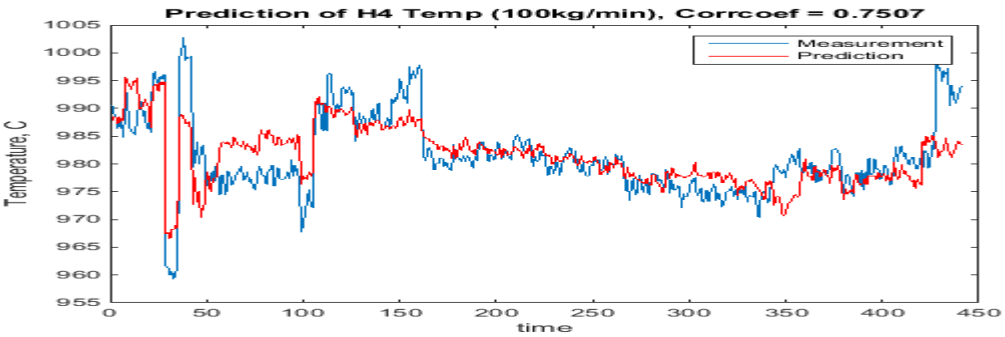

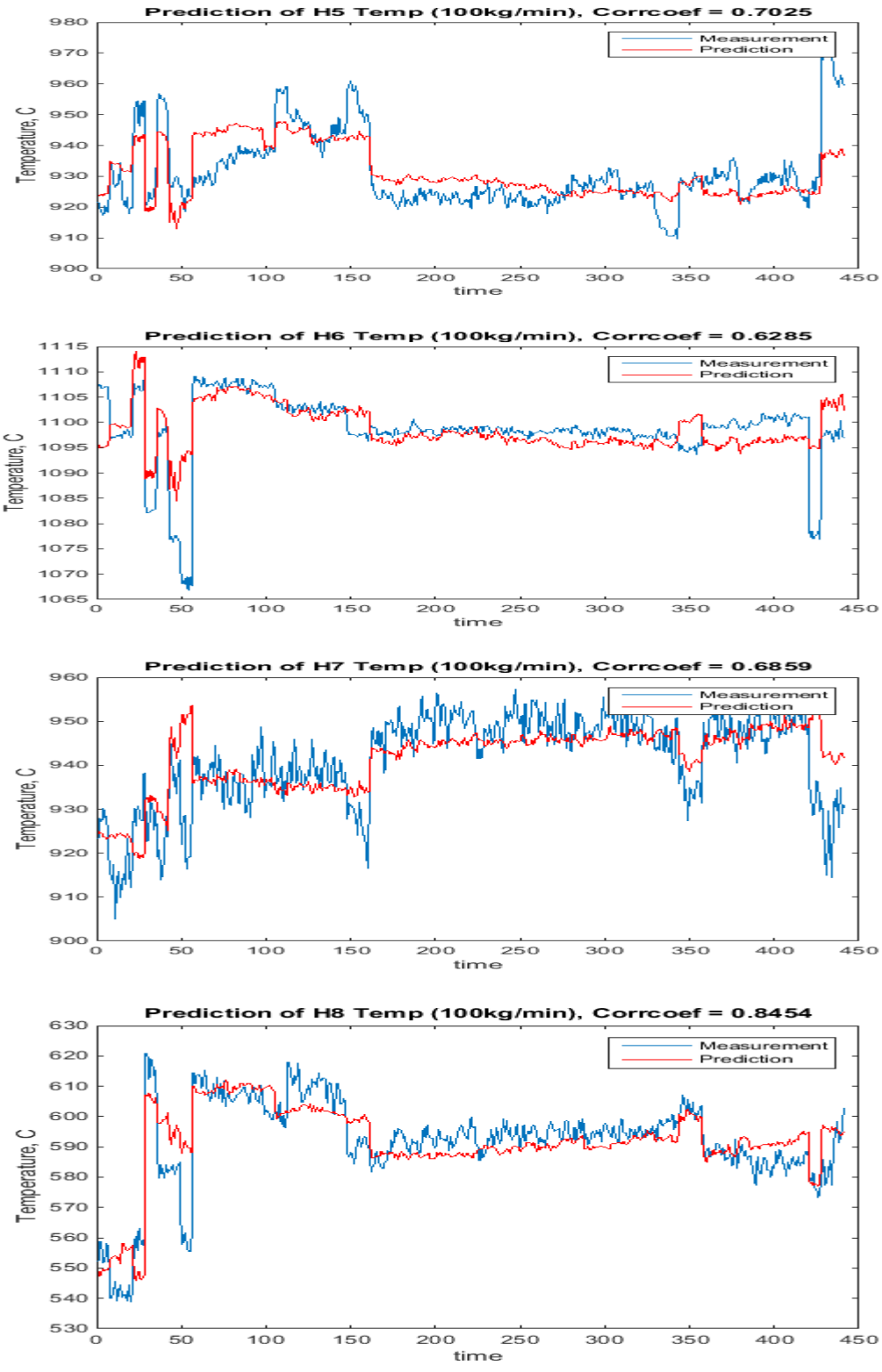

Figures 53-60: Prediction of gas temperature profiles in hearths 1 to 8 using gas flows and walls temperature for Feed rate 100 kg/min

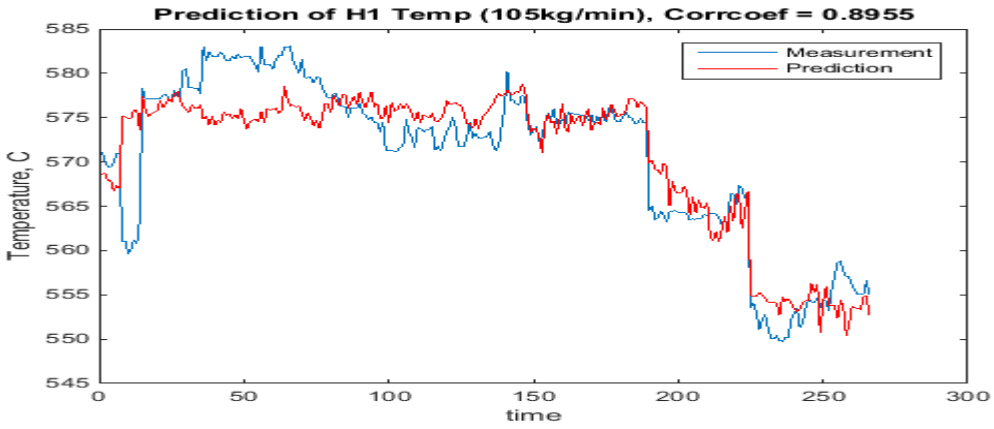
Prediction of H1 Temp (105kg/min), Corrcoef = 0.8955
Measurement
Prediction
Temperature, C
time

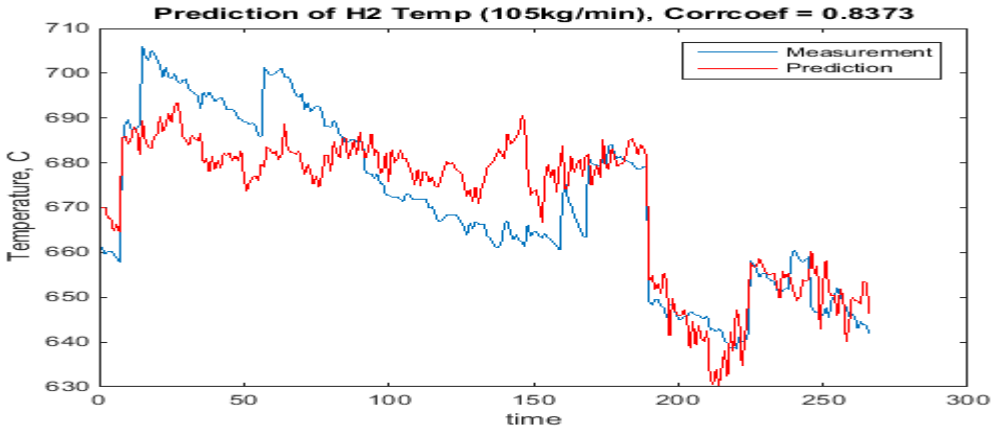
Prediction of H2 Temp (105kg/min), Corrcoef = 0.8373
Measurement
Prediction
Temperature, C
time

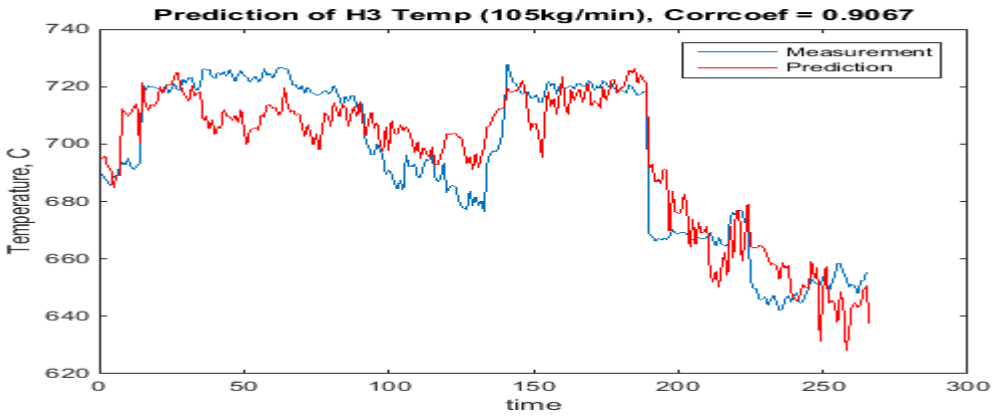
Prediction of H3 Temp (105kg/min), Corrcoef = 0.9067
Measurement
Prediction
Temperature, C
time

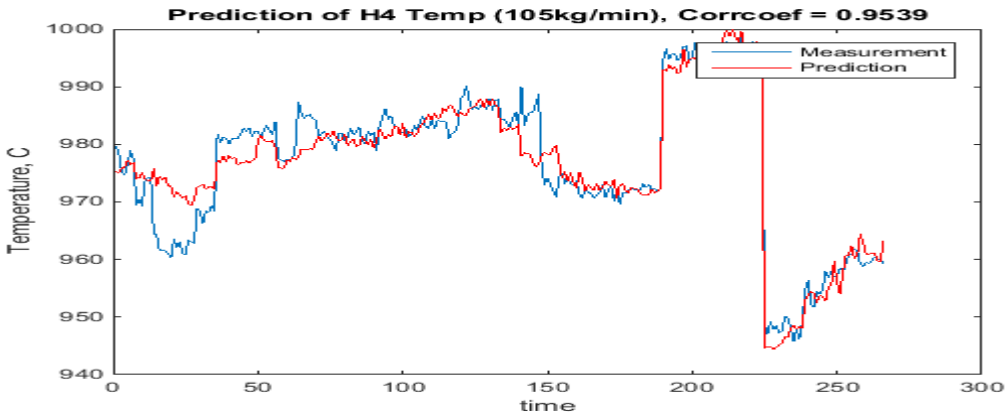
Prediction of H4 Temp (105kg/min), Corrcoef = 0.9539
Measurement
Prediction
Temperature, C
time

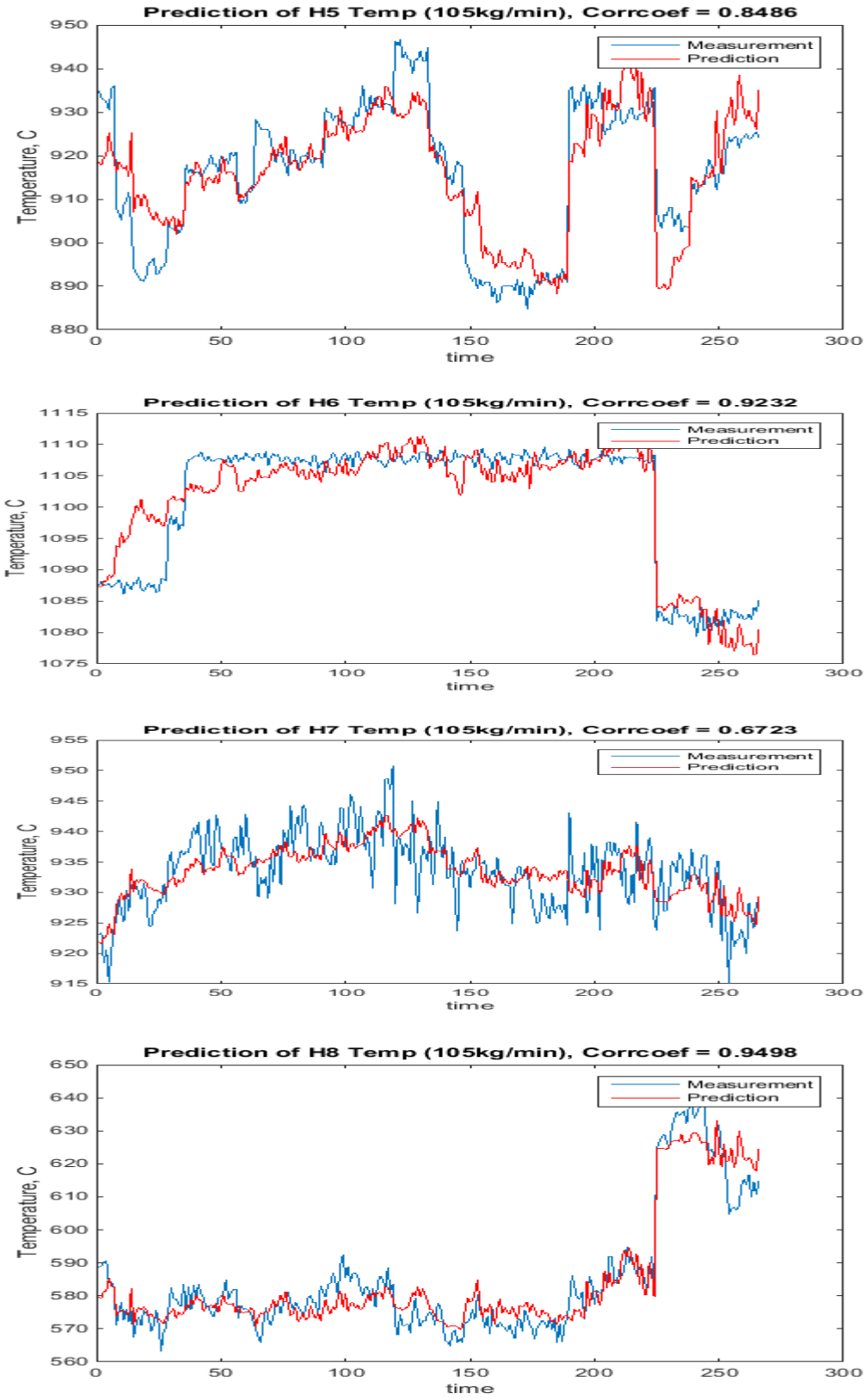

Figures 60-67: Prediction of gas temperature profiles in hearths 1 to 8 using gas flows and walls temperature for Feed rate 105 kg/min

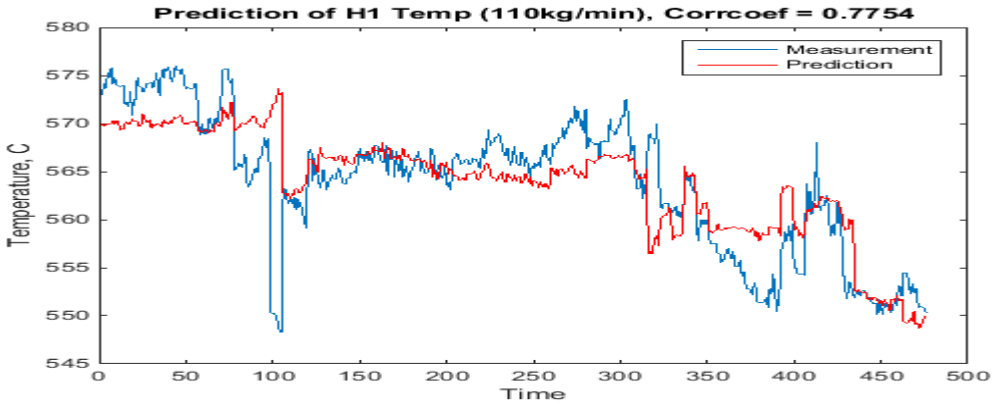
Prediction of H1 Temp (110kg/min), Corrcoef = 0.7754
Measurement
Prediction
Temperature, C
Time

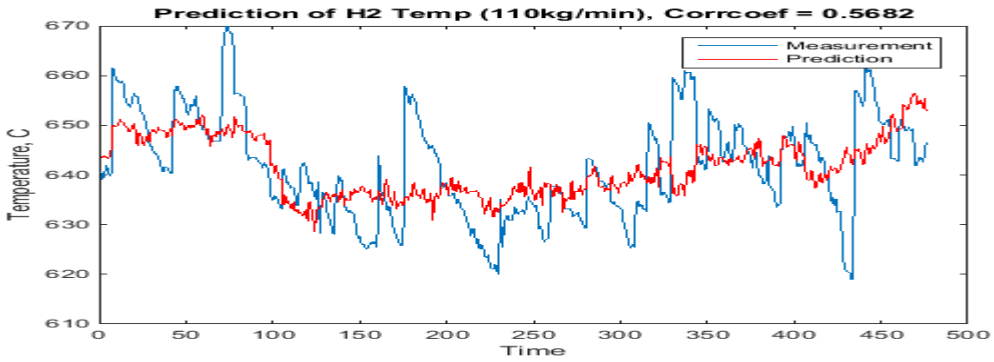
Prediction of H2 Temp (110kg/min), Corrcoef = 0.5682
Measurement
Prediction
Temperature, C
Time

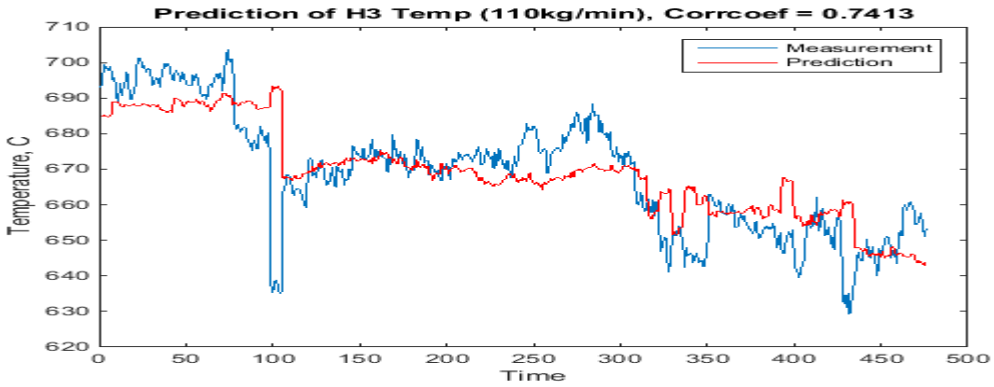
Prediction of H3 Temp (110kg/min), Corrcoef = 0.7413
Measurement
Prediction
Temperature, C
Time

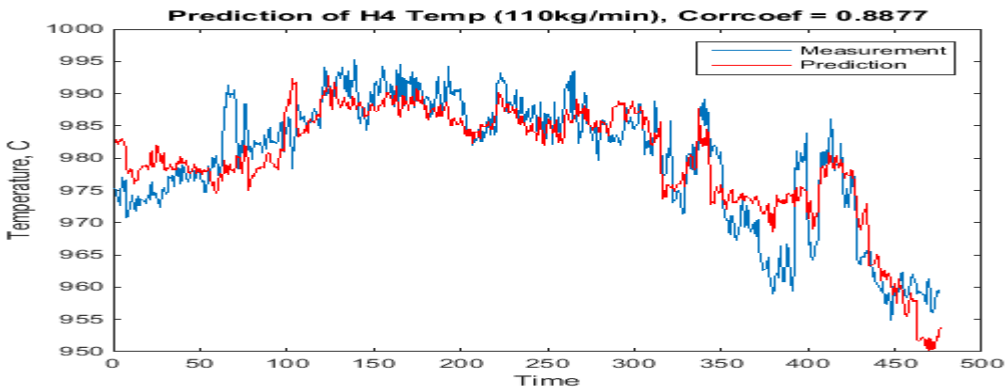
Prediction of H4 Temp (110kg/min), Corrcoef = 0.8877
Measurement
Prediction
Temperature, C
Time

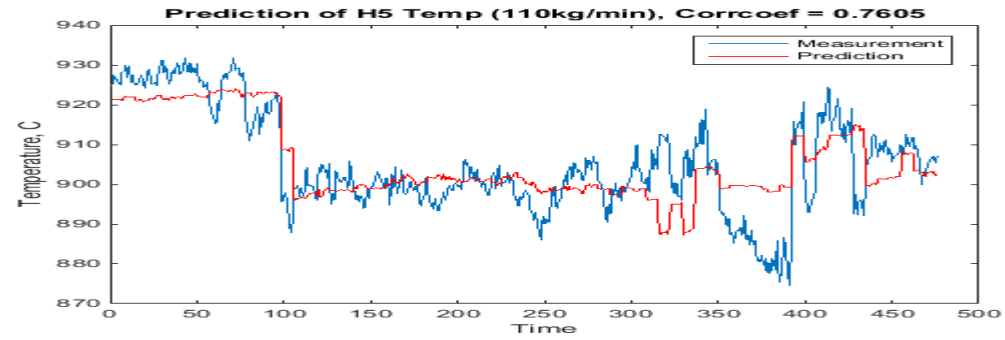

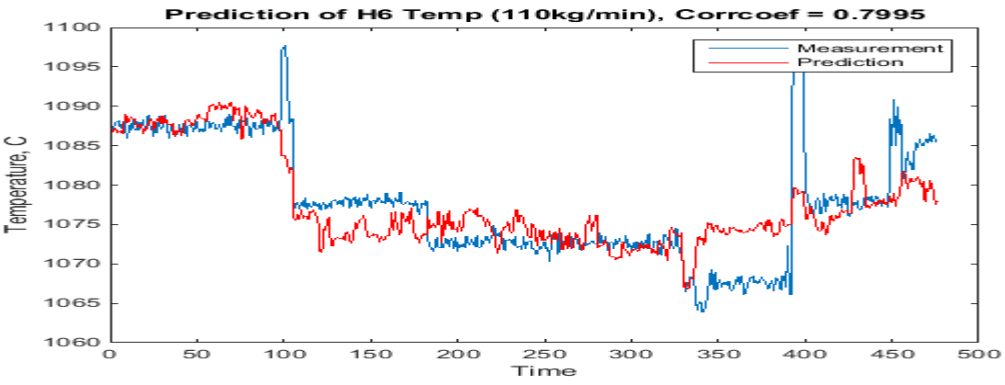

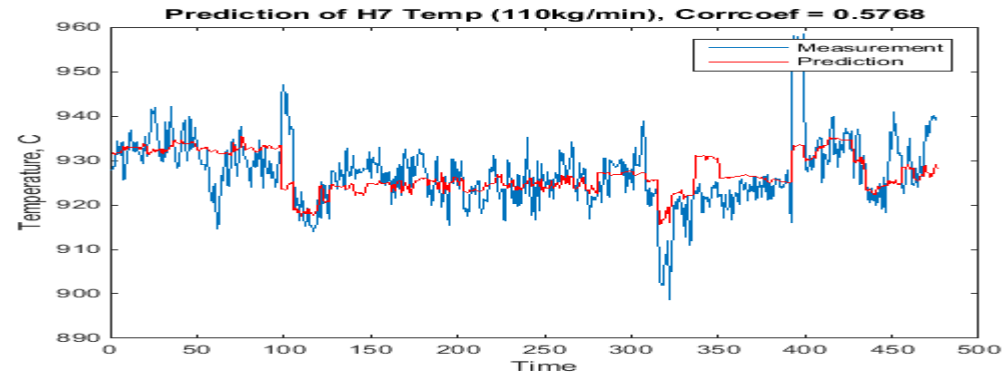

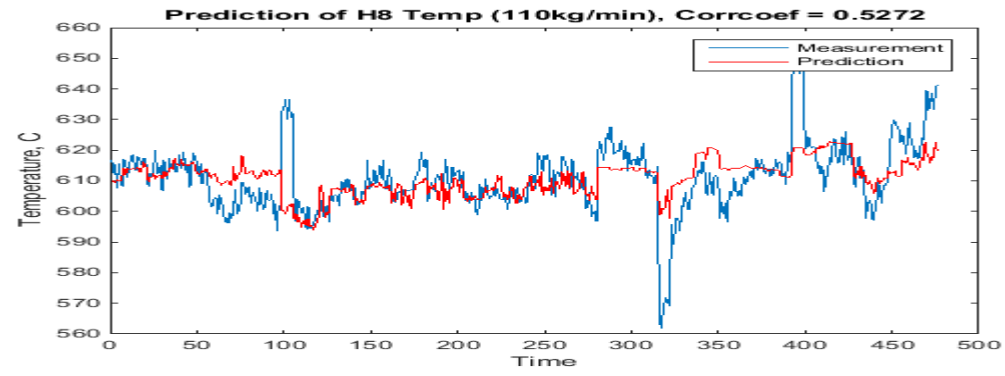

Figures 68-75: Prediction of gas temperature profiles in hearths 1 to 8 using gas flows and walls temperature for Feed rate 110 kg/min

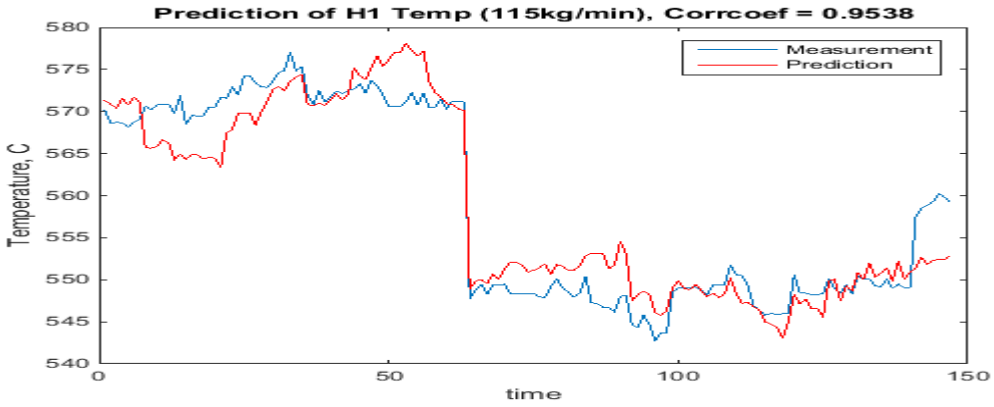
Prediction of H1 Temp (115kg/min), Corrcoef = 0.9538
Measurement
Prediction
Temperature, C
time

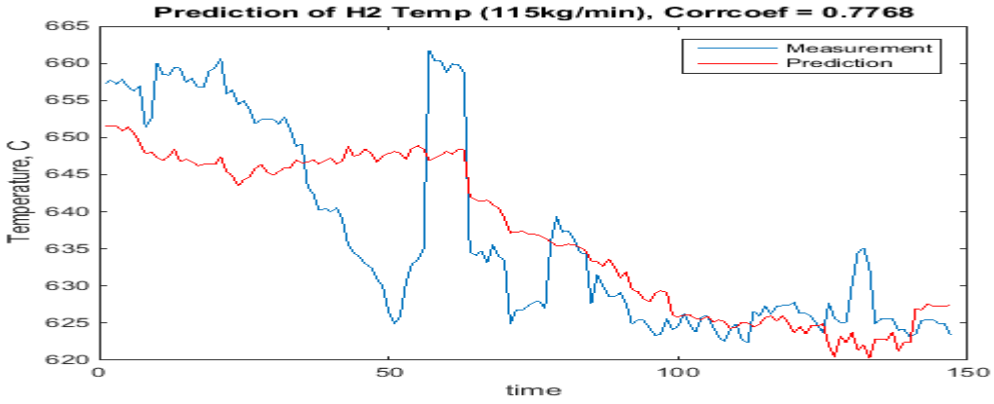
Prediction of H2 Temp (115kg/min), Corrcoef = 0.7768
Measurement
Prediction
Temperature, C
time

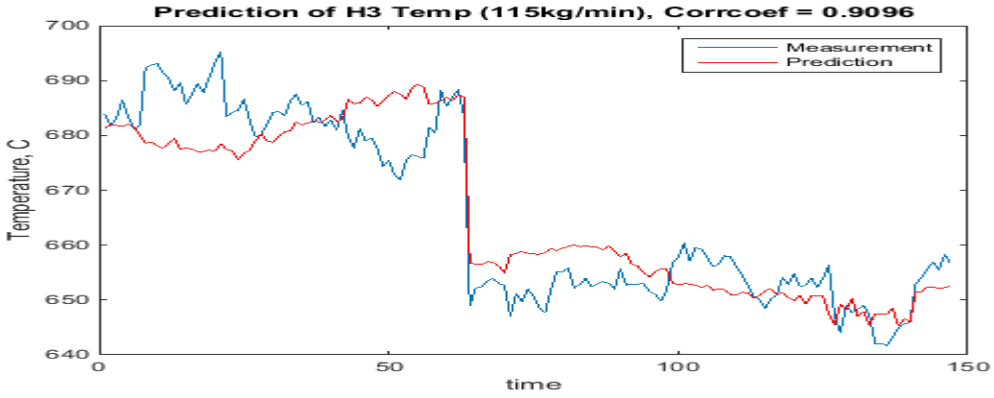
Prediction of H3 Temp (115kg/min), Corrcoef = 0.9096
Measurement
Prediction
Temperature, C
time

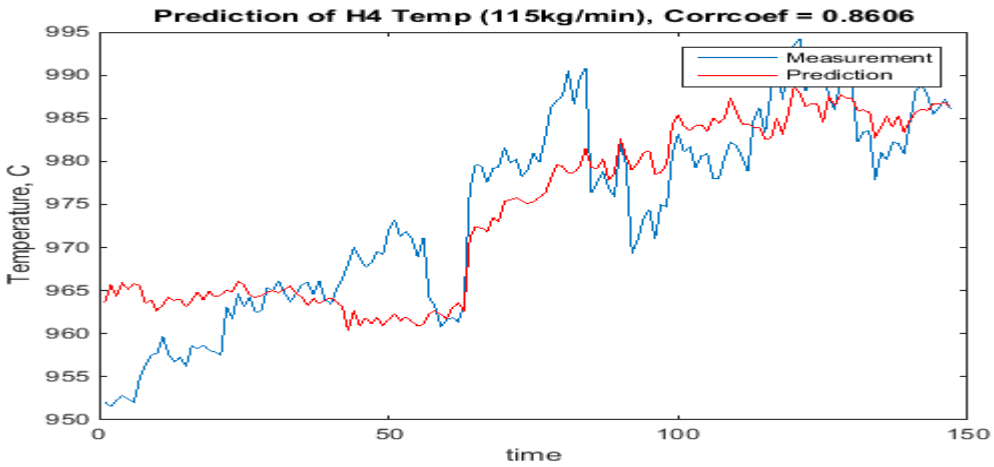
Prediction of H4 Temp (115kg/min), Corrcoef = 0.8606
Measurement
Prediction
Temperature, C
time

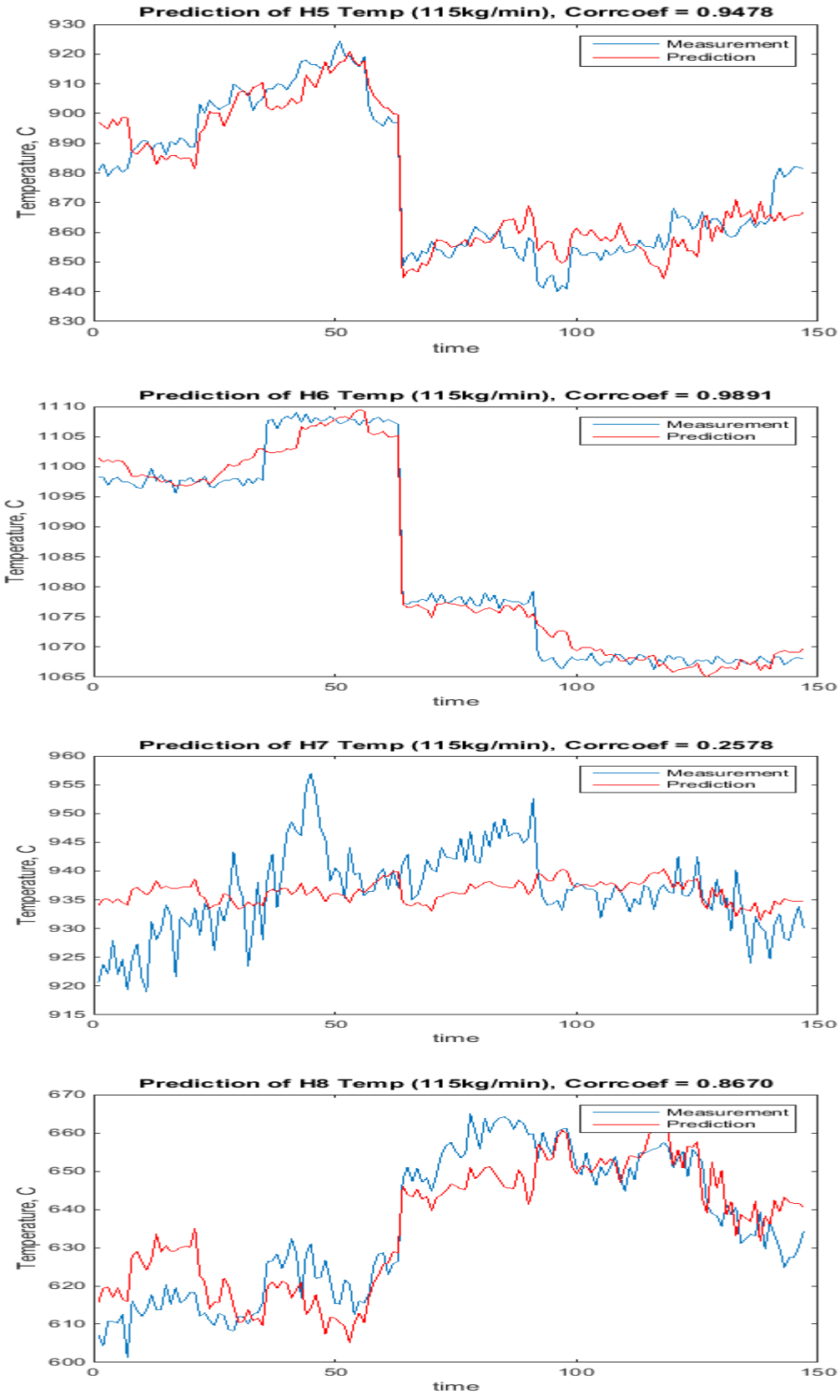

Figures 76-83: Prediction of gas temperature profiles in hearths 1 to 8 using gas flows and walls temperature for Feed rate 115 kg/min

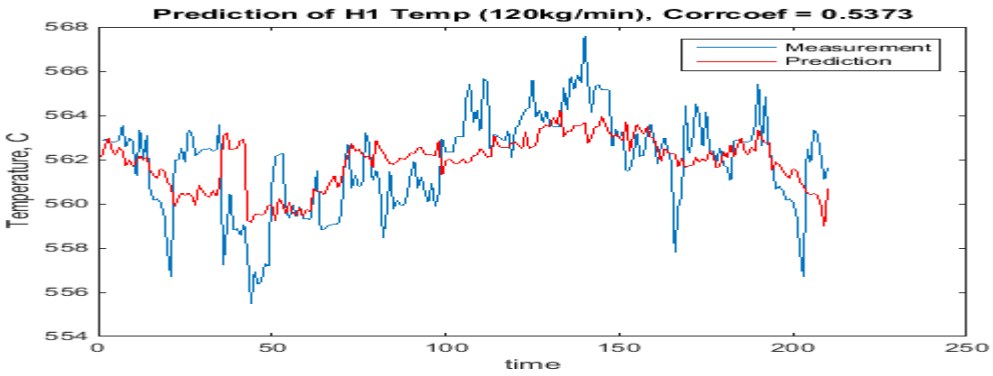
Prediction of H1 Temp (120kg/min), Corrcoef = 0.5373
Measurement
Prediction
Temperature, C
time

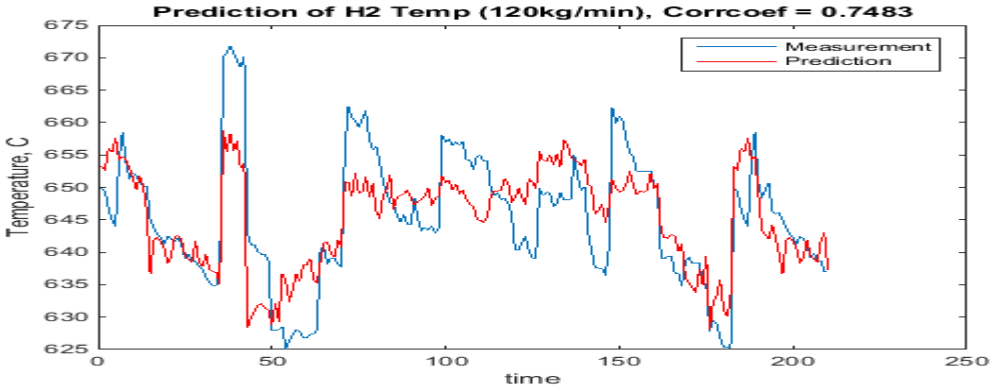
Prediction of H2 Temp (120kg/min), Corrcoef = 0.7483
Measurement
Prediction
Temperature, C
time

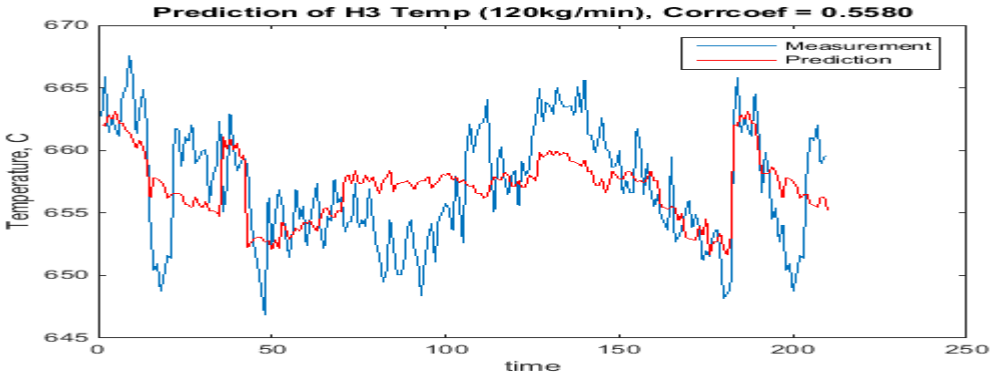
Prediction of H3 Temp (120kg/min), Corrcoef = 0.5580
Measurement
Prediction
Temperature, C
time

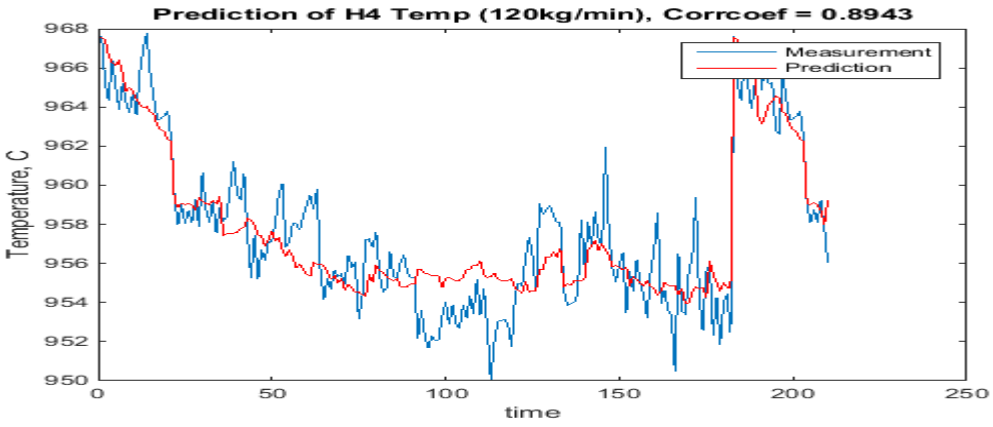
Prediction of H4 Temp (120kg/min), Corrcoef = 0.8943
Measurement
Prediction
Temperature, C
time

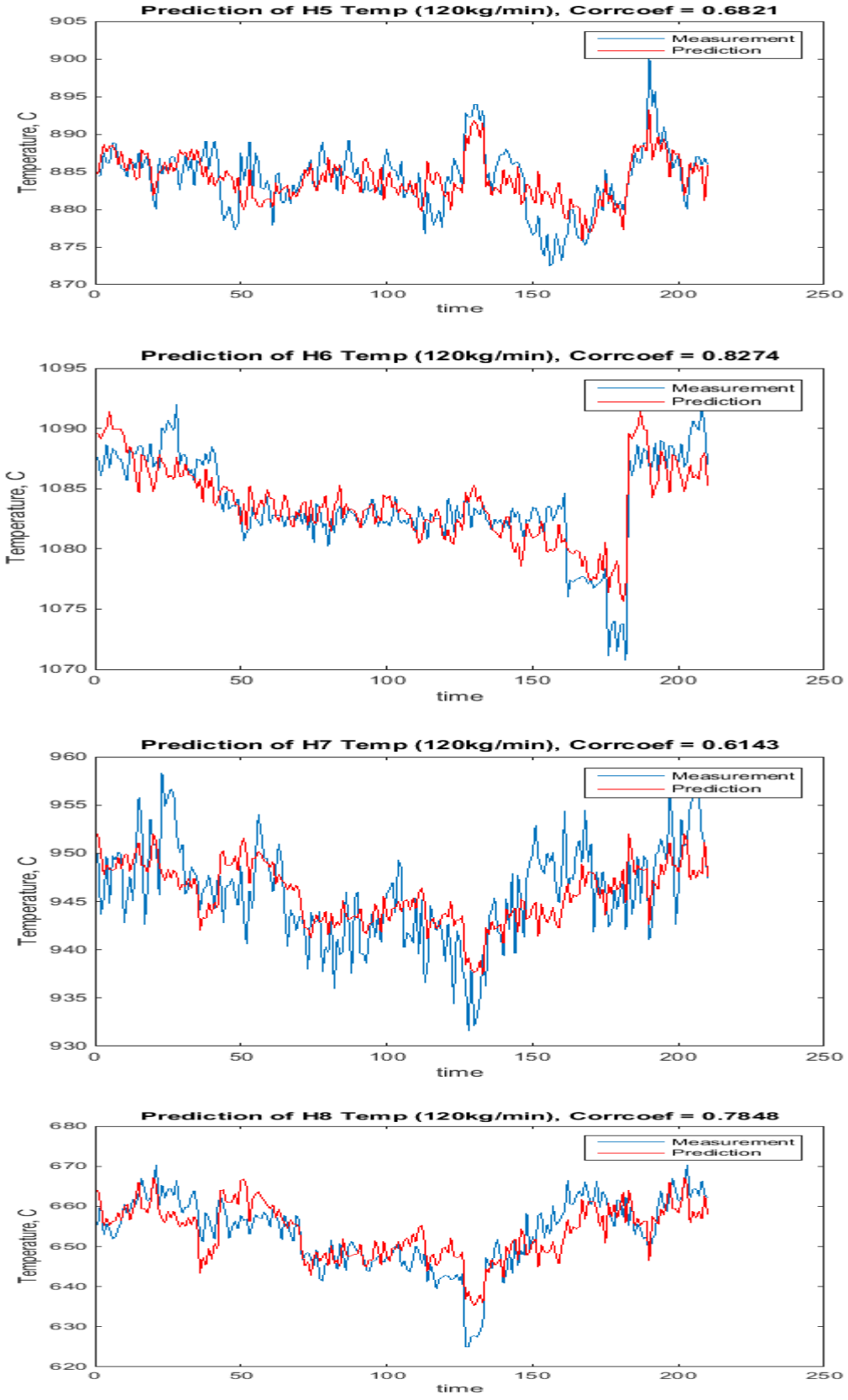

Figures 84-91: Prediction of gas temperature profiles in hearths 1 to 8 using gas flows and walls temperature for Feed rate 120 kg/min

6. Prediction of Gas temperature profiles using Methane gas flows, Furnace Walls temperature and delayed gas temperatures (Dynamic Models).

Figures 92 to 131 are the results of PLS for prediction of gas temperature profiles in hearths 1 to 8 for feed rates 100, 105, 110, 115, 120 kg/min.

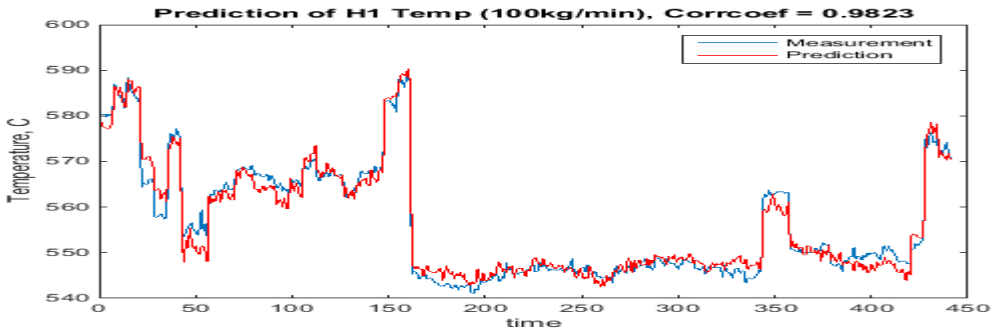

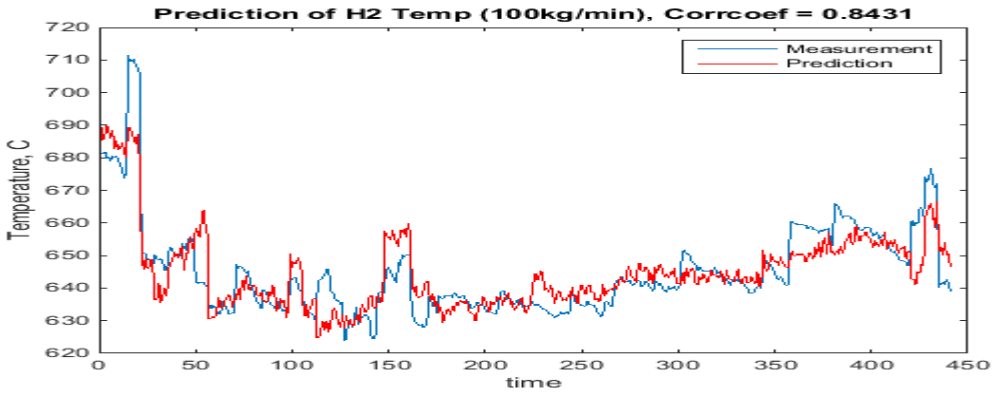

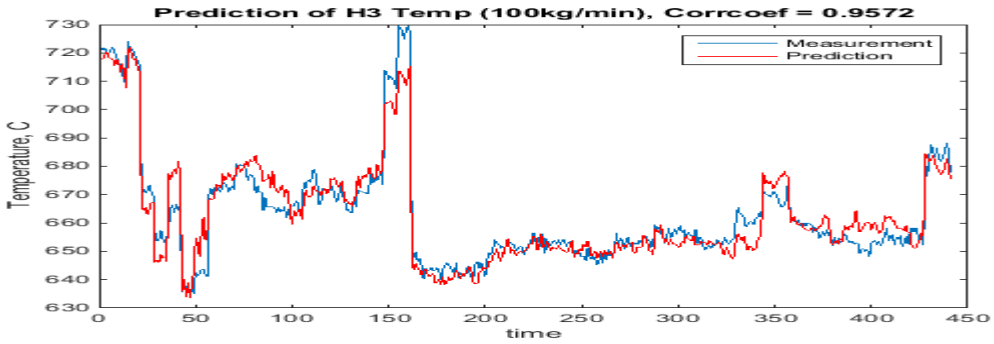

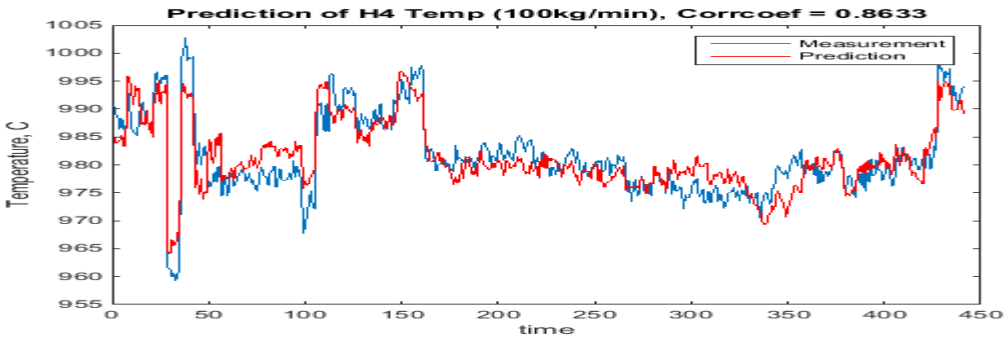

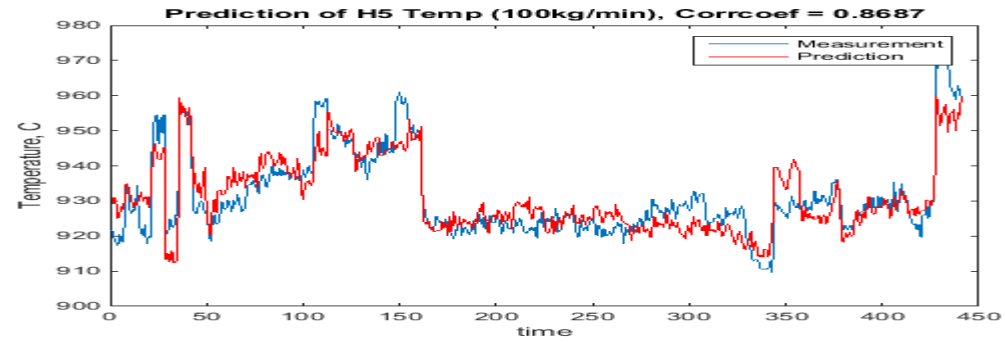

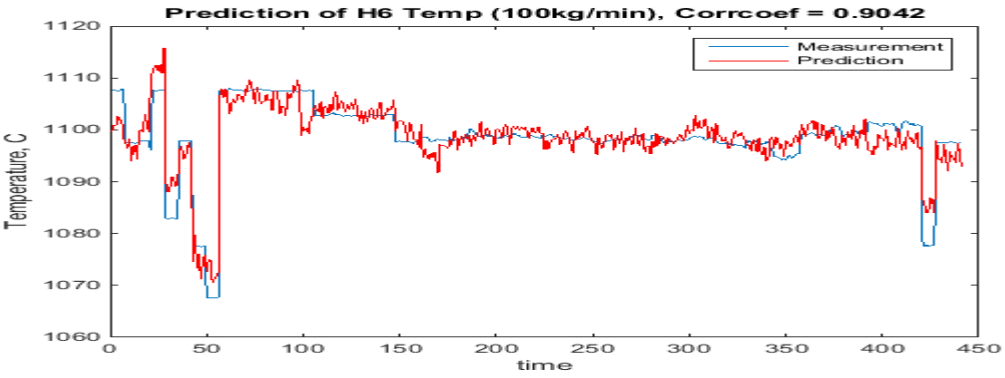

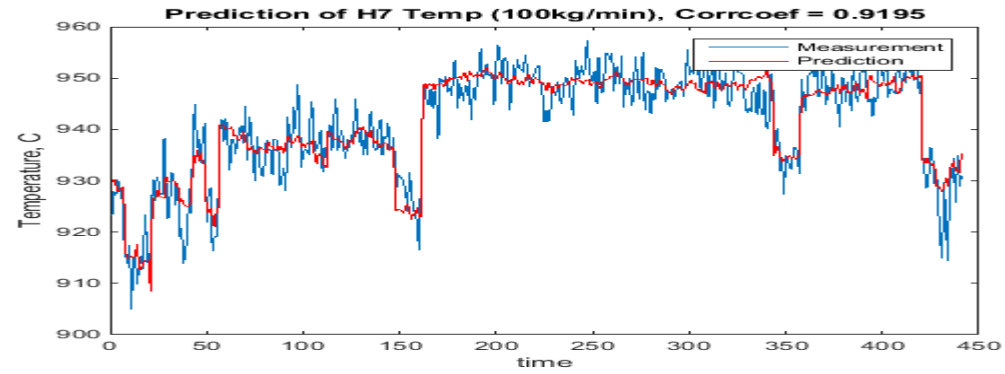

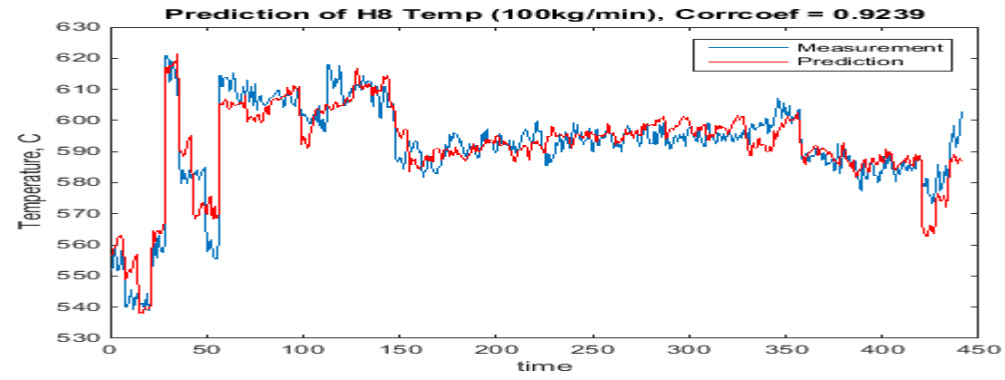

Figures 92-99: Prediction of gas temperature profiles in hearths 1 to 8 using gas flows, walls temperature and delayed gas temperatures for Feed rate 100 kg/min

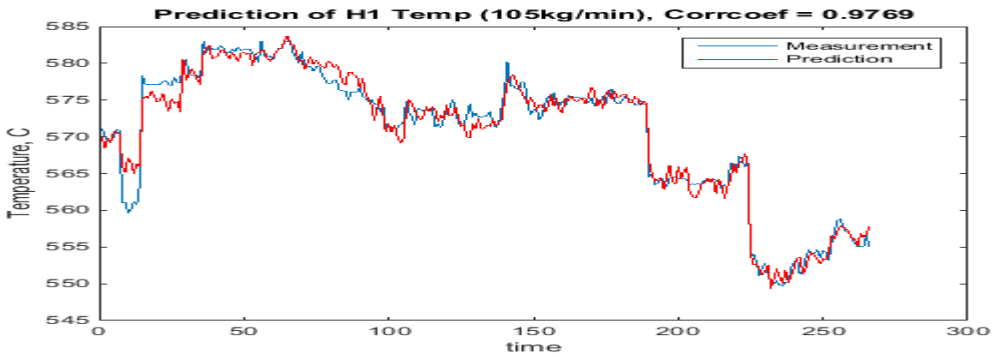
Prediction of H1 Temp (105kg/min), Corrcoef = 0.9769
Measurement
Prediction
Temperature, C
time

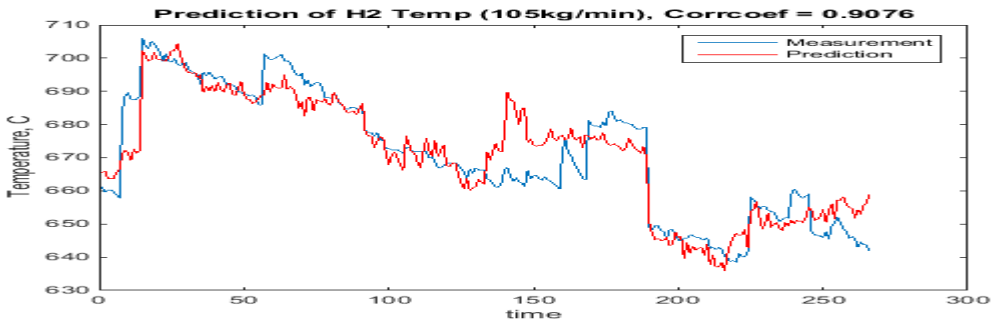
Prediction of H2 Temp (105kg/min), Corrcoef = 0.9076
Measurement
Prediction
Temperature, C
time

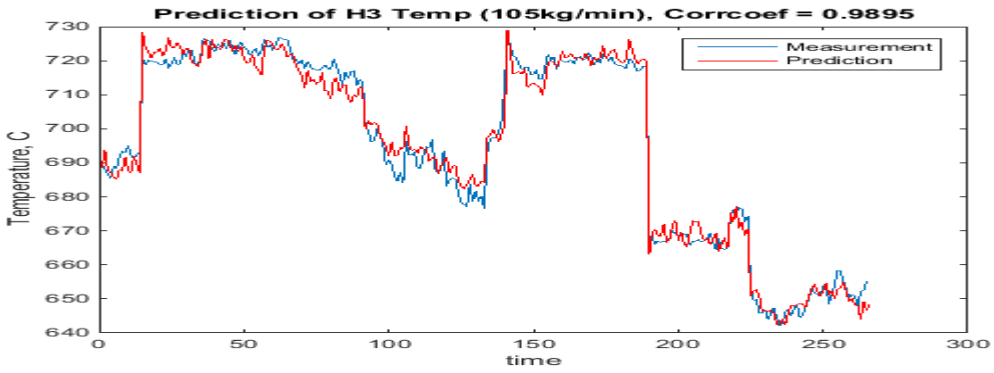
Prediction of H3 Temp (105kg/min), Corrcoef = 0.9895
Measurement
Prediction
Temperature, C
time

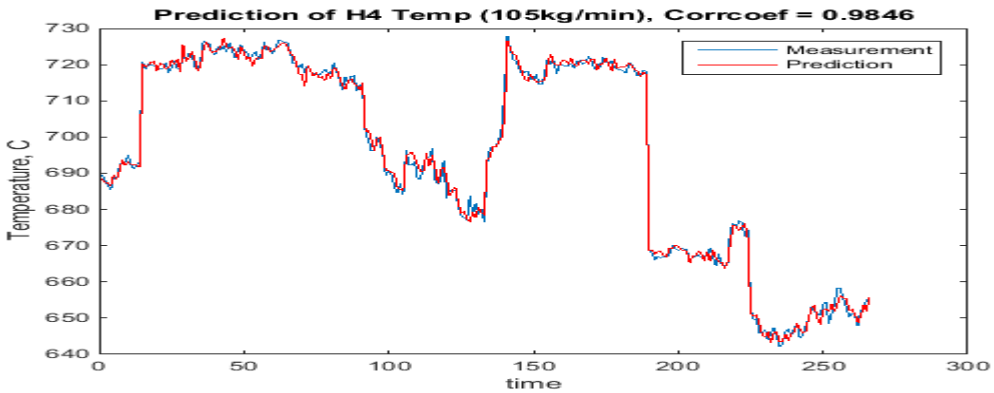
Prediction of H4 Temp (105kg/min), Corrcoef = 0.9846
Measurement
Prediction
Temperature, C
time

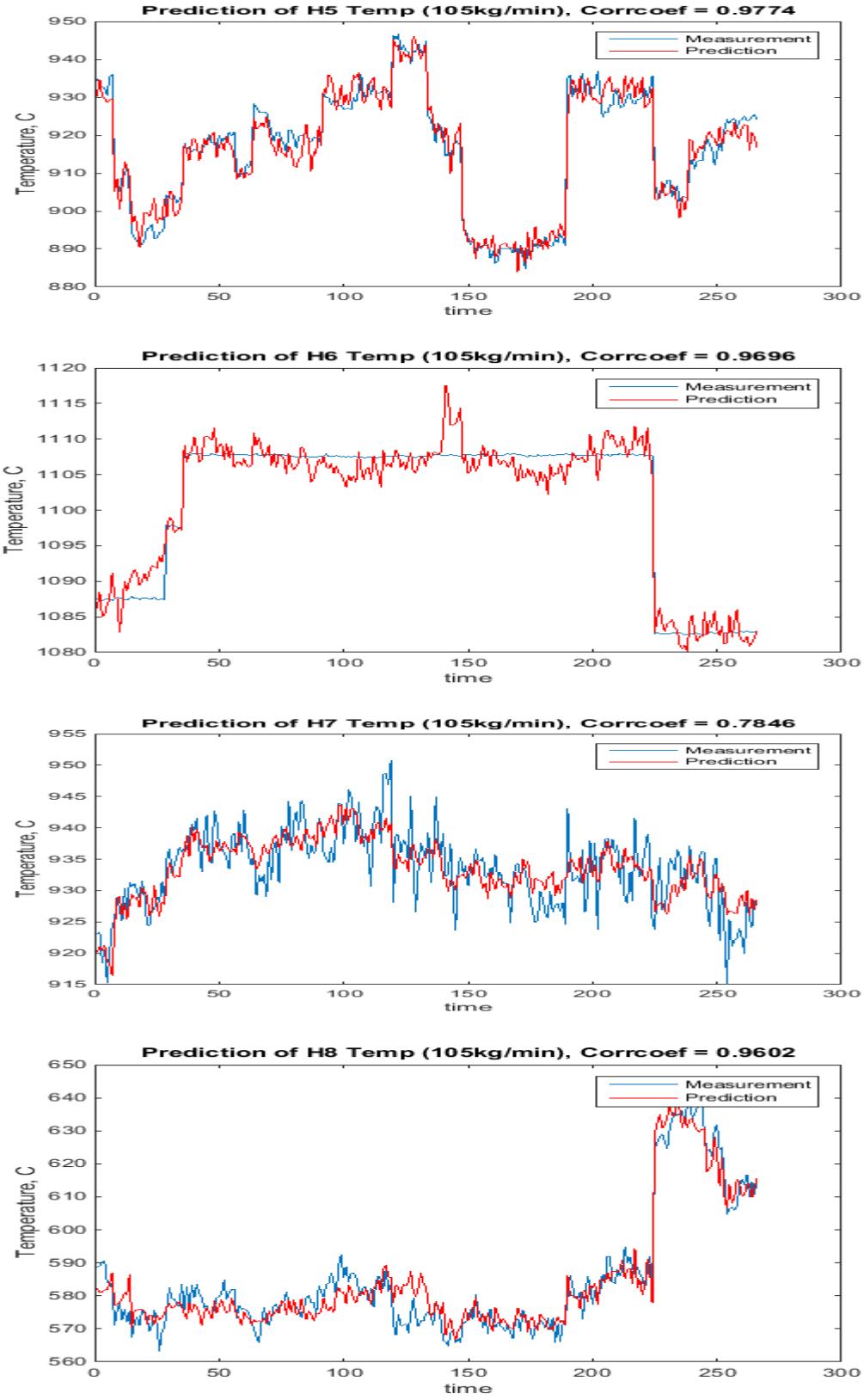

Figures 100-107: Prediction of gas temperature profiles in hearths 1 to 8 using gas flows, walls temperature and delayed gas temperatures for Feed rate 100 kg/min

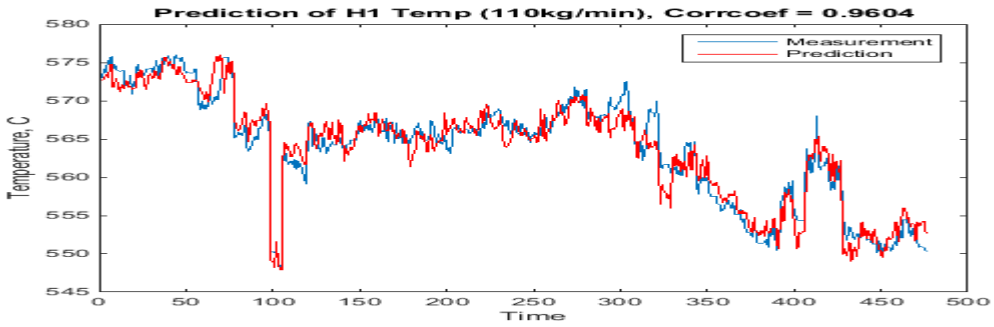
Prediction of H1 Temp (110kg/min), Corrcoef = 0.9604
Measurement
Prediction
Temperature, C
Time

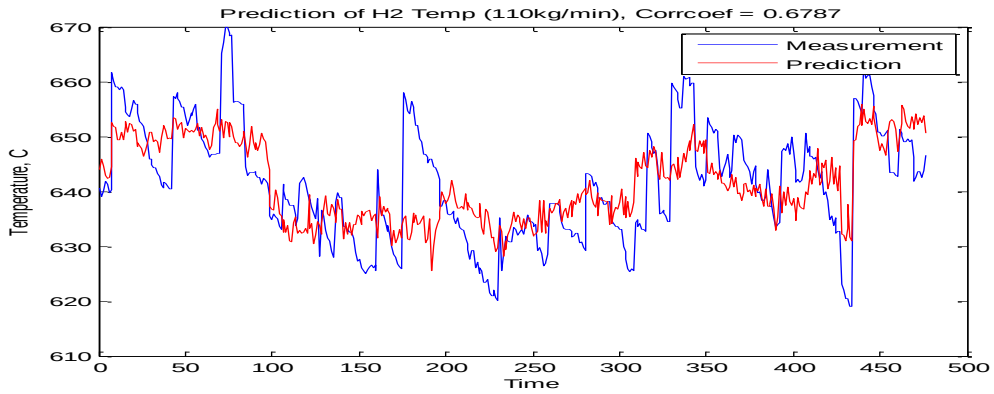
Prediction of H2 Temp (110kg/min), Corrcoef = 0.6787
Measurement
Prediction
Temperature, C
Time

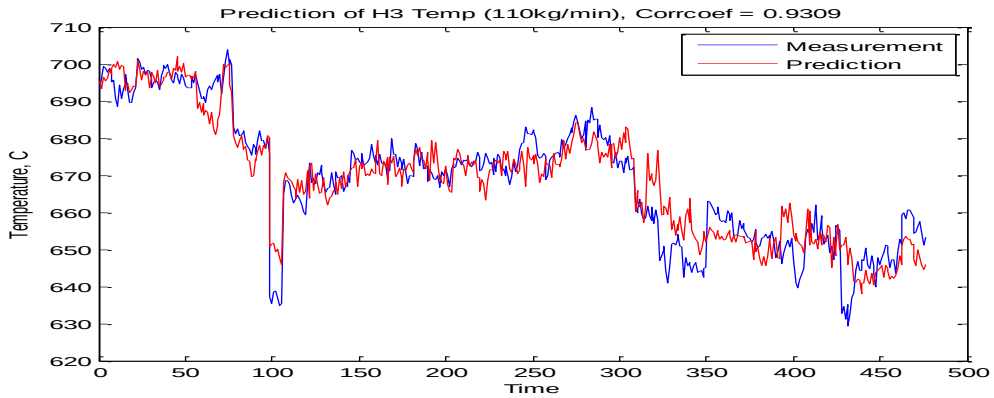
Prediction of H3 Temp (110kg/min), Corrcoef = 0.9309
Measurement
Prediction
Temperature, C
Time

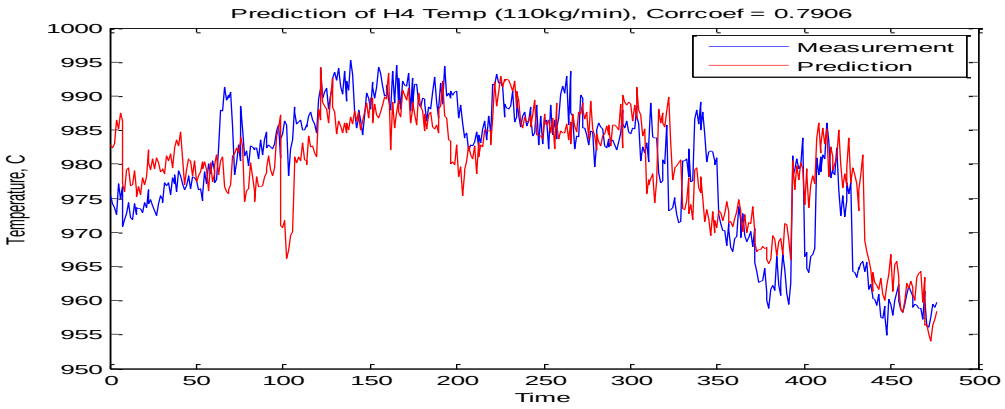
Prediction of H4 Temp (110kg/min), Corrcoef = 0.7906
Measurement
Prediction
Temperature, C
Time

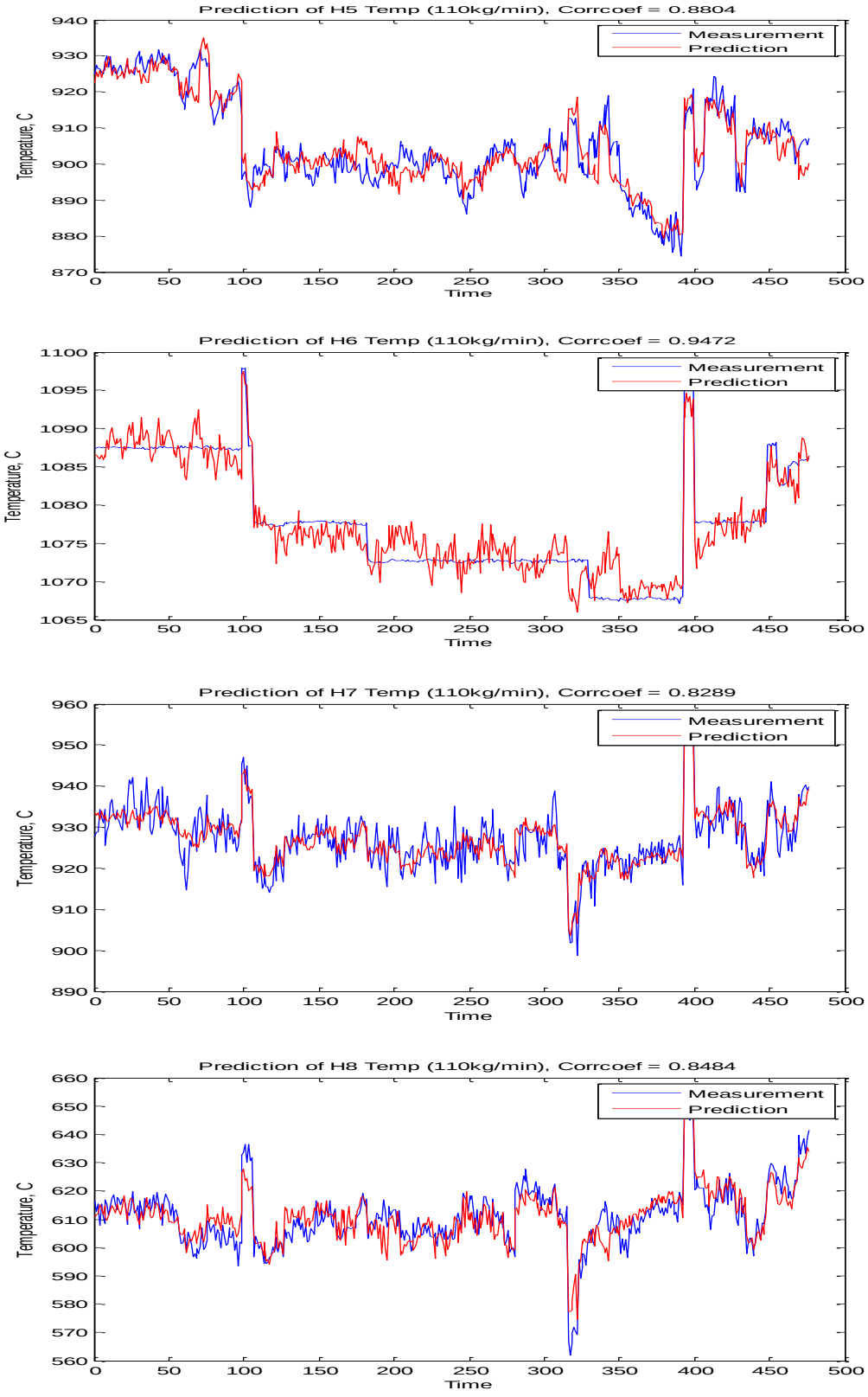

Figures 108-115: Prediction of gas temperature profiles in hearths 1 to 8 using gas flows, walls temperature and delayed gas temperatures for Feed rate 100 kg/min

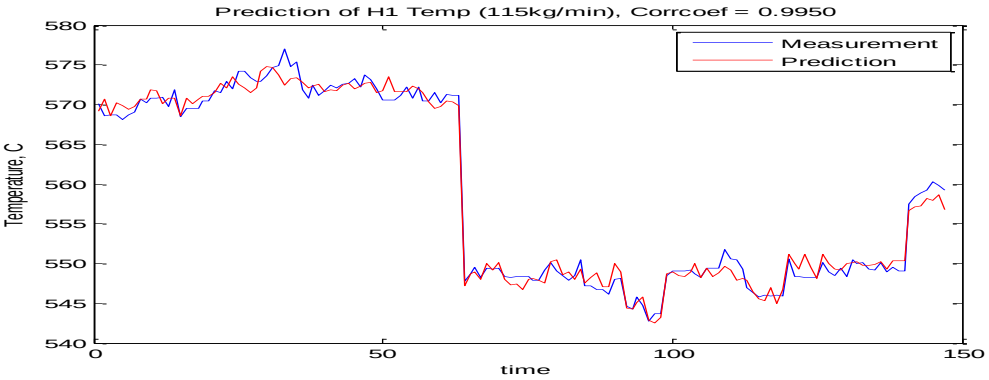
Prediction of H1 Temp (115kg/min), Corrcoef = 0.9950
Measurement
Prediction
Temperature, C
time
580
575
570
565
560
555
550
545
540
0
50
100
150

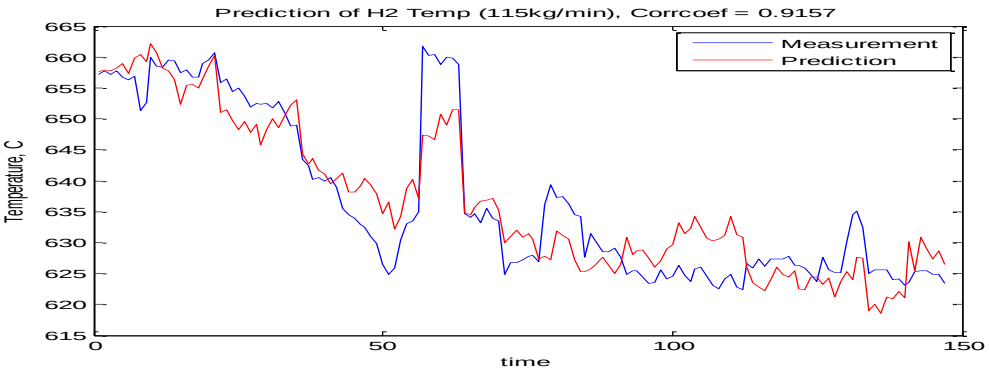
Prediction of H2 Temp (115kg/min), Corrcoef = 0.9157
Measurement
Prediction
Temperature, C
time
665
660
655
650
645
640
635
630
625
620
615
0
50
100
150

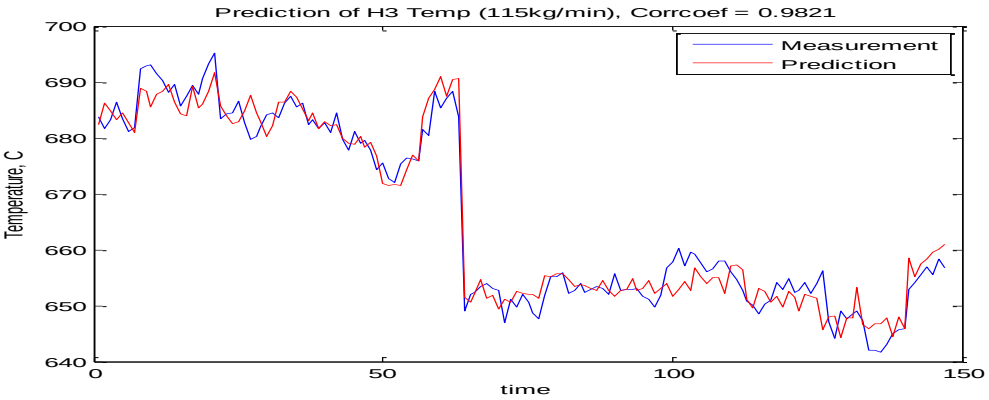
Prediction of H3 Temp (115kg/min), Corrcoef = 0.9821
Measurement
Prediction
Temperature, C
time
700
690
680
670
660
650
640
0
50
100
150

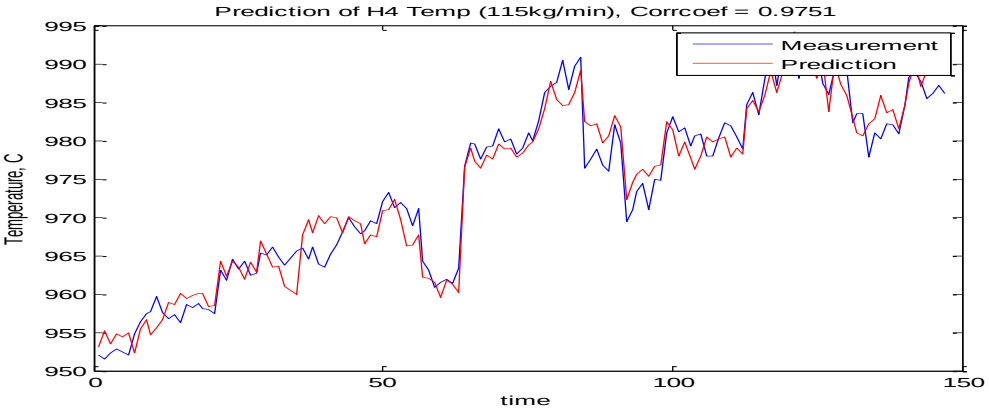
Prediction of H4 Temp (115kg/min), Corrcoef = 0.9751
Measurement
Prediction
Temperature, C
time
995
990
985
980
975
970
965
960
955
950
0
50
100
150

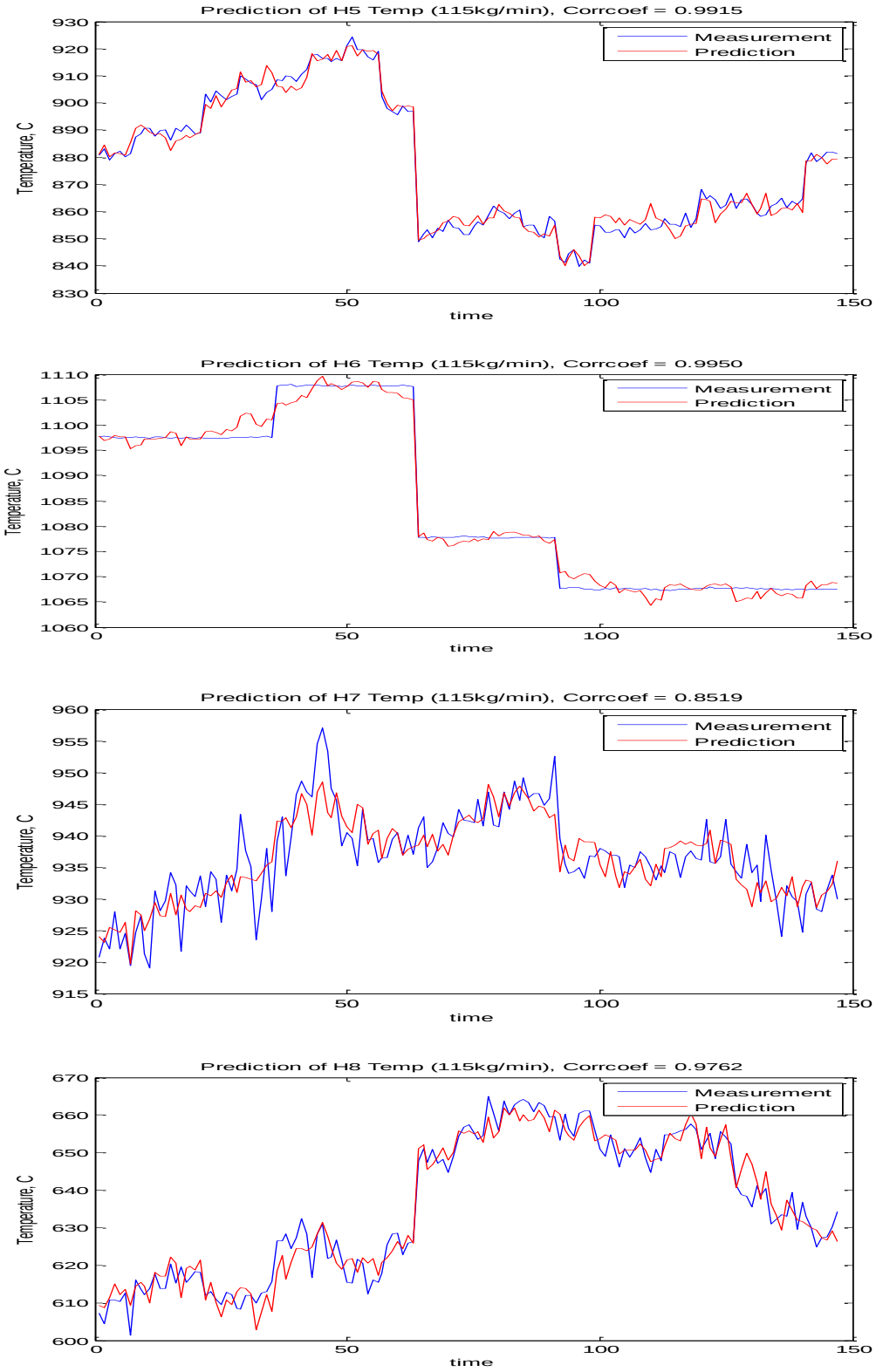

Figures 116-123: Prediction of gas temperature profiles in hearths 1 to 8 using gas flows, walls temperature and delayed gas temperatures for Feed rate 115 kg/min

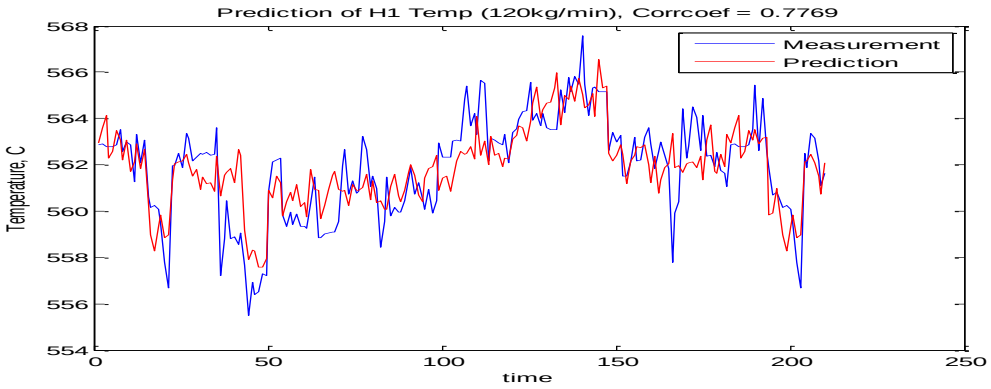
Prediction of H1 Temp (120kg/min), Corrcoef = 0.7769
Measurement
Prediction
Temperature, C
time
568
566
564
562
560
558
556
554
0
50
100
150
200
250

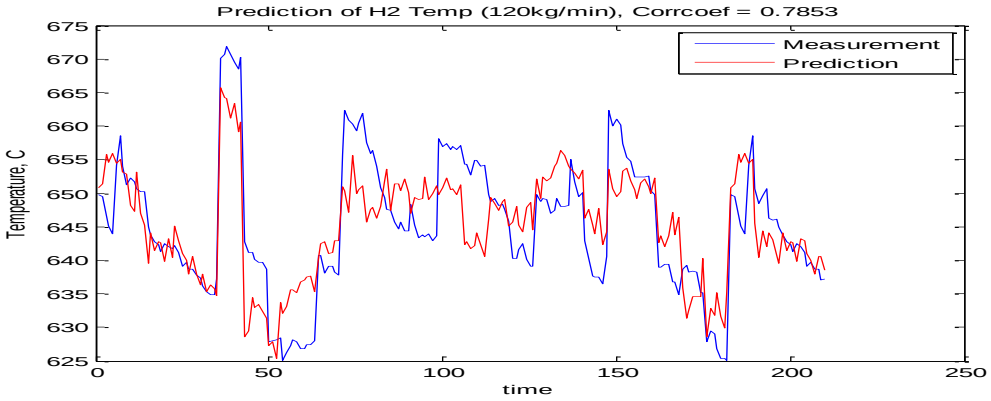
Prediction of H2 Temp (120kg/min), Corrcoef = 0.7853
Measurement
Prediction
Temperature, C
time
675
670
665
660
655
650
645
640
635
630
625
0
50
100
150
200
250

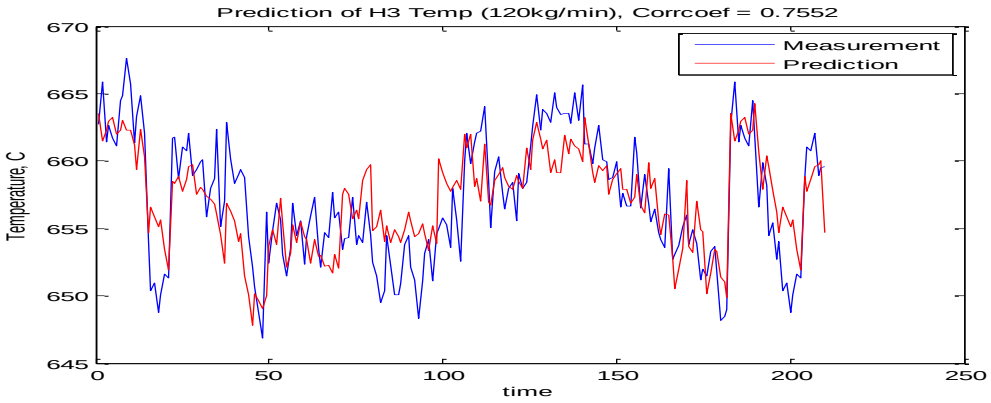
Prediction of H3 Temp (120kg/min), Corrcoef = 0.7552
Measurement
Prediction
Temperature, C
time
670
665
660
655
650
645
0
50
100
150
200
250

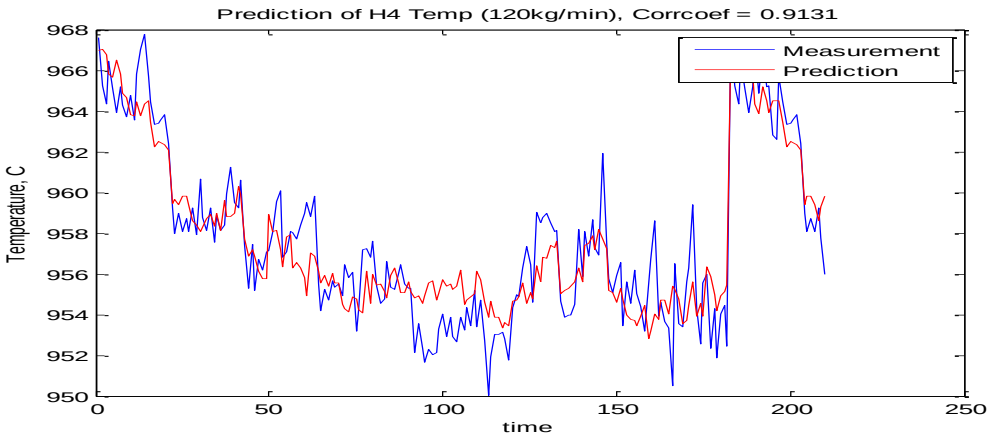
Prediction of H4 Temp (120kg/min), Corrcoef = 0.9131
Measurement
Prediction
Temperature, C
time
968
966
964
962
960
958
956
954
952
950
0
50
100
150
200
250

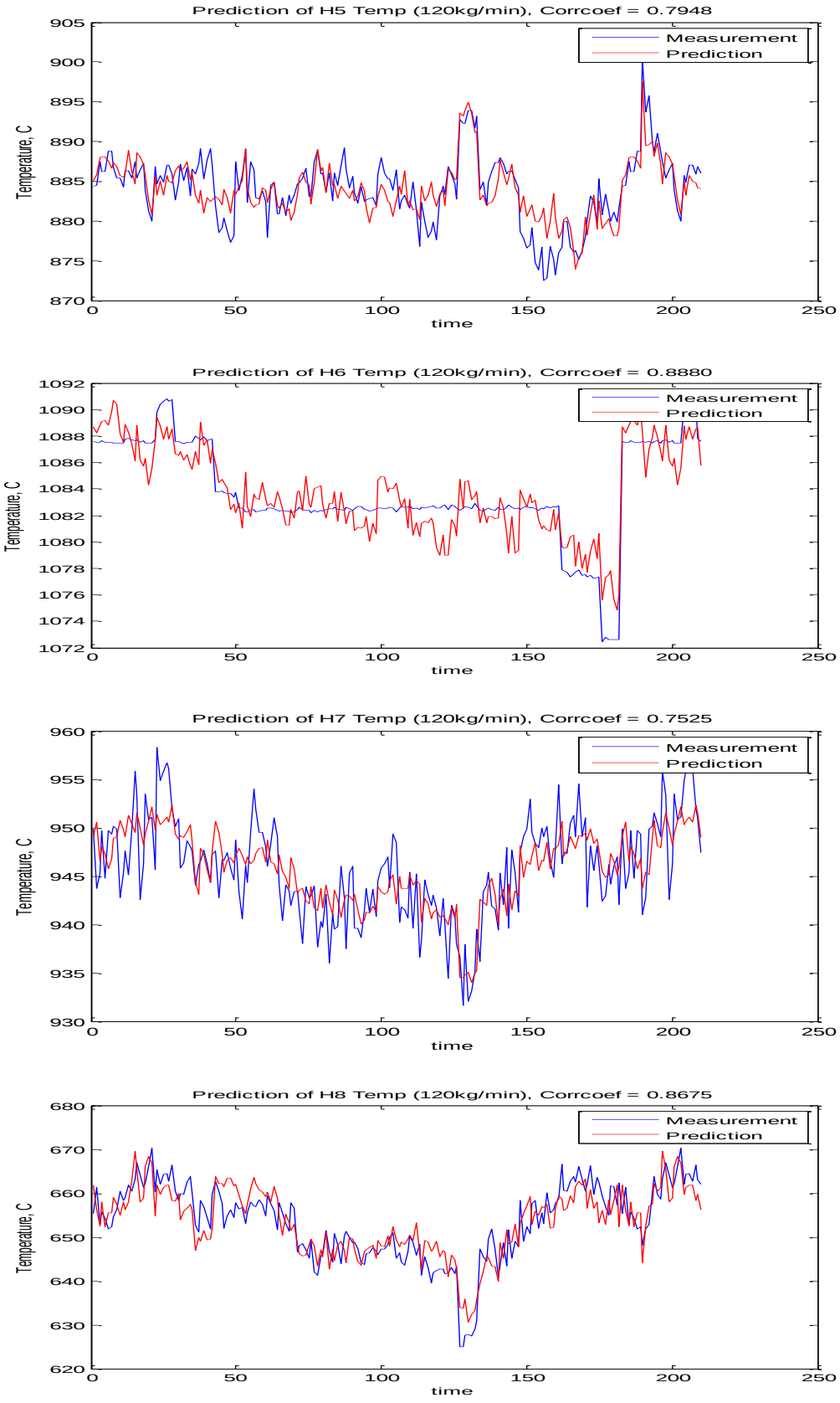

Figures 124-131: Prediction of gas temperature profiles in hearths 1 to 8 using gas flows, walls temperature and delayed gas temperatures for Feed rate 120 kg/min

7. Prediction of Gas temperature profiles using the ratios of Methane gas flows to each burner, Furnace Walls temperature and the delayed gas temperatures (Dynamic Models).

Figures 132 to 131 are the results of PLS for prediction of gas temperature profiles in hearths 1 to 8 for feed rates 100, 105, 110, 115, 120 kg/min.

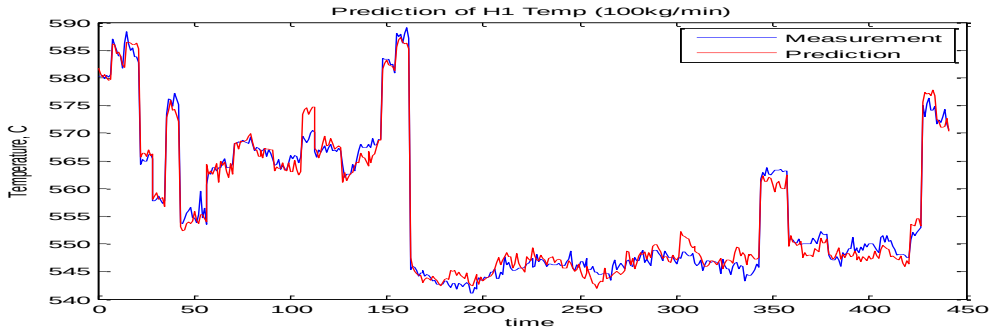

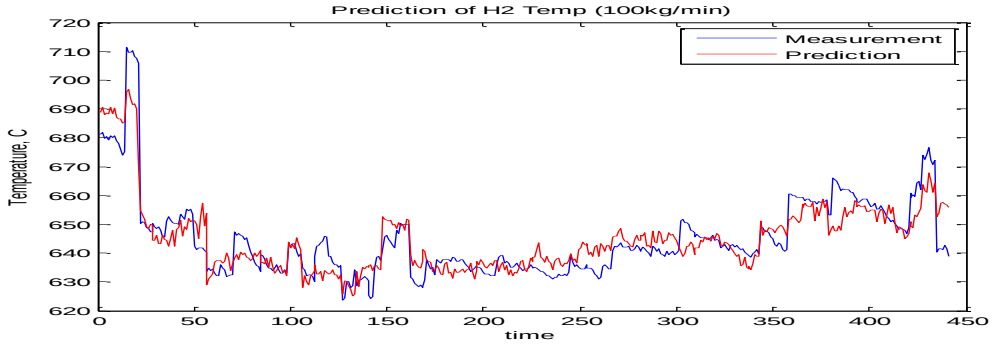

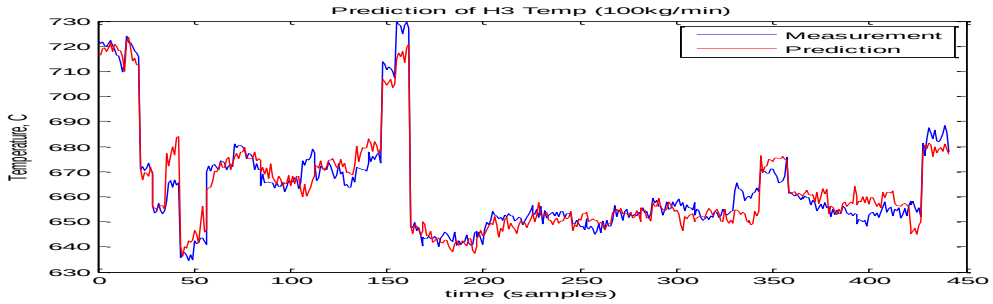

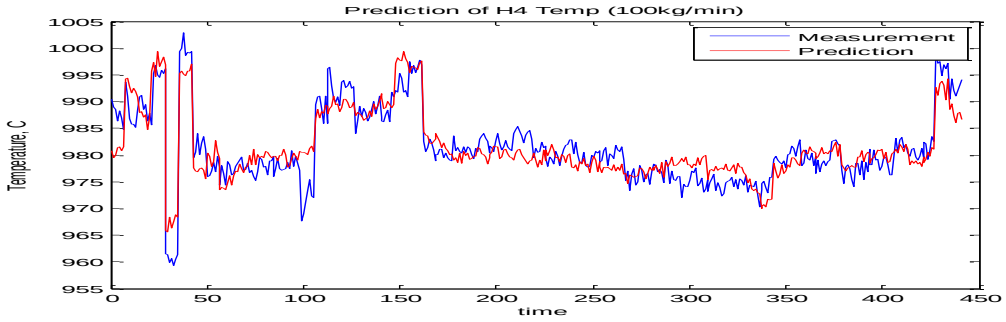

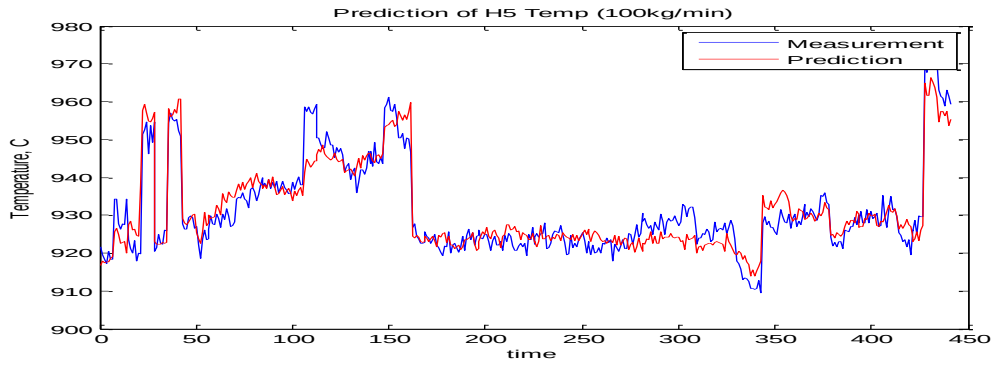
Prediction of H5 Temp (100kg/min)
Measurement
Prediction
Temperature, C
time

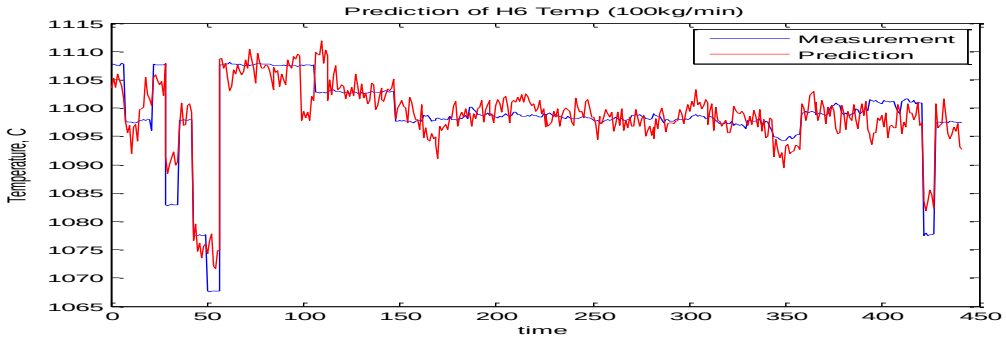
Prediction of H6 Temp (100kg/min)
Measurement
Prediction
Temperature, C
time

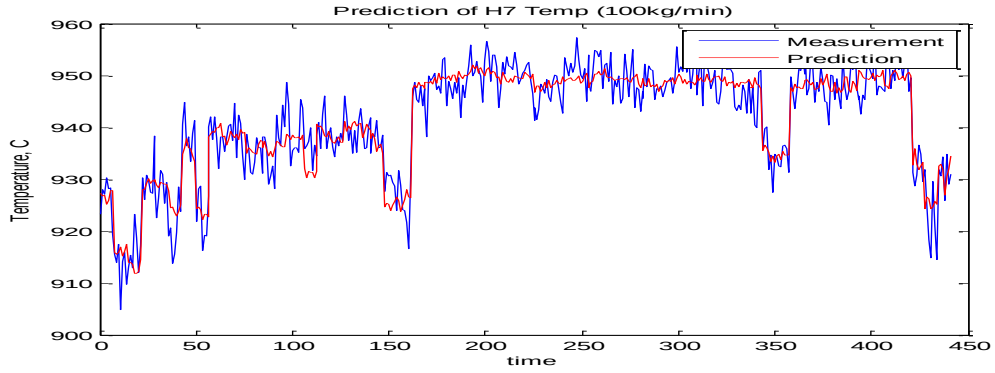
Prediction of H7 Temp (100kg/min)
Measurement
Prediction
Temperature, C
time

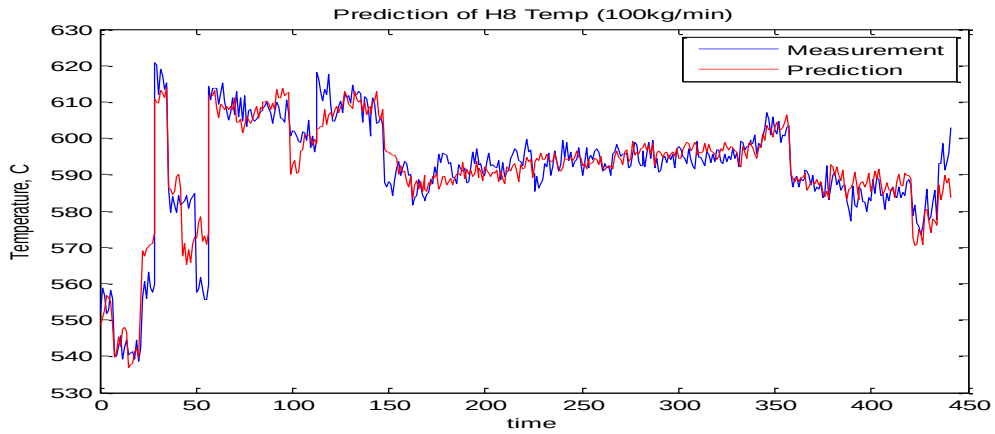
Prediction of H8 Temp (100kg/min)
Measurement
Prediction
Temperature, C
time

Figures 124-139: Prediction of gas temperature profiles in hearths 1 to 8 using the individual gas flow to each burner, walls temperature and delayed gas temperatures for Feed rate 100 kg/min

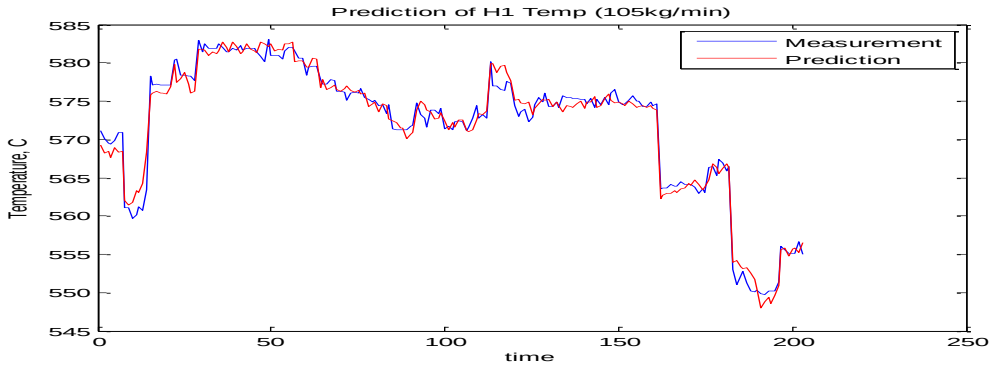

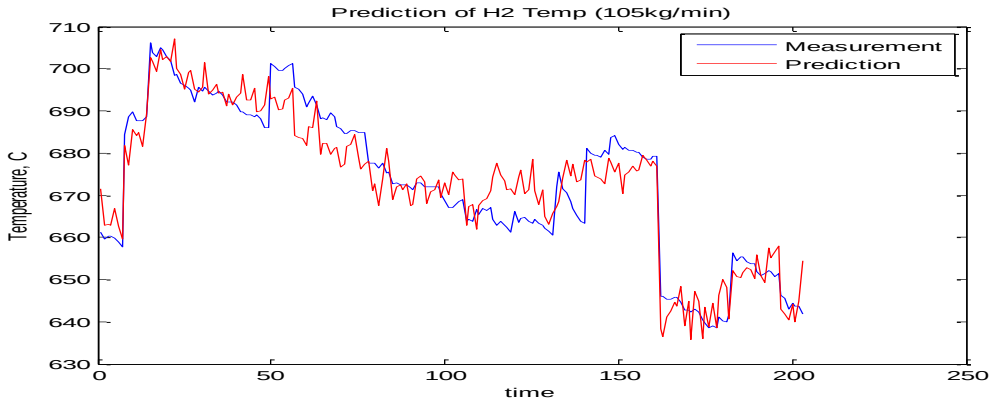

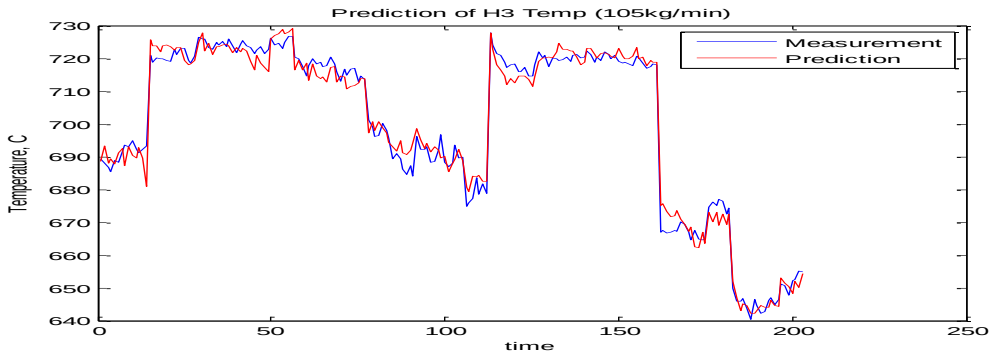

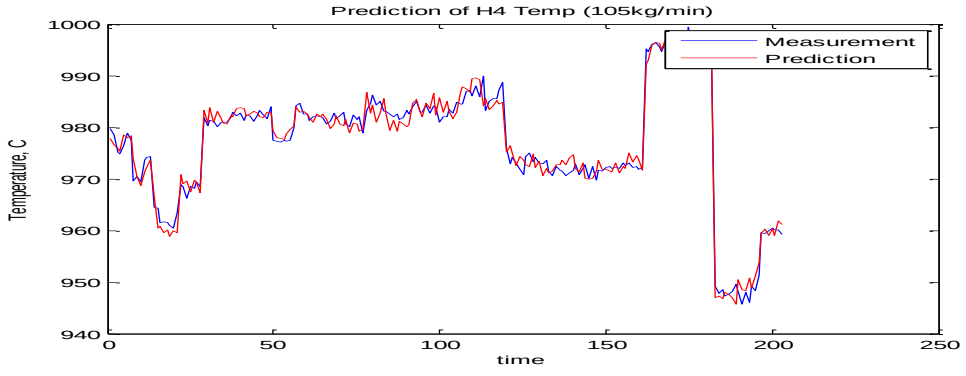

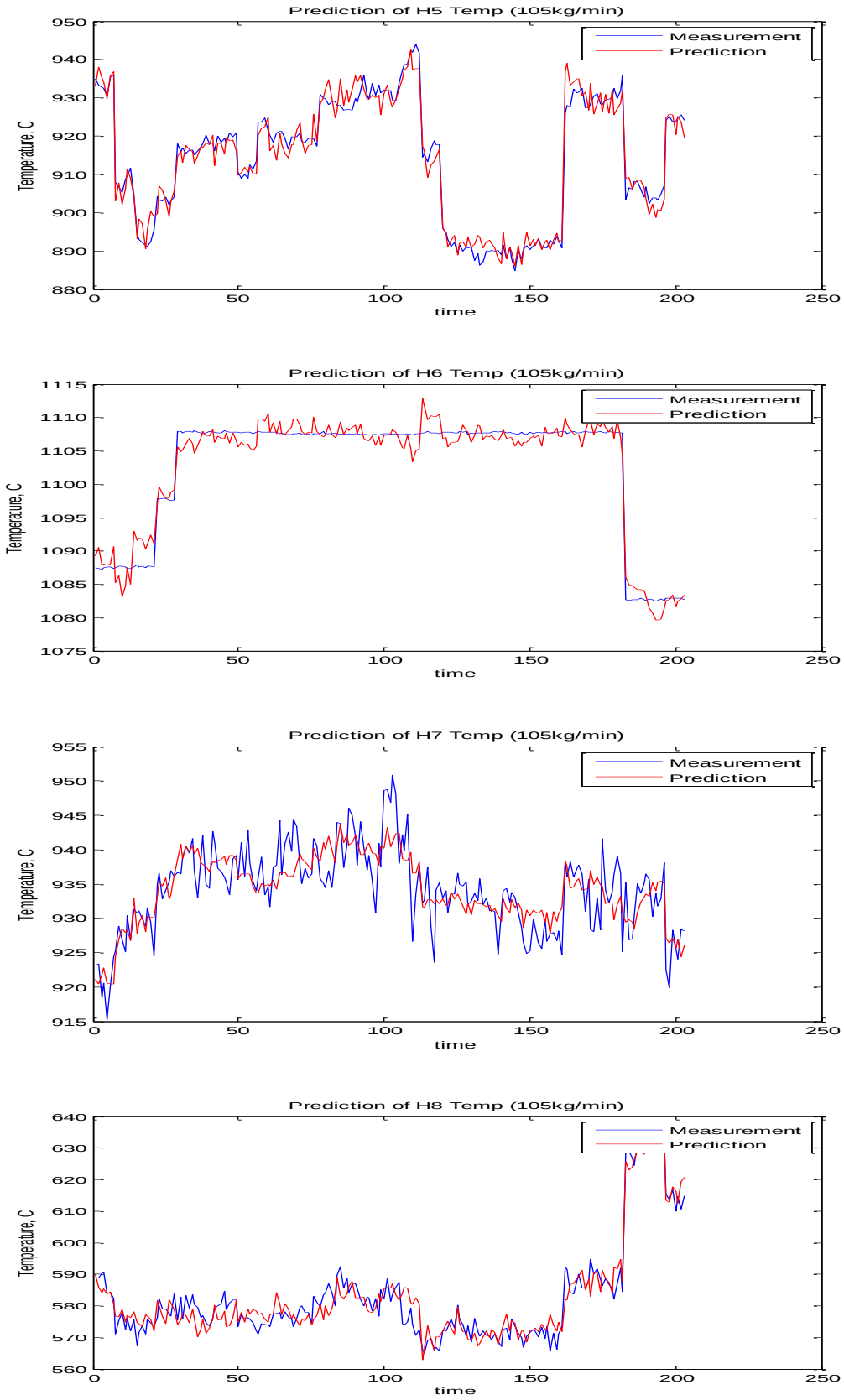

Figures 140-147: Prediction of gas temperature profiles in hearths 1 to 8 using the individual gas flow to each burner, walls temperature and delayed gas temperatures for Feed rate 105 kg/min

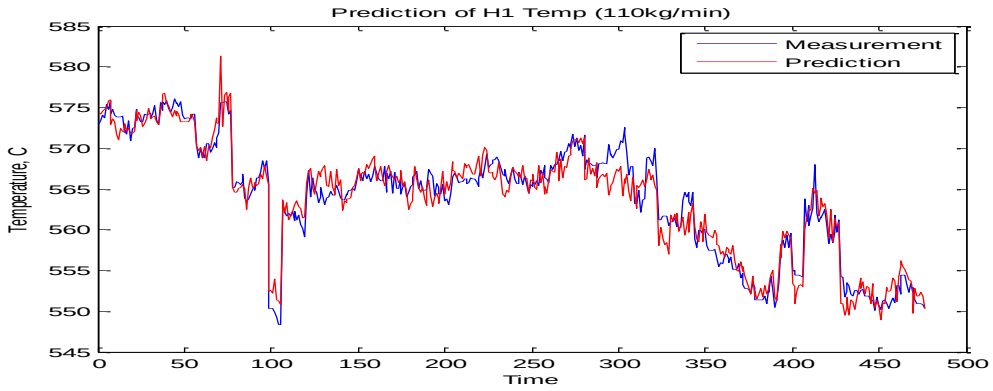
Prediction of H1 Temp (110kg/min)
Measurement
Prediction
Temperature, C
Time

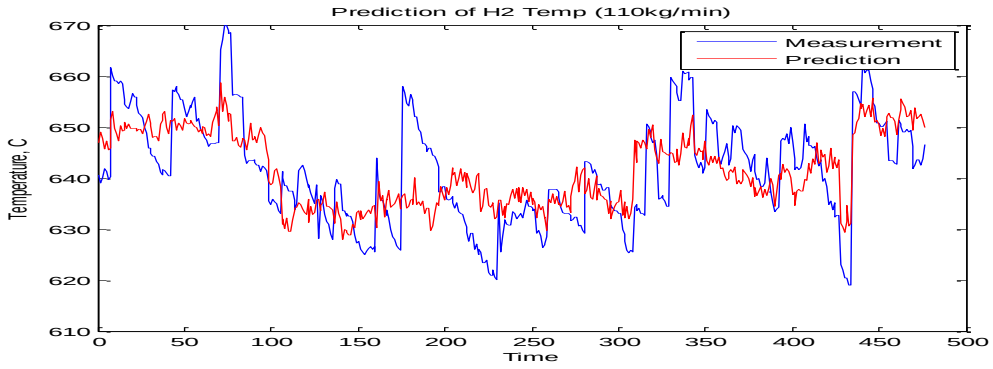
Prediction of H2 Temp (110kg/min)
Measurement
Prediction
Temperature, C
Time

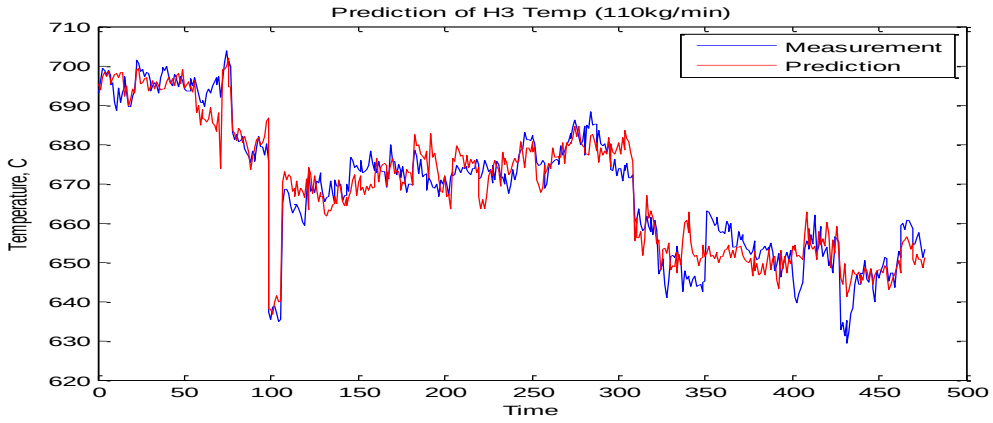
Prediction of H3 Temp (110kg/min)
Measurement
Prediction
Temperature, C
Time

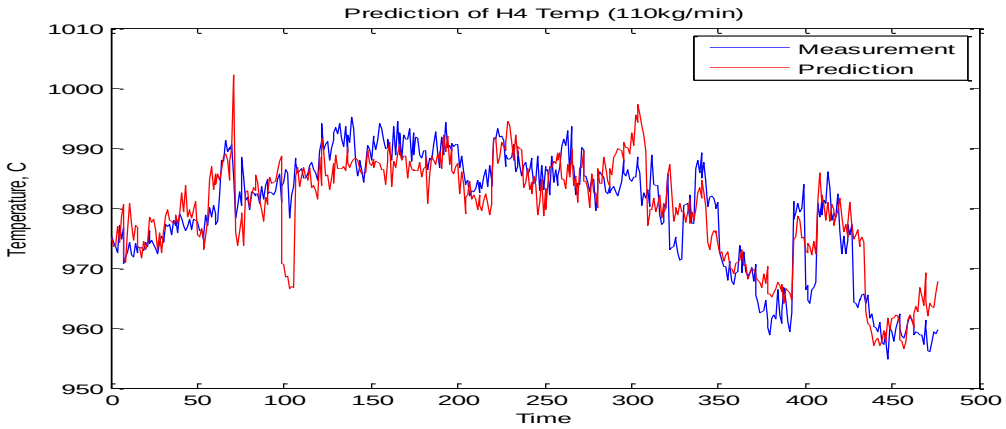
Prediction of H4 Temp (110kg/min)
Measurement
Prediction
Temperature, C
Time

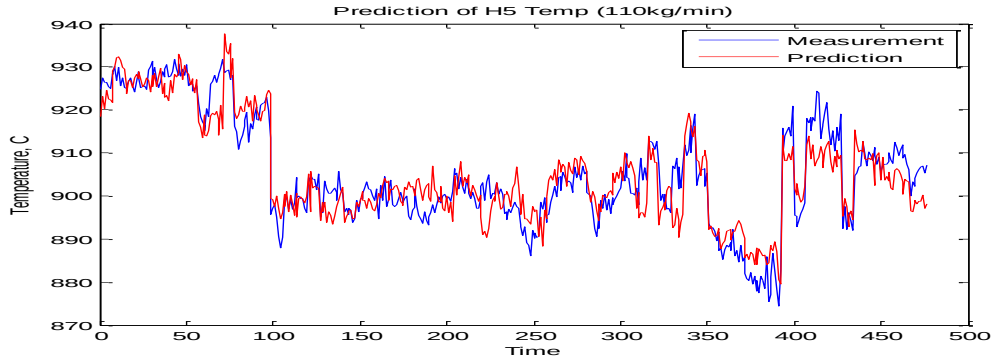

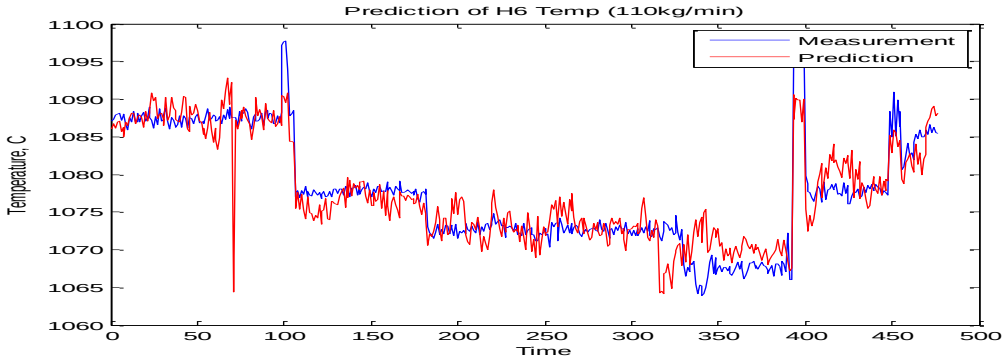

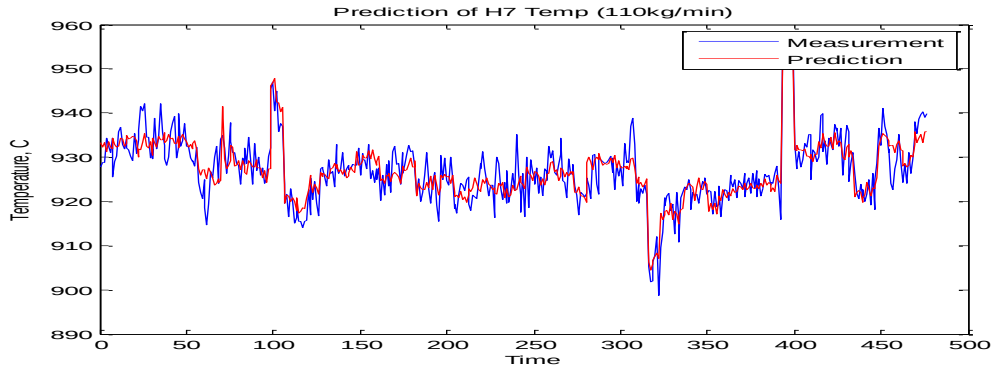

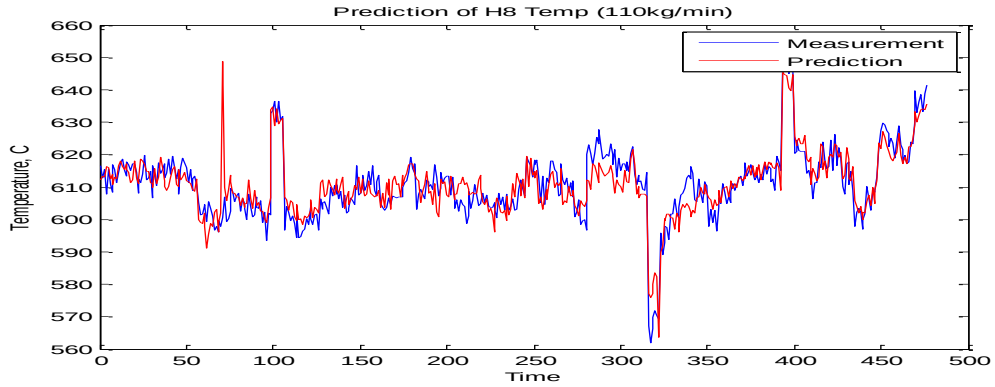

Figures 148-155: Prediction of gas temperature profiles in hearths 1 to 8 using the individual gas flow to each burner, walls temperature and delayed gas temperatures for Feed rate 110 kg/min

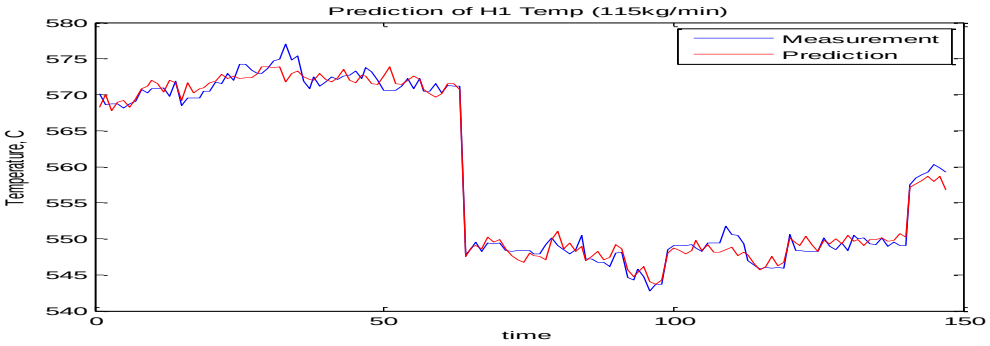
Prediction of H1 Temp (115kg/min)
Measurement
Prediction
Temperature, C
time
580
575
570
565
560
555
550
545
540
0
50
100
150

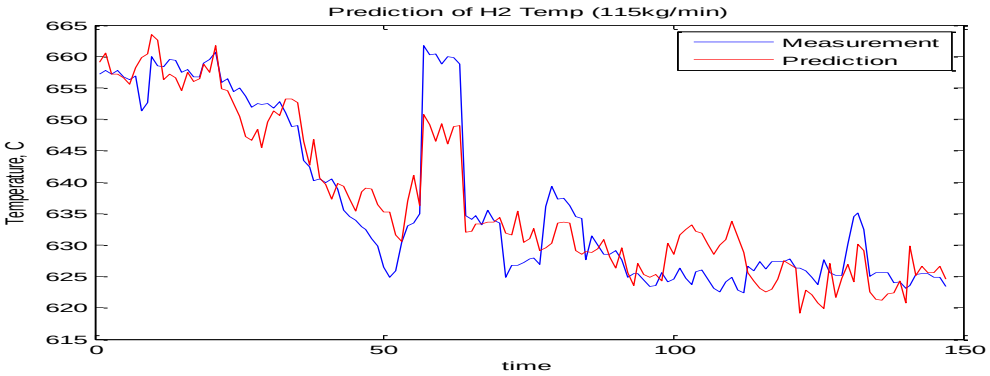
Prediction of H2 Temp (115kg/min)
Measurement
Prediction
Temperature, C
time
665
660
655
650
645
640
635
630
625
620
615
0
50
100
150

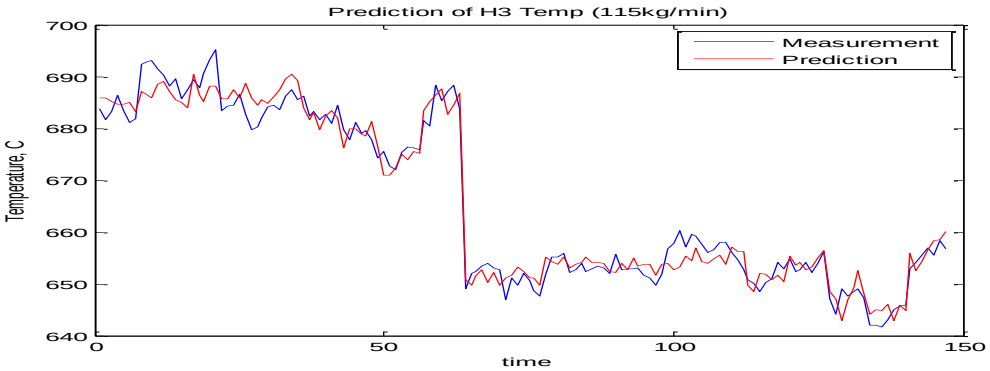
Prediction of H3 Temp (115kg/min)
Measurement
Prediction
Temperature, C
time
700
690
680
670
660
650
640
0
50
100
150

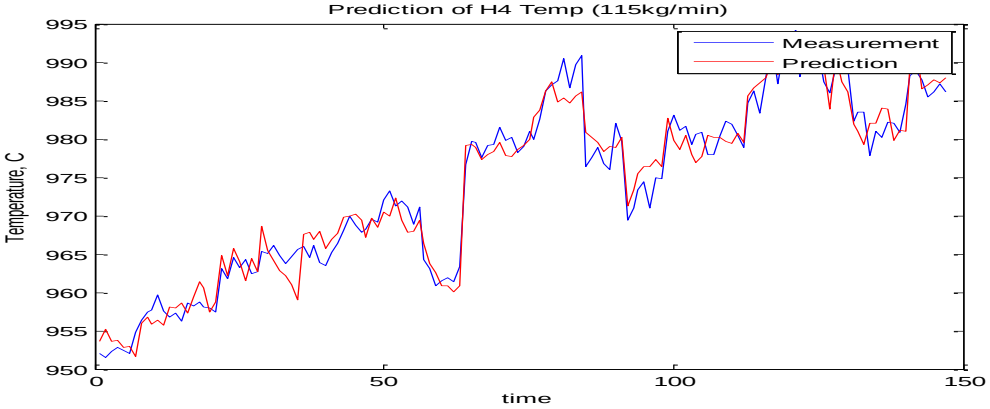
Prediction of H4 Temp (115kg/min)
Measurement
Prediction
Temperature, C
time
995
990
985
980
975
970
965
960
955
950
0
50
100
150

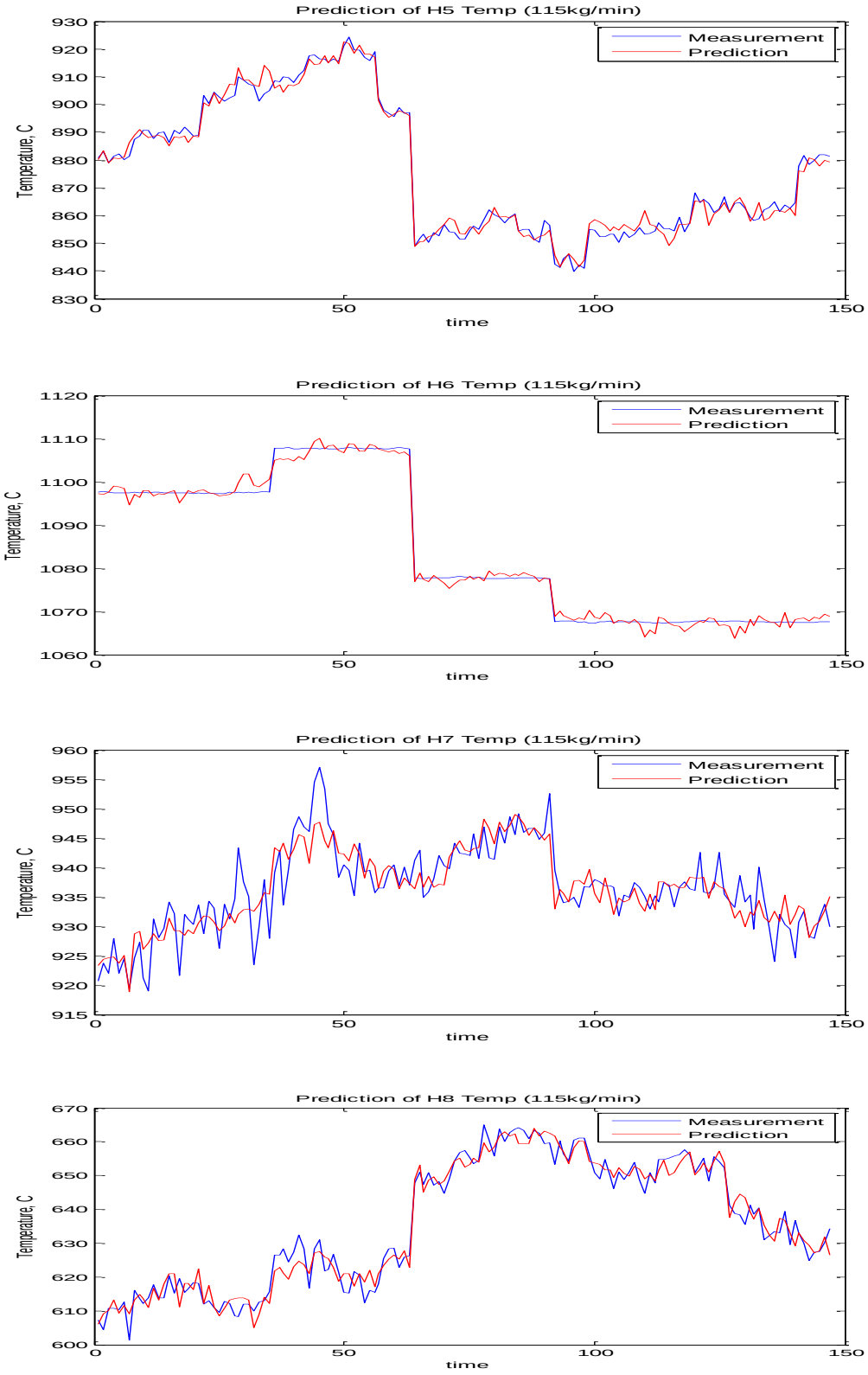

Figures 156-163: Prediction of gas temperature profiles in hearths 1 to 8 using the individual gas flow to each burner, walls temperature and delayed gas temperatures for Feed rate 115 kg/min

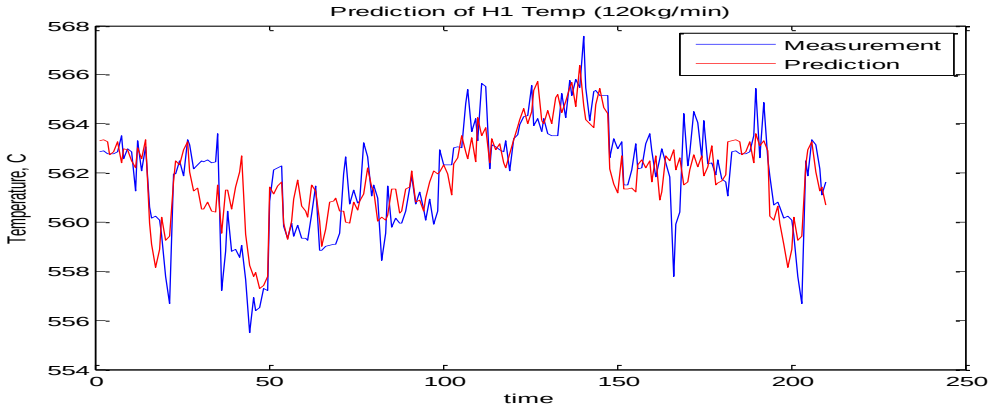
Prediction of H1 Temp (120kg/min)
Measurement
Prediction
Temperature, C
time
568
566
564
562
560
558
556
554
0
50
100
150
200
250

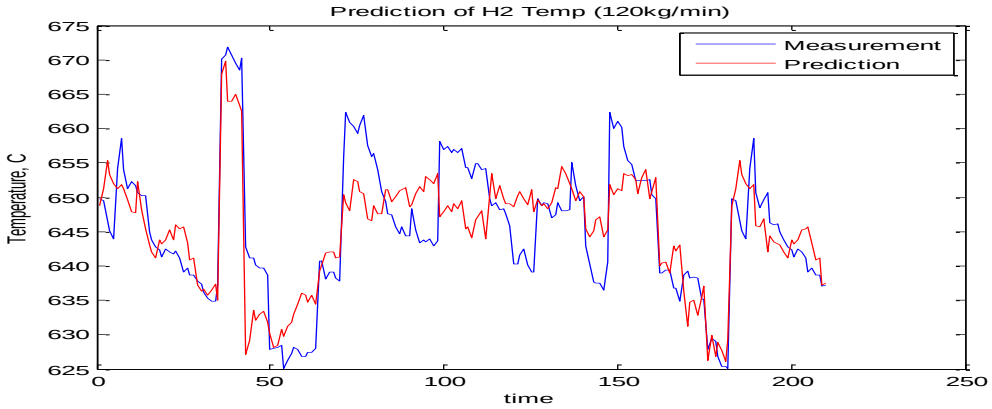
Prediction of H2 Temp (120kg/min)
Measurement
Prediction
Temperature, C
time
675
670
665
660
655
650
645
640
635
630
625
0
50
100
150
200
250

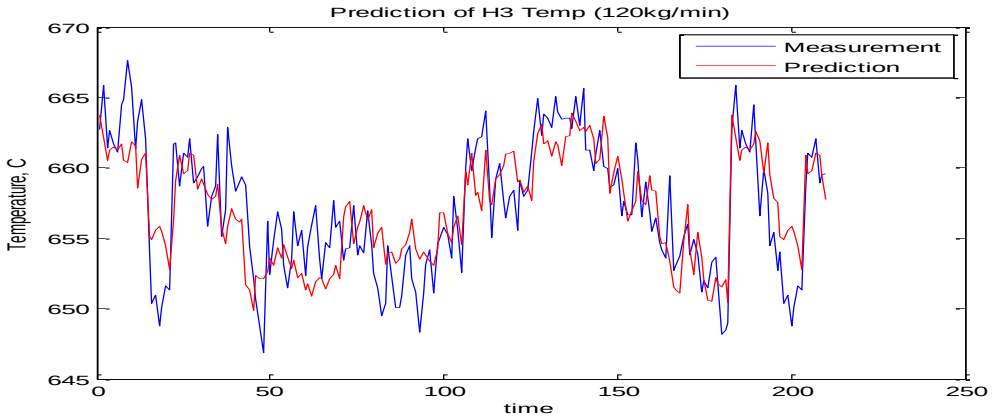
Prediction of H3 Temp (120kg/min)
Measurement
Prediction
Temperature, C
time
670
665
660
655
650
645
0
50
100
150
200
250

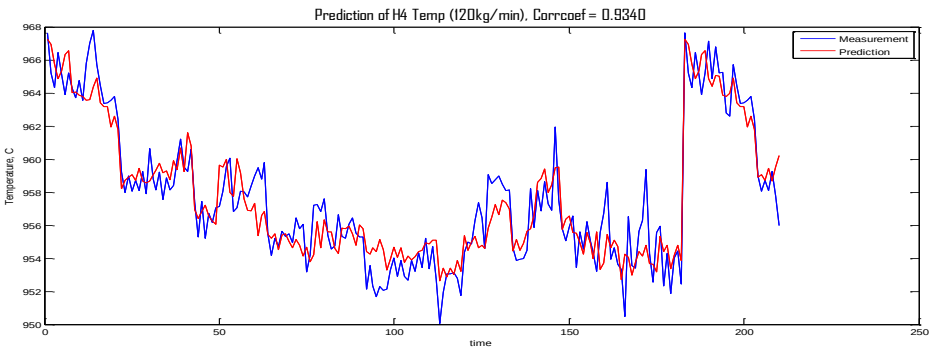
Prediction of H4 Temp (120kg/min), Corrcoef = 0.9340
Measurement
Prediction
Temperature, C
time
968
966
964
962
960
958
956
954
952
950
0
50
100
150
200
250

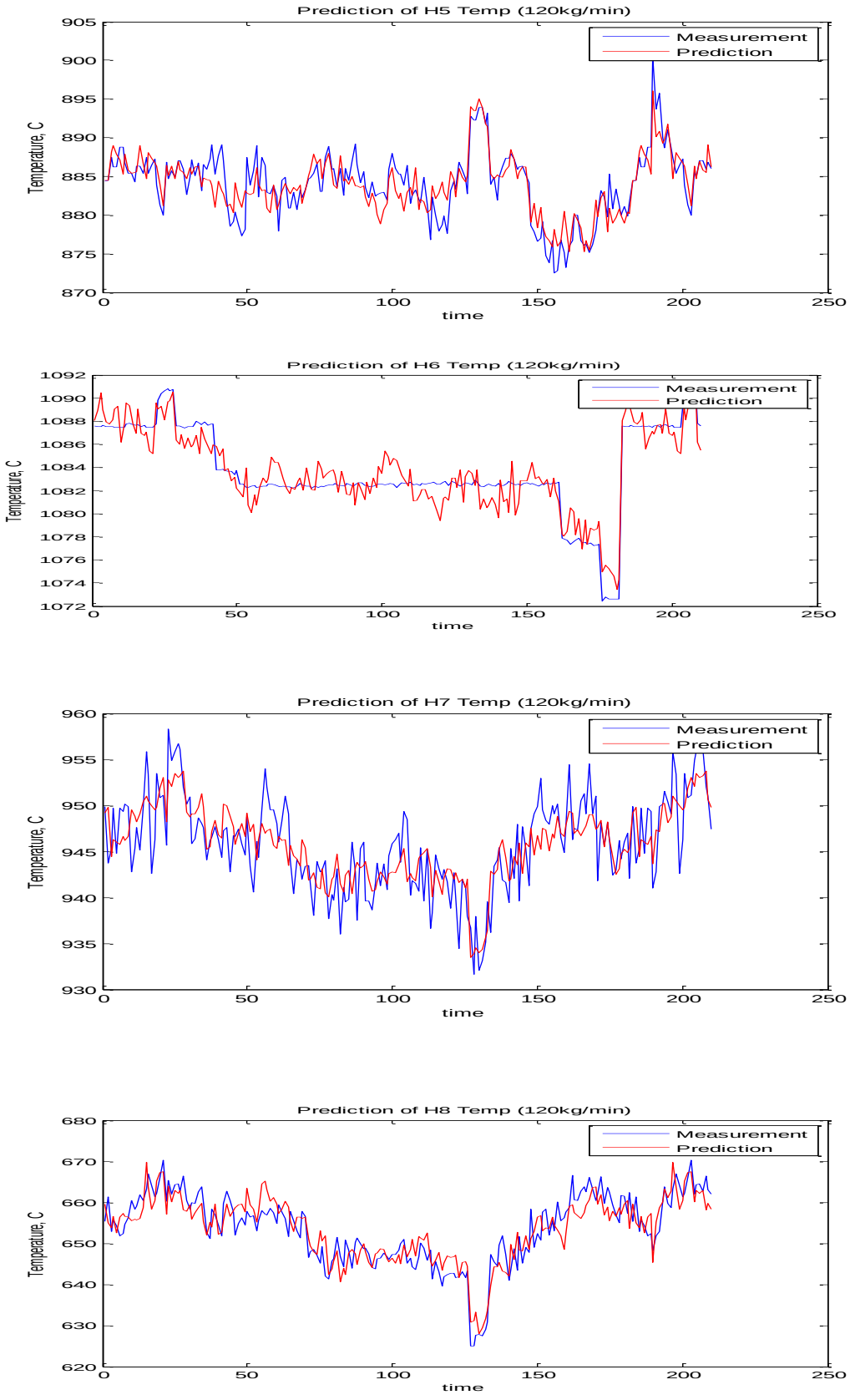

Figures 164-171: Prediction of gas temperature profiles in hearths 1 to 8 using the individual gas flow to each burner, walls temperature and delayed gas temperatures for Feed rate 120 kg/min